

Design and Analysis of a Novel Low Loss Homopolar Electrodynamic Bearing

TORBJÖRN A. LEMBKE



Doctoral Thesis in
Electrical Machines and Drives
Stockholm, Sweden 2005



KTH Electrical Engineering



KTH Electrical Engineering

TRITA-ETS-2005-02
ISSN-1650-674X
ISRN KTH/R-0504-SE
ISBN 91-7178-032-7

Design and Analysis of a Novel Low Loss Homopolar Electrodynamic Bearing

Torbjörn A. Lembke

Doctoral Dissertation
Stockholm 2005

ELECTRICAL MACHINES AND POWER ELECTRONICS
DEPARTMENT OF ELECTRICAL ENGINEERING
ROYAL INSTITUTE OF TECHNOLOGY
SWEDEN

*Submitted to the School of Electrical Engineering, KTH,
in partial fulfilment of the requirements for the degree of
Doctor of Philosophy*

Printed in Stockholm, Sweden
Universitetservice US AB, 2005

TRITA-ETS-2005-02
ISSN-1650-674X
ISRN KTH/R-0504-SE
ISBN 91-7178-032-7

*To my wife
Ann-Sofie
and my sons
Johannes & Fredrik*

Abstract

A novel homopolar electrodynamic bearing, together with a suitable permanent magnet drive, have been developed for high-speed applications where low losses and high reliability are essential and exclude the use of ball bearings, and yet where active magnetic bearings offer a too complex system solution. Considered applications are small turbomolecular vacuum pumps, and maintenance free flywheels for energy storage in remote telecom and satellite systems. Other upcoming areas where these bearings offer interesting technical and economic solutions are compressors for fuel cells and heat pumps, applications which normally suffer from short bearing lifetime.

Unlike active magnetic bearings, forces are produced in electrodynamic bearings without any control electronics, thanks to stabilizing eddy currents induced by permanent magnets. In the novel homopolar concept eddy current losses are reduced to a minimum using a homopolar design with ring magnets instead of multipole or Halbach arrays.

Currents and forces are simulated using steady state 3D-FEM analysis, which can take velocity into account using an implemented Minkowski transform. From these results an analytical model has been developed, and the results are compared. The results are converted into useful rotordynamic data that is easily understood by machine engineers.

The bearing has been experimentally tested in a rebuilt turbomolecular vacuum pump up to 90,000 rpm. Bearing forces have been accurately measured on a specially designed spring suspended scales, in which the bearing rotor is powered with the permanent magnet drive. Comparison of measured data with results from the 3D-FEM analysis shows excellent agreement.

Keywords: *Homopolar bearing, Electrodynamic bearing, Induction bearing, Eddy current bearing, High-speed drive, Permanent magnet drive, Halbach rotor, Flywheel for energy storage*

Preface

This work was initiated in 1997 in order to investigate an invention made by the author two years earlier in the field of electrodynamic levitation. Having finished his M.Sc thesis [5] in 1990 on the design of magnetic induction bearings, the author continued to develop these bearings, also known as electrodynamic bearings, for SKF and later also for the German vacuum industry until 1994. However, though the bearings met the specifications set by the application engineers, the losses generated by these bearings were still too high to meet the requirements from a broader market, and it was also felt that they could not be reduced to acceptable levels solely by optimizing the bearing parameters. A completely new approach was needed; a development task that the author initially carried out from his newly founded company Magnetel.

The homopolar induction bearing saw the crack of dawn in 1995. It has a simple geometric design that promises very low losses, but it soon turned out that the bearing was remarkably difficult to analyze. Nothing similar had ever been published, and the computational tools required to simulate the bearing had barely been developed.

Professor Dave Rogers at the University of Bath was contacted, who at the time was developing a 3D-FEM software. He and his staff delivered a version of the software, which they had optimized especially for this application. Thanks to the software it was, for the first time ever, possible to visualize how the currents are induced in the bearing, and from these results the first steps towards an analytical model could be taken.

At that time also Prof. Chandur Sadarangani at the Royal Institute of Technology in Stockholm was involved, and the current research project started at his department, the department of Electrical Machines and Power Electronics, in 1997. Professor Sadarangani has a long experience in eddy current calculations regarding different types of electrical machines, and he and his staff has contributed to a better analytical understanding of the bearing.

Two test rigs were made to verify the analytical and computer simulated results. The conformity of the results is striking. However, during the experimental phase of the project, it was discovered that the existing rotordynamic theories available did not correctly take eddy current losses and its effect on stability into consideration, which caused difficulties to interpret some of the dynamic effects of the first test rig. Nevertheless, several test runs up to 90 000 rpm were performed with this rig. The second rig was made to enable very accurate measurements at lower speeds. Low speed involves much interesting physics, but is difficult to simulate in the

computer, since it causes instability in the Newton-Raphson equation solver. Thus low speed measurements bring additional scientific values.

The original contributions of this work to the public knowledge on magnetic bearings are believed to be:

- The development of a low loss homopolar electrodynamic bearing concept with cylindrical conductors for high-speed operation.
- Parametric optimization using 3D-FEM simulations of the bearing.
- Development of a simplified analytical model of the bearing, which explains the fundamental physics, and which is accurate enough to comply with FEM data.
- Measurements of bearing forces and losses for various magnet configurations.
- Development of a high-speed airgap BLDC motor with low radial forces.
- Better understanding of rotordynamic influence from eddy currents taking both resistance and inductance into consideration.

Acknowledgement

First of all I would like to express my deepest gratitude to my supervisor Prof. Chandur Sadarangani at the department of Electrical Machines and Power Electronics at the Royal Institute of Technology in Stockholm, who has guided me through this long and challenging project.

I gratefully acknowledge the financial support by the Swedish Business Development Agency in Stockholm (NUTEK) and by Magnet AB in Uppsala.

Without the help and kindness from Prof. Dave Roger and Prof. Roger Hill-Cottingham from the University of Bath regarding the 3D-FEM simulations, I doubt it would have been possible to find ways to simulate this novel bearing concept.

Prof. Hans-Peter Nee has been of great help in cross checking my theories. He also helped me to bring understanding to some of the complicated 3D effects, which I gladly, and without comment, will neglect in this report.

Many thanks to Mats Leksell, my roommate who helped me to interpret the induction bearing in terms of induction generator terminology. He has also encouraged me during the project, and has taught me the way of life in his introduction movie "Dante Doktorand" for new employees.

Cheerful and encouraging comments were provided en masse by Peter Bennich, who as a power quality researcher immediately saw the possibilities with magnetically levitated flywheels.

Marcus Granström at Magnet AB has been of great help in making the 3D-CAD generated pictures of the bearings. Per Uselius at Magnet AB and Jan Olov Brännvall at the institutions laboratory, have done great jobs in finding mechanical solutions and putting the machines together.

A new motor was developed for the high speed test spindle, and I especially want to thank Louis Lefevre for his thorough analysis of that motor, and to Dag Bergkvist at Magnet AB and Matthias Milde who did a great job in trying to understand the hand written winding diagrams from the author.

Without Göte Bergh, practical things would simply not work at the department, and it will be a great loss for all of us when he soon retires.

Finally, the support of my wonderful wife Ann-Sofie has been invaluable. She has encouraged me to continue, and patiently believed me every time I told her this thesis would soon be finished.

Stockholm, April 2005

Torbjörn A. Lembke

Contents

1	GENERAL INTRODUCTION.....	1
1.1	HIGH SPEED DRIVES AND NEW BEARING REQUIREMENTS.....	1
1.2	CONVERTING CONVENTIONAL MACHINES FOR HIGH SPEED	3
1.2.1	<i>Mechanical limitations</i>	3
1.2.2	<i>Solutions</i>	4
1.3	MAGNETIC BEARINGS OPENS UP FOR NEW MACHINE DESIGNS.....	5
1.4	OVERVIEW OF COMMERCIAL MAGNETIC BEARINGS	7
1.4.1	<i>The Earnshaw stability criterion</i>	7
1.4.2	<i>Classical active magnetic bearings, AMB</i>	9
1.4.3	<i>Permanent magnet bearings, PMB</i>	9
1.4.4	<i>Superconducting bearings, SCB</i>	11
1.5	MARKET NEED FOR LESS COMPLICATED MAGNETIC BEARINGS.....	12
1.6	ELECTRODYNAMIC REPULSION –THE KEY TO SIMPLICITY?	13
1.6.1	<i>Basic operation</i>	13
1.6.2	<i>Advantages</i>	14
1.6.3	<i>Drawbacks</i>	14
1.7	RESEARCH MOTIVATIONS AND OBJECTIVES.....	15
2	PREVIOUS WORK ON EDDY CURRENT REDUCTION.....	17
2.1	THE NULL FLUX SCHEME	17
2.2	HOMOPOLAR CONCEPTS	20
2.2.1	<i>Axial flux concept</i>	21
2.2.2	<i>Radial flux concept</i>	22
2.2.3	<i>Homopolar bearings with rotor windings</i>	23
2.3	AXIAL FLUX GYROSCOPE STABILIZED BEARINGS.....	25
3	GENERAL ON EDDY CURRENTS AND LOSSES IN HOMOPOLAR ELECTRODYNAMIC BEARINGS.....	27
3.1	CONCENTRIC OPERATION	27
3.2	ECCENTRIC OPERATION AND COMPARISON WITH INDUCTION GENERATORS	29
3.3	SEPARATION OF LIFT FORCE AND STIFFNESS.....	32
3.4	THE PRINCIPLE BEHIND ZERO LOSS BEARING OPERATION	34
3.5	A BEARING WITHOUT LOSSES – IS IT REALISTIC?	35
4	DESIGN OF THE RADIAL FLUX HOMOPOLAR INDUCTION BEARING.....	37
4.1	GENERAL COMMENTS ON ELECTRODYNAMIC BEARING DESIGN.....	37
4.2	BEARING DESCRIPTION AND DRAWINGS	38
4.2.1	<i>Inner rotor bearing for spindles and turbines</i>	39
4.2.2	<i>Outer rotor bearing for flywheels</i>	41

4.2.3	Intermediate rotor bearing for hollow shafts and pumps	42
4.3	AUXILIARY BEARINGS	43
5	BEARING ANALYSIS.....	45
5.1	PURPOSE OF THE ANALYSIS	45
5.2	ANALYTICAL METHOD	45
5.3	MAGNETIC CIRCUIT	48
5.3.1	Magnetic circuit of an inner rotor bearing.....	48
5.3.2	Magnetic circuit of an outer rotor bearing.....	50
5.3.3	Magnetic circuit of an intermediate rotor bearing	50
5.4	EDDY CURRENT CIRCUITS.....	52
5.4.1	Eddy currents induced due to eccentricity.....	52
5.4.1.1	Induced voltage	59
5.4.1.2	Resistance.....	64
5.4.1.3	Skin depth	68
5.4.1.4	Inductance	69
5.4.2	Eddy currents induced by lateral motion.....	74
5.4.2.1	Constant speed	74
5.4.2.2	Vibrations.....	77
5.4.2.3	Low frequency whirl	80
5.4.2.4	High frequency whirl	81
5.4.2.5	Synchronous whirl.....	82
5.4.3	Stray eddy currents.....	83
5.5	BEARING FORCES	84
5.6	LOSSES	89
5.7	STIFFNESS	93
5.8	DAMPING	97
5.9	ROTOR DYNAMICS.....	100
5.9.1	Equations of motion.....	103
5.9.2	Static Equilibrium.....	105
5.9.3	Load Range.....	106
5.9.4	Stability.....	107
5.10	COMPARISON WITH BALL BEARING STANDARDS.....	108
6	FEM -SIMULATIONS.....	109
6.1	SIMULATION METHOD	109
6.1.1	Software.....	110
6.1.2	Platform.....	110
6.2	MODEL GEOMETRY OF THE STUDIED BEARINGS.....	111
6.3	SYMMETRY PLANES AND BOUNDARIES.....	112
6.4	MESH GENERATION	113
6.4.1	Mesh generation in Mega.....	113
6.4.2	Comments on automatic mesh generation.....	113
6.4.3	Square or triangular elements?	113
6.4.4	Structure of the manually generated mesh	113
6.4.5	Influence of mesh size.	116
6.5	SOURCES AND REGIONS.....	118

6.6	EDDY CURRENT DISTRIBUTION	119
6.6.1	<i>Field diffusion</i>	121
6.6.2	<i>Importance of flux derivatives</i>	122
6.7	BEARING FORCES	123
6.8	BEARING LOSSES	130
6.9	PARAMETRIC OPTIMIZATION OF BEARING GEOMETRY	132
6.9.1	<i>Influence of scaling</i>	133
6.9.2	<i>Adding intermediate magnets</i>	134
6.9.3	<i>Optimization of magnet length</i>	135
6.9.4	<i>Optimization of rotor length</i>	140
6.9.5	<i>Optimization of magnet width</i>	142
6.9.6	<i>Leakage flux reduction</i>	144
7	MOTOR	147
7.1	BACKGROUND.....	147
7.2	CONCEPT	148
7.3	BACK-EMF	153
8	EXPERIMENTAL VALIDATION OF THE PROTOTYPES	155
8.1	PROTOTYPE 1; VACUUM PUMP	155
8.2	TEST RUNS.....	157
8.3	PROTOTYPE 2; SPRING SUSPENDED SCALES.....	163
8.4	BEARING PARTS.....	169
8.5	CALIBRATION OF BEARING CENTER	170
8.6	TEST RESULTS	171
8.6.1	<i>Eccentricity dependent properties</i>	171
8.6.2	<i>Stiffness versus speed</i>	175
8.7	COMPARISON WITH FEM CALCULATIONS	178
8.8	THERMAL ANALYSIS.....	179
9	CONCLUSIONS AND SUGGESTIONS FOR FUTURE RESEARCH	181
9.1	CONCLUSIONS	182
9.2	SUGGESTIONS FOR FUTURE RESEARCH	183
	REFERENCES	185
	APPENDIX 1	189
	SIMPLE HANDS-ON RULES FOR DESIGNING INDUCTION BEARINGS	189
	APPENDIX 2	191
	MODEL GEOMETRIES	191
	APPENDIX 3	193
	PATENTS	193

List of symbols

Symbol	Unit	Description
B	T	Magnetic flux density
B_r	T	Remanent flux density
d_i	m	Inner diameter of inner magnet
C	Ns/m	Damping coefficient
D_i	m	Outer diameter of inner magnet
d_r	m	Inner diameter of conducting rotor
D_r	m	Outer diameter of conducting rotor
d_o	m	Inner diameter of outer magnet
D_o	m	Outer diameter of outer magnet
f	Hz	Frequency
F_x, F_{xb}	N	Bearing force x-component in bearing coordinate system
F_y, F_{yb}	N	Bearing force y-component in bearing coordinate system
F_{xs}	N	Bearing force x-component in stator coordinate system
F_{ys}	N	Bearing force y-component in stator coordinate system
F_z	N	Bearing force in z direction
F_b, F_r	N	Total bearing force caused by displacement Δr
F_v	N	Phase delayed damping force proportional to rotor translational velocity v
F_d	N	Damping force caused by external non-rotating damper
g_n	m	Nominal airgap
K	N/m	Bearing stiffness
k_y	N/m	Bearing stiffness in y direction
k_x	N/m	Bearing stiffness in x direction
k_{yx}, k_c	N/m	Cross coupling stiffness
l_m	m	Axial length of magnet
l_w	m	Axial length of iron pole shoes at ends
l_r	m	Length of conducting bearing rotor
l_1, l_2, l_3	m	Lengths of eddy current circuit
m	kg	Mass of rotor
m	Am	Magnetization
M_x	Nm	Moment about x axis
M_y	Nm	Moment about y axis
M_z	Nm	Moment about z axis, brake moment
p	-	Number of poles in heteropolar bearing

r, φ, α	m, rad	Fixed spherical coordinates of rotor position
w_m	m	Width of magnet cross section.
w_1, w_2, w_3	m	Widths of eddy current circuit
x_0, x_1, x_r	m	Fixed, translating and rotating x-coordinates
y_0, y_1, y_r	m	Fixed, translating and rotating y-coordinates
$z_0, z_1,$	m	Fixed and translating y-coordinates
x_s	m	Stator coordinate axis perpendicular to displacement
y_s	m	Stator coordinate axis parallel to displacement
z_s	m	Stator axial coordinate about which stator is symmetric
α	rad	Attitude angle
ρ	Ωm	Resistivity of rotor
ρ_0, ρ_r	m	Fixed and rotating radial cylindrical coordinates
θ	rad	Force angle, defined as the complimentary angle between the force and the displacement.
σ	$\Omega^1 m^{-1}$	Conductivity of rotor
τ	m	Pole width
ω	s^{-1}	Rotational speed
ω_n	s^{-1}	Natural frequency of undamped vibrations
Ω, ω_w	s^{-1}	Whirl frequency

1 General introduction

The benefits of using modern high-speed technology instead of using conventional machines are becoming apparent to an ever-increasing number of engineers. Higher power density and better efficiency are advantages usually sought for, thus leading to smaller machines with lower power consumption. Hand held screwdrivers and mobile power generators are applications where these advantages become obvious, and the number of applications is likely to increase in the future.

1.1 High speed drives and new bearing requirements

What is the definition of a high-speed machine? Some years ago the answer would definitely have been that there is a sharp line between motors running at network frequency and motors running faster. However, with the widely spread use of power converters the limit is now moving upwards. During the past ten years turbomolecular pumps operating at 90,000 rpm have been mass-produced showing that the technology is mature. These pumps are often referred to as high-speed turbo pumps.

Recently the term very high speed machines was launched referring to the recent research at MIT on small 0.1 kW turbogenerators operating at between 1 and 2 million rpm.

Probably the fastest machine ever made was a motor made for splitting steel balls. It levitated the balls in a magnetic field and forced them to rotate at 18 million rpm so that they would burst.

An engineer designing a high-speed machine will have to tackle other types of problems than usually treated by courses in electrical engineering. Questions like how to reduce air drag losses and how to eliminate eddy current losses or how to treat problems concerning rotor dynamics and vibration control are likely to occur.

A special type of problem that many engineers regard to be the most difficult one, is the choice of bearings. At high speed the lifetime of a ball bearing is very limited. This may not matter for some applications as is the case for a hand held screwdriver that only operates a few seconds at a time, but for other applications the lifetime is crucial.

In some environments the noise level determines the choice of bearings. If the rotor is not perfectly balanced, or maybe it creeps with time and gets

1 General introduction

unbalanced, a bearing with high stiffness will transfer the vibrations to the housing and should thus be avoided.

In other cases the bearing must be lubrication free, for instance in hydrocarbon free environments like the medical process industry or the vacuum industry.

Maintenance free operation is often required, something that lubricated bearings can not deliver.

Bearings like ceramic ball bearings, air bearings or fluid bearings are often used, all with their special limitations. It is not surprising that a new class of bearings, **magnetic bearings**, is becoming very popular in designing high-speed machines.

Magnetic bearings exist in several different types, all of them offering non-contact operation. Thus they all have very long lifetime. They are lubrication free and thus maintenance free. They have low stiffness and thus does not transmit vibrations to the housing. They are quiet. And they have very low losses, even at very high speed. If it would not be for the price these bearings would surely be the ultimate choice.



Fig. 1.1. Homopolar induction bearing compared to a spherical ball bearing.

1.2 Converting conventional machines for high speed

This report will deal with the possibility to make a low-price magnetic bearing that still offers most of the advantages you expect from this emerging and promising new bearing technology. The bearing will be referred to as the radial flux homopolar induction bearing, Fig. 1.1.

1.2 Converting conventional machines for high speed

When inverters are used to increase the speed of a conventional machine, without changing the machine design, the bearing lifetime is reduced. Also vibrational problems are likely to occur. At very high speed centrifugal forces need to be taken into careful consideration. Below, these mechanical limitations will be studied, and different solutions will be discussed.

1.2.1 Mechanical limitations

As the speed of a bearing increases, the centrifugal forces will increase. To a certain limit the use of low density ceramic balls instead of steel balls can reduce the centrifugal force, but this does not help very much since the force increases linearly with weight and quadratically with speed. So the best way to increase the lifetime is often to reduce the diameter. If the load is too high for a smaller bearing, two bearings can be used in line. In this case a so-called paired couple of bearings is often used to reduce the bearing axial gap. The important thing is to reduce the diameter and thus the peripheral speed of the bearing.

However, this method is contradictory to the desire to maintain the torque while increasing the speed, since the same torque has to be transmitted through a thinner shaft, which can lead to torsional vibrations and fatigue stress. Thus the torque during normal operation in such applications has to be reduced in order to enable the use of a thinner shaft.

Reducing the diameter has another disadvantage: it reduces the frequency of the first bending mode, which makes high speed operation more demanding and increases the need for appropriate damping. See Fig. 1.2a.

1 General introduction

1.2.2 Solutions

The solution is to use large diameter bearings that still offer long lifetime. This makes magnetic bearings the ideal choice. Fig. 1.2b. Today, magnetic bearings are used in a variety of applications, so the main question is seldom whether or not magnetic bearings can do the job. The question is what kind of magnetic bearing, or bearing combination, that should be used to fulfill the mechanical specifications within given economical constraints. This sometimes results in interesting bearing combinations. Often used are combinations of passive and active magnetic bearings. Another popular hybrid is the combination of passive magnetic bearings and ball bearings. Finally air bearings and passive magnetic bearings are sometimes used together. A description of these types of magnetic bearings is given in Section 1.4 “Overview of commercial magnetic bearings”.

With the introduction of cost effective induction bearings the number of possible bearing combinations increase. The induction bearing is of particular interest at peripheral speeds over 200 m/s. At this speed sheet steel rotors used in active magnetic bearings can hardly withstand the centrifugal forces, while an induction bearing with an aluminum cylinder can easily operate at such speeds.

Thanks to the simplicity of the induction bearings they can open up for new machine designs since they neither require rotating magnets nor bearing rotors of sheet steel. In Chapter 1.3 two applications will be shown where the use of induction bearings is particularly beneficial.

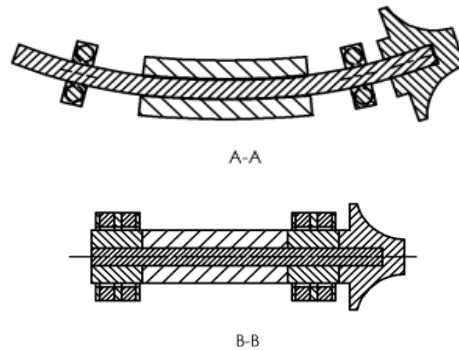


Fig. 1.2. Compressor with a) ball bearings and b) magnetic bearings.

1.3 *Magnetic Bearings opens up for new machine designs*

If magnetic bearings are considered early when developing a new machine, completely new designs are possible. Often there is no need for a shaft at all. The bearings and the motor can then be integrated into the load, thus reducing the size and the mechanical complexity of the whole machine. This concept is especially useful for gasturbines, centrifuges, pumps, flywheels, gyroscopes and other direct driven applications.

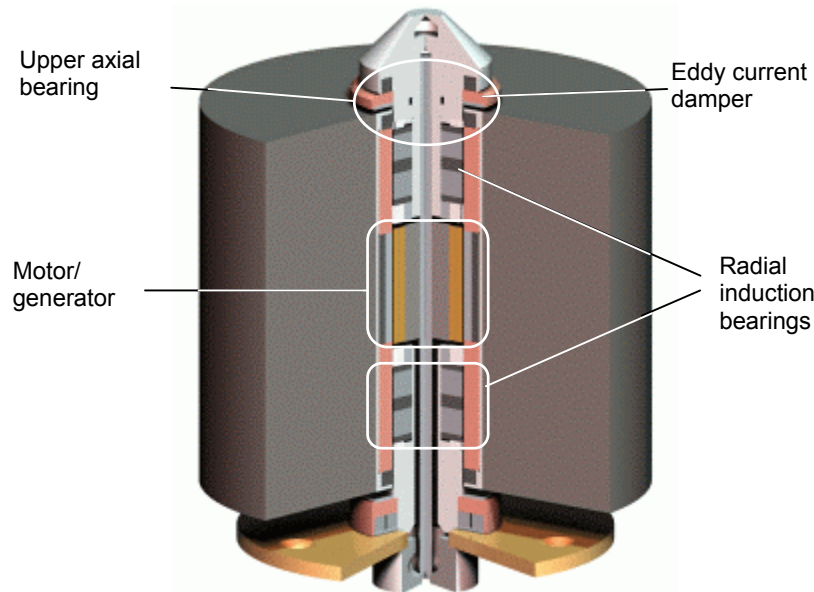


Fig. 1.3. High speed flywheel for energy storage.

A flywheel without shaft [24] is shown in Fig. 1.3, and has obvious advantages over conventional flywheel designs. Similar flywheels are already manufactured and marketed by AFSTrinity Flywheel Corporation [23]. The drive and the bearings can be integrated in the design without the need for a long thin shaft. In this particular design two radial homopolar induction bearings and one passive axial bearing of permanent magnet type are used. For efficiency reasons, an outer rotor permanent magnet machine is used for motor and generator mode.

The shaft is often the weak point in conventional flywheels, due to bending problems at high speed and due to the very large torque when the machine

1 General introduction

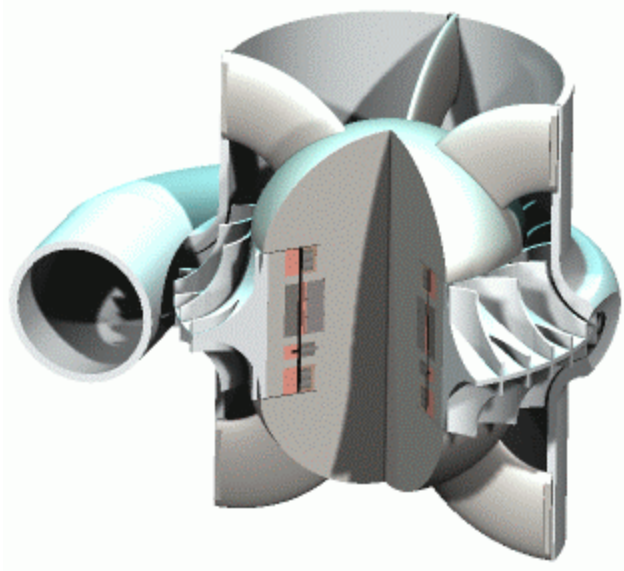


Fig. 1.4. Gas expander with integrated drive unit.

operates as a generator. Especially flywheels used for power quality applications, which have to deliver very high power during short periods, suffer from these torque peaks.

Turbines is another group of applications where magnetic bearings offer interesting design possibilities. Fig. 1.4 shows a picture of a novel design of a gas expander made by the author. The bearings and the generator are integrated in the impeller.

Avoidance of a flexible shaft with additional damping arrangements, and elimination of the complex oil jet injection lubrication systems increases the reliability of the total system as the number of moving parts are reduced. Also the price of the system as a whole will probably be lower than for conventional turbine designs. If low maintenance requirements are crucial, the magnetic bearing is the natural choice.

Active magnetic bearings will most likely do the job for most applications, but for the designs in Fig. 1.3 and 1.4 it is important to get rid of the emergency ball bearings. In these cases induction bearings with integrated touch down bearings [27] may be better suited in order not to have to decrease the diameter or to increase the length of the shaft.

1.4 Overview of commercial magnetic bearings

A magnetic bearing is a contact free bearing wherein the load is carried by magnetic forces. Furthermore the magnetic field is generated in such a way that it provides necessary stiffness and damping for the rotor to be levitated safely during operation.

Magnetic bearings have been available on the market for about 30 years. Usually they are divided into two categories, often referred to as either active or passive depending on whether an electronic control system is being used or not.

This nomenclature has been around for quite a while even though it is rather unfortunate and sometimes gives rise to misunderstandings.

It would certainly be more clarifying to classify magnetic bearings according to the physical cause of the force, as H. Bleuler [12] has done. He divides the bearings in two groups, reluctance force bearings and electrodynamic bearings. Then each group is divided into five respectively four categories depending on how the magnetic force is generated.

Some bearing categories are of only limited academic interest, while others have found many useful applications. Based on Bleulers [12] classification some of the most technically and commercially important bearing types will be presented below. But first we need to take a closer look at the general stability criterion for magnetic bearings.

1.4.1 The Earnshaw stability criterion

As early as 1842 Earnshaw [1] was able to show that it is impossible for an object to be suspended in stable equilibrium purely by means of magnetic or electrostatic forces.

Let V be the scalar magnetic potential at a point, proportional to the scalar product of \vec{B} at that point and the constant magnetization \vec{m} for a single magnetic pole on the suspended object. Then according to the Laplace Eq. (1.1) the sum of the second derivatives is zero,

$$\frac{d^2V}{dx^2} + \frac{d^2V}{dy^2} + \frac{d^2V}{dz^2} = 0 \quad (1.1)$$

1 General introduction

In order for a magnetic pole to experience no magnetic force and have no tendency to move, it is necessary that

$$\frac{dV}{dx} = \frac{dV}{dy} = \frac{dV}{dz} = 0. \quad (1.2)$$

This is the condition for a maximum or a minimum in the potential V . Only at a potential minimum is the equilibrium stable. The condition for a potential minimum is that its second derivative is positive. At best, two of the second derivatives can be made to be positive, then, according to the Laplace equation, the third has to be negative. In that direction the equilibrium will be unstable. The theorem has been derived for a single pole. However, recently Lang [25] was able to show that the theorem can be applied to a magnet as a whole.

In order to achieve stability in all directions it is necessary to add a dynamic term, which can be either an electromagnetic or a mechanical one. Adding an electromagnetic term will exchange the Laplace equation into the Poisson equation, which is used in active magnetic bearings and electrodynamic bearings. When a mechanical force derivative is added it can be done directly into Eq. (1.1). For the bearing to be of the non-contact type the preferred mechanical forces are either gyroscopic or fluid dynamic.

Gravitation is for instance not possible to utilize as a means of stabilizing the bearing, since it has only negligible derivatives. Say that we want to compensate the vertical magnetic force F_y with a gravitational force $-mg$. Then the total potential energy V_{tot} should be used instead of the magnetic potential V , the latter being denoted V_{mag} below to avoid confusion. Unfortunately this does not change anything in the Laplace equation (1.1) since the second term remains unchanged as shown below:

$$\begin{aligned} \frac{d^2 V_{tot}}{dy^2} &= \frac{d^2}{dy^2} \int F_{y,tot} dy = \frac{d^2}{dy^2} \int (F_{y,mag} - mg) dy = \\ &= \frac{dF_{y,mag}}{dy} - \frac{d}{dy} (mg) = \frac{dF_{y,mag}}{dy} = \frac{d^2 V_{mag}}{dy^2} \end{aligned} \quad (1.3)$$

Thus, gravity does not improve the stability of a levitating magnet.

What is said above can be applied to other constant forces as well, like air drag in a windmill. They cannot be fully levitated by permanent magnets alone. However, other air forces like the wedge effect in an air bearing can be used for stabilisation since that force has a space derivative defined by the airgap.

1.4.2 Classical active magnetic bearings, AMB

An active magnetic bearing is a typical example of an advanced mechatronics product. All AMB:s on the market today utilize attracting reluctance forces generated by strong stator electromagnets acting on a ferromagnetic rotor. The magnetic equilibrium reached in this way is inherently unstable. Thus an analog or digital controller is used to stabilize the bearing. Contactless sensors are used to measure the rotor position. Any deviation from the desired position results in a control signal that via the controller and the amplifiers changes the current in the electromagnet so that forces are generated to pull the rotor back so that stability is maintained [12].

Currently only attractive forces are used, but theoretically also repulsive forces could be used for actively controlled levitation. This is the reason why active bearings are sometimes referred to as attracting bearings, while passive bearings are often referred to as repulsive.

The advantages with active bearings over passive bearings are obvious as they offer the possibility to change and adapt the controller algorithms according to machine dynamics. The disadvantages are equally clear and are related to the cost of the bearing. Also reliability is a problem as the controller is dependent on high power quality and thus need energy back up.

Today active magnetic bearings are found in a variety of applications like compressors, gas turbines, motors, flywheels, gyroscopes, fans and machine tool spindles.

1.4.3 Permanent magnet bearings, PMB

One of the first successful commercial products where magnetic bearings offered true added value to the customer was the turbomolecular vacuum pump. With lubrication free magnetic bearings it was possible to manufacture hydrocarbon free pumps – a great achievement at that time.

The first mass produced pump of this kind had one passive magnetic bearing on the high vacuum side and one ball bearing on the exhaust side. The magnetic bearing consisted of concentrically arranged repulsive ring magnets, Fig. 1.5. To the left a bearing with a single magnet pair, and to the right two oppositely directed pairs are used. The latter configuration gives almost 3 times the stiffness compared to the former one. An optimization of PMB geometry was recently done by Lang & Fremerey [9], who showed that many thin magnets should be used instead of a few thick ones.

1 General introduction

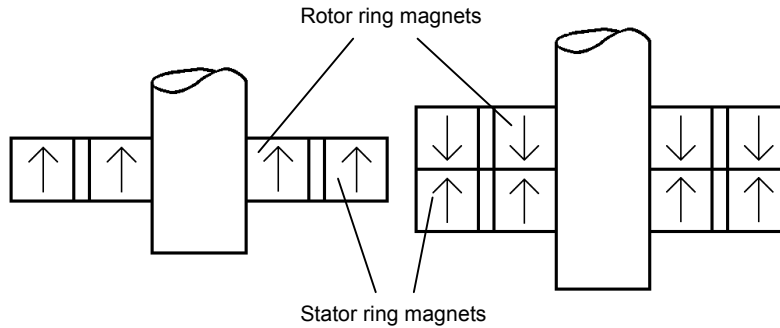


Fig. 1.5. Passive magnetic radial bearings.

For low speed applications it is convenient to let the inner rings be mounted on the rotor, while for high speed applications it is better to let the outer rings rotate due to the centrifugal forces, in which case these forces are used more advantageously in keeping the rotating magnets in place.

When the term passive magnetic bearing is mentioned in this report as well as in most literature this is the magnet arrangement usually referred to.

Attractive magnetic forces from permanent magnets could have been used as well, but as the geometry for such bearings is slightly more complicated they are seldom used.

All passive bearings of these kinds have one thing in common. According to the Earnshaw theorem they are unstable in at least one direction. For the pump mentioned above the repulsive bearing is strongly unstable in the axial direction. This is compensated for by the use of one ball bearing that prevents the bearing from moving axially.

The next progress was made when the axial stability from the ball bearing could be exchanged for an active magnetic axial bearing. In this case two repulsive radial bearings were used. This concept was originally developed by Gilbert [28] and was later used by S2M in Vernon for flywheels for gyroscopic stabilization of satellites. Later, Boden & Fremerey in Jülich modified this concept for use in the turbomolecular vacuum pumps, X-ray tubes and other industrial applications [20]. In 1999 Fremerey and Kolk [19] presented a 500 Wh flywheel for energy storage based on this concept.

1.4.4 Superconducting bearings, SCB

A superconductor has by definition two properties that makes it ideal for magnetic bearings. The first one is the Meissner effect which makes the superconductor act like a perfect diamagnet. A permanent magnet placed above a superconducting surface will "see" a mirror image under the surface polarized so that the force is repulsive. This levitation is stable in the vertical direction, and indifferent in the horizontal direction. If the real magnet moves the image moves too, thus maintaining the repulsive force vertical.

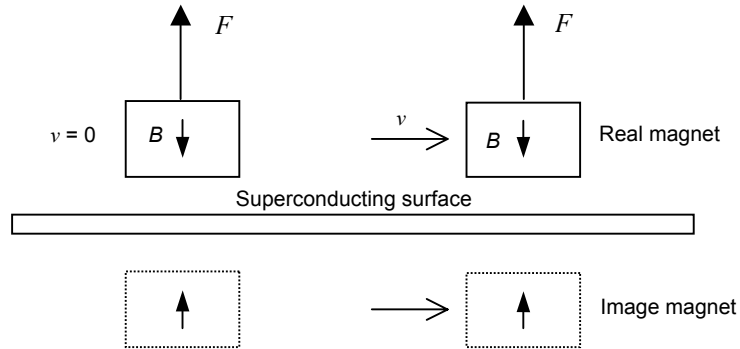


Fig. 1.6. Repulsive force due to the Meissner effect

The modern high temperature superconductors have a built in defect that at a first glance makes them even more interesting for magnetic bearings. If the magnet is placed close to the surface before the superconductor has been cooled down to its superconducting state, not all the flux is expelled when the temperature is decreased again. This method is called field quenching. Some of the field is "frozen" into the superconductor due to an effect called flux pinning. This frozen field stabilizes the magnet in both radial and axial direction. If the surface is turned upside down the magnet does not fall down.

The author, at that time employed by SKF, evaluated this effect in 1990 [5] for use in magnetic bearings, but it was found that the long time stability of such bearings was limited. It was then predicted that when used in a rotating machine exposed to vibrations, then according to the hysteresis loop caused by flux pinning the bearing would slowly move in the direction of the static load and eventually touch down. Later research on superconducting bearings at Argonne national lab and many other places have proved this to be true. This is regarded to be a major drawback for this bearing technology.

1 General introduction

The second effect defining a superconductor is the zero resistance. This effect has been used to make strong electromagnets for magnetically levitated test trains. In this case the bearing principle is not the superconducting one, but the electrodynamic one. The superconductors are just used to replace the permanent magnets that would otherwise have been used. In this case the track is made of aluminium, not superconductors.

It is theoretically possible, but hardly practical, to use the superconductor as the conducting member in an electrodynamic bearing. Due to bad mechanical properties and due to large hysteresis losses this may be found not to work properly. As is nowadays well known, the AC losses in a superconductor are quite large.

1.5 *Market need for less complicated magnetic bearings*

There is an increasing demand for small uncomplicated stand alone bearings for various mass produced applications with special bearing requirements.

Low noise levels are desired in office and household environments. Especially where people need to stay concentrated. Ventilation fans, computer fans and hard drives are typical applications where the pay back time for an investment in more silent equipment is just a few additional effective working hours.

Oil free bearings are important in chemical, biomedicine and biotech applications. Hydrocarbon free environment is necessary in analytical instruments, and in the large electronics manufacturing area.

Maintenance free operation is important in unmanned stations for telecom, television and space industry. Space industry can still afford active magnetic bearings, but the highly competing telecom market need to reduce investment costs to a minimum.

Low energy loss is important in all kinds of energy generation and energy storage applications. It is also important for applications where energy is limited like in battery-powered electronics and vehicles.

Despite the market need, there are no magnetic bearings available on the market that does not require either an electronic control unit or cryogenic cooling equipment. Thus there are no bearings available for the huge markets that small and mass-produced products represent.

1.6 Electrodynamic repulsion –the key to simplicity?

"Electrodynamic bearings" is a large group of magnetic bearings, all of them based on the electrodynamic repulsion principle. They offer many similarities with induction generators, which is the reason they in this dissertation are frequently referred to as "induction bearings". "Eddy current bearings" is another term often used in patent applications, also referring to this group of bearings.

1.6.1 Basic operation

The electrodynamic principle is based on Lenz' law. According to this law a change of magnetic flux through a conductor will induce a voltage in the conductor in such a way that a current is produced that tries to maintain the magnetic flux at the original level. In reality this means that any changing electromagnetic flux will be reflected on a conducting surface, thus giving rise to repulsive forces. The maximum force is generated at infinitely high speed. This force can be calculated as if there is a mirror image of the real magnet on the opposite side of the surface. This is very much like the superconducting effect described earlier, and the bearings are equally strong, at least for high frequencies. At low frequency an electromagnetic bearing has very low lift force. Thus at low speed induction bearings will touch down on landing bearings.

Fig. 1.7 illustrates the electrodynamic levitation principle applied to a linear bearing where a moving magnet levitates above a conducting plate. The plate could as well be a set of short circuit coils. At zero speed there is no change of flux and thus no eddy currents are induced and no force arise. At high speed eddy currents I^+ and I^- are induced and the mirror effect develops. However, the mirror is incomplete and phase shifted due to the finite speed and the resistance in the conducting plate. The phase shift changes the angle

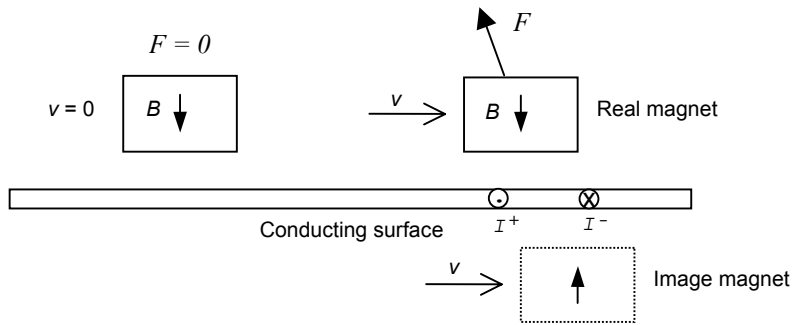


Fig. 1.7. The electrodynamic levitation principle.

1 General introduction

of the resultant force F so that there is also a brake force component. The force F acts between the magnet and the induced currents, but can also be calculated as the force between the real magnet and its image, which was done by the author [5] in 1990. It may seem a little bit confusing that the mirror comes ahead of the real magnet, but this is a natural result from the fact that the eddy currents are induced from the change of the flux from the real magnet, which always comes before the flux itself. The brake force is well known from linear induction motor theory where it is reversed and used for traction.

Instead of moving permanent magnets an alternating magnetic field can be generated by coils connected in a resonant circuit. However, the ohmic losses in the ac-coils in such a bearing tends to be rather high, so such bearings are mostly investigated for very small or very light applications. The large ohmic losses is the reason for permanent magnets being used instead of electromagnets.

If extremely large forces are desired, the permanent magnets can be exchanged for superconducting coils carrying DC-current. This is the case for some linear electrodynamic bearings that have been proposed for a variety of large magnetically levitated vehicles like trains and rocket launchers. These devices are often referred to as maglevs. In these cases strong superconducting magnets are needed to produce the desired lift force. Some of these applications have already been built and tested and are likely to be of some importance for future transportation.

1.6.2 Advantages

Like superconducting bearings, induction bearings can provide stable levitation without control electronics. However, unlike superconductors they do not need cooling, which make them very attractive from a commercial point of view.

Induction bearings operates more silently than active magnetic bearings, since there is no amplifier noise being transmitted to the rotor and housing.

Induction bearing rotors are preferably made of bulk aluminum or copper conductors. These have the shape of discs or cylinders, which facilitates high-speed operation. Compared to active or passive magnetic bearings, where the rotor material is soft iron respectively brittle permanent ceramic magnets, the induction bearing rotor enables higher speed.

1.6.3 Drawbacks

Large-scale electrodynamic maglev systems have already been successfully demonstrated. However, trying to apply electrodynamic bearings for small

1.7 Research motivations and objectives

and medium size rotating machines is not as easy. Scaling properties makes it difficult to reduce the losses and an attempt is likely to result in an induction heater rather than in a functional bearing.

Many attempts to decrease the eddy current losses have been done in the past, and a review will be given in Chapter 2. However, though many inventors did great work, none of their bearings are available on the market today, the remaining losses being the main issue. Other problems that sometimes are discussed are rotordynamic stability problems due to internal losses.

Finally, these bearings require some kind of starting bearing, since the lift force is low at low speed.

1.7 Research motivations and objectives

The current research and development of stand-alone induction bearings is an attempt to fill this giant gap between on one side market and environmental need and technological achievements on the other. It also seems clear that high-speed technologies will play an important role in the not too far future. It might even be apt to talk about a technology shift where heavy, noisy and dirty industrial machines are exchanged for small high-speed clean and silent ones.

In addition to the market need, which is described in Chapter 1.5, there is also increasing political issues concerning electrical power quality, which sometimes is contradictory to the demands on increased amounts of distributed wind power generation. Rapidly emerging technologies related to Internet and telecom require better power quality than the power grid alone is able to supply. Energy storage in large flywheels on magnetic bearings may prove to be a very efficient way of increasing wind power without losing grid stability and power quality.

Though active magnetic bearings, which are already on the market, may seem to be the obvious choice for the products mentioned, at least from a technical point of view, they do not always convince the purchaser. Will active magnetic bearings ever be cheap in mass production? What about training programs for the staff? How is the problem with back up power to the bearings to be solved?

When this project started it was felt that if there will ever be a great breakthrough for high speed applications in general and magnetic bearings in particular, someone needs to look at these questions seriously.

In 1996 the Swedish National Board for Industrial and Technical Development, NUTEK, and Magnet AB (Publ) agreed on funding the

1 General introduction

current research project about a new type of induction bearing based on the homopolar design.

The objectives of this research are:

- To simulate the magnetic properties of the homopolar induction bearing using 3-dimensional finite element analysis.
- To verify the results experimentally.
- To develop a qualitative understanding of the bearing physics.
- To convert the results into useful rotordynamic data which can readily be used by machine engineers.

2 Previous work on eddy current reduction

Of the different magnetic bearing concepts presented in the introduction, it clearly seems that electrodynamic repulsion offer the simplest means of magnetic levitation, requiring neither electronics nor cooling systems. However, due to well-known losses from bearings based on this concept, the applicability is limited to machines that normally utilize additional heaters. In order to gain access to a broader market, it is necessary to reduce the eddy current losses generated in these bearings. In the following sections a survey will be given on different new designs that have been proposed in order to solve the problem.

2.1 The null flux scheme

The first successful method of reducing eddy current losses is known to have been presented by Powell & Danby [2], who patented their solution in 1969 for use in a ground transportation vehicle. Later, several authors have proposed means of reducing eddy current losses in linear electrodynamic bearings for magnetically levitated trains, maglevs, based their results. Powell & Danby introduced what they called the “null flux scheme”, Fig. 2.1b, which means that the magnets can be arranged in such a way that they do not induce currents until they are needed. Compare Fig. 2.1a and Fig. 2.1b. In Fig. 2.1a an additional lower magnet is added which induces a second eddy current on the lower surface of the conducting plate. The upper and the lower currents do not interfere, since the skin depth prevents them from penetrating into each other. However, in Fig. 2.1b the conducting plate

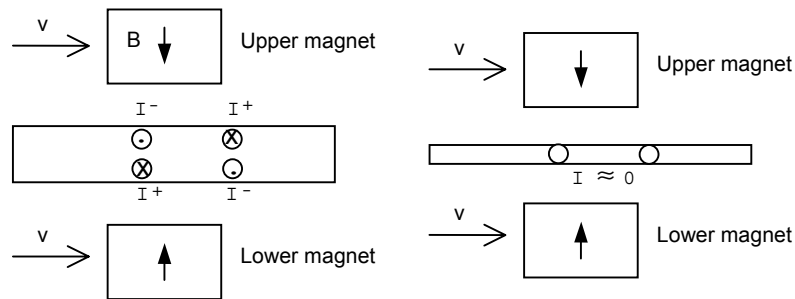


Fig. 2.1 a, b. The null flux scheme.

2 Previous work on eddy current reduction

is thinner than one skin depth so that the eddy currents almost completely eliminate each other. This is true as long as the plate is centered between the magnets in the “null flux region” where there is no flux perpendicular to the plate. When any deviation occurs, the field is no longer zero and repulsive eddy currents are induced.

Sacerdoti et al. [4] utilize this effect in a thrust bearing which they combined with passive radial bearings and reported losses that were “not too high”.

In 1990 the author [5] demonstrated a prototype with eddy current bearings where the linear null flux scheme was applied to axial as well as radial bearings. The rotor weight was 1 kg and the speed was 12 000 rpm. In order to further minimize the losses a minimum of magnets was used, which resulted in a low stiffness. Despite the low stiffness it was possible to demonstrate full magnetic levitation, using only permanent magnets and rotating aluminum discs and tubes. The weight of the rotor was unloaded from the bearings by a separate set of permanent magnets. Thus the lowest possible speed was not determined by the lift force, since the separate lift magnets produced a constant lift force, but by the rotordynamic stability. At 8,000 rpm the rotor centered and the maximum speed tested was 14,000 rpm.

It was also possible to safely run through critical speeds thanks to integrated plain bearings/dampers. The concept was promising, but the losses were still far too high.

Between 1991 and 1995 much work was done by the author to increase the stiffness and to reduce the losses. During this period the basic design that was used for both thrust bearings and journal bearings was the heteropolar eddy current bearing with permanent magnets, see Fig. 2.2. Due to the similarities with an induction generator with large slip the bearing was referred to as the “Magnetic Induction Bearing”, MIB, or simply “induction bearing”.

The goal during this period was to make a thrust bearing that produced a stiffness of 1 N/mm for each Watt of power dissipation at a speed of 100 m/s measured as the speed over the magnets. When this goal was reached the research project was ended, although it seemed possible to reduce the losses even further.

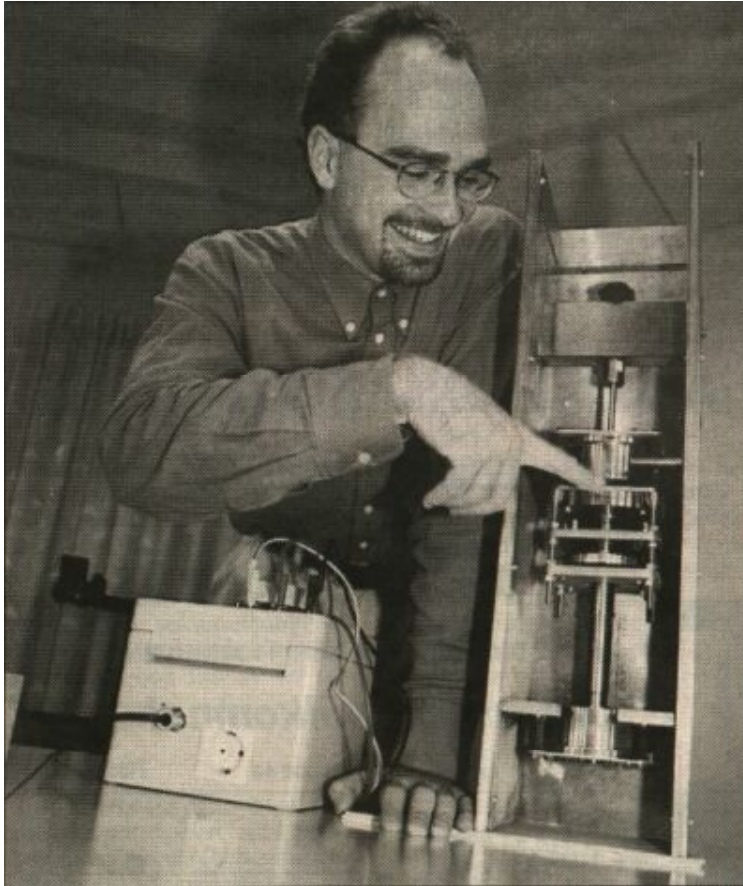


Fig. 2.2. Heteropolar induction bearings designed by the author at SKF in 1990.

In 1998 R.F.Post [7] presented an interesting solution to the eddy current problem in heteropolar radial bearings by simply using a wire wound rotor with the coils connected to minimize the undesired currents. In Fig. 2.3 a prototype of Post's bearing is shown, modified and built by the group of Passive Magnetic Bearings in Lausanne. For axial stabilization passive axial repulsive bearings are suggested.

Instead of reducing the radial flux as Sacerdoti [4], Powell & Danby [2] and the author [5] did, he series connected the coils in such a way that the induced voltages eliminated each other.

2 Previous work on eddy current reduction



Fig. 2.3. A prototype from Lausanne where Richard Post's bearing is evaluated.

All these concepts, including the latter solution from Post [7], can all be described as multipole or heteropolar bearings. They all work according to the principle of eddy current reduction by letting either the induced voltages or the penetrating fluxes counteract each other. The result is the same.

A drawback with the null flux scheme presented by Powell and Danby [2] is that the null flux region is infinitely thin. Thus the conducting part of the rotor, whether it is a bulk material or made up of coils, also needs to be infinitely thin in order not to produce any losses. This in turn requires that the speed is infinitely high; otherwise the rotor can't repel the flux lines.

A practical design needs a certain material thickness. What was needed was a bearing concept that allows a strong flux to penetrate the conductor without inducing unnecessary eddy currents. This leads to solutions involving homopolar magnetic flux.

2.2 Homopolar concepts

Recent research in Japan, Switzerland and USA has shown that it is possible to get around some of the problems above by using a homopolar magnetic field instead of a heteropolar field.

In a bearing with a homopolar field there are no induced voltages that need to be eliminated like in the multipole bearings above. Filatov [10] introduced the term “Null-E magnetic bearings” for this bearing concept, to distinguish it from the previously described “Null flux bearings”. The circular design avoids the induction of any unnecessary eddy currents, as long as the rotor is centered in the bearing stator. The result is the same, but the homopolar concept is much simpler as no winding is required to avoid all the unnecessary eddy currents. Homopolar bearings, as we will denote them, can be of either of the axial flux or radial flux type.

2.2.1 Axial flux concept

A simple axial flux homopolar bearing can look like the left bearing in Fig. 2.4. The advantage of an axial type design is that the magnetic flux path is very effective with a relatively small airgap. Eddy currents are induced in the bearing disc, which rotates in the airgap. The disadvantage with this design is that the eddy current path is rather ineffective thus increasing the total resistance of the electric circuit. Another disadvantage is that the disc can only utilize about half of the flux, at a given instance of time. The remaining flux is used to build up an area with a strong flux gradient in which the rotor can move when it is not centered.

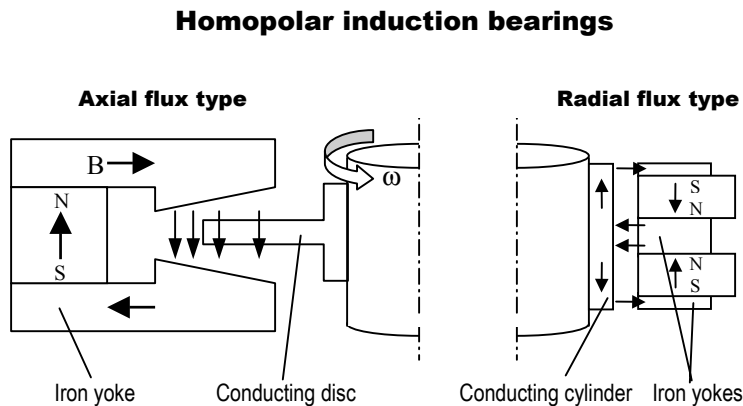


Fig. 2.4. Axial and radial homopolar bearing concepts.

2 Previous work on eddy current reduction

2.2.2 Radial flux concept

The current research by the author on radial flux homopolar bearings is an attempt to overcome some of the above mentioned problems with axial flux bearings. A comparison between the axial flux and the radial flux concepts is made in Fig. 2.4.

The radial flux concept differs from the axial flux bearing in that the rotor has no disc, but only a conducting cylinder into which the flux penetrates in radial direction, Fig. 2.4 right. If a typical flux path is considered, the effective airgap is larger than for the axial flux bearing. However, the active length of the eddy current path is relatively shorter than in the axial flux bearing, thus resulting in a more effective concept. From Fig. 2.4 it is also clear that the radial flux concept is more compact and requires less space than the axial one.

Radial flux homopolar bearings are studied also by H. Bleuler and J. Sandtner at the Group of Passive Magnetic Bearings in Lausanne, Switzerland. During the Seventh International Conference on Magnetic Bearings in Zurich, August 2000, they reported stable levitation at 9,000 rpm, Fig. 2.5.



Fig. 2.5. Swiss rotor with air turbine and homopolar bearings.

2.2.3 Homopolar bearings with rotor windings

Instead of bulk rotor disks and cylinders it is possible to use rotating short-circuited windings instead. The advantage is that the induced eddy currents can be lead into desired current paths, and that stray eddy currents due to badly oriented magnets thus will have a much less negative effect on losses. With coils it is also possible to series connect an electric circuit in order to improve certain bearing characteristics.

Filatov et al. [13] have shown that a simple circuit like a series inductance has a positive influence on low speed stability for axial type homopolar bearings. This is due to the increased phase delay, which has a positive effect on the direction of the restoring force.

Filatov [10] made a bearing prototype, Fig. 2.6, which was able to levitate at speeds from 21 - 40 Hz. The low speed limit was set by the damping properties, and the high speed limit by the material strength. Damping turned out to be a crucial point, so he had to add additional damping by connecting stator mounted damping coils to an external electrical circuit.

The obvious disadvantage with rotating coils and rotating circuits is that they are not well suited for very high speed applications due to the centrifugal load on each component. In this aspect bulk conductors are much better. For this reason Filatov had to optimize his bearing for low speed operation, though with better rotor materials his bearing could certainly have been used at higher speed too. At higher speed he would likely not have needed the additional damping electronics, since damping requirements decreases with increasing speed. Recently, Filatov et al. [14] were able to show that inductance has a positive effect on stability also when it appears in the stationary damping coils.

The work by Filatov et al. [13], [14] is important in more than one way. Though nowadays quite a few reports on passive levitation are published, very few of them contain any analytical explanations to the bearing behaviours. Filatovs work includes several analytical approaches that forms a solid foundation for future work. Thus in this report their nomenclature will be adopted to the bearing analysis.

2 Previous work on eddy current reduction

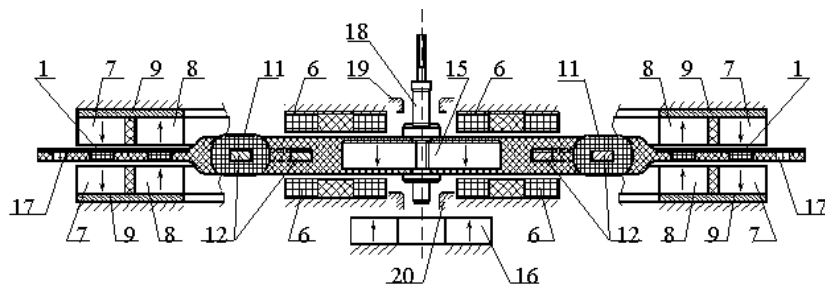
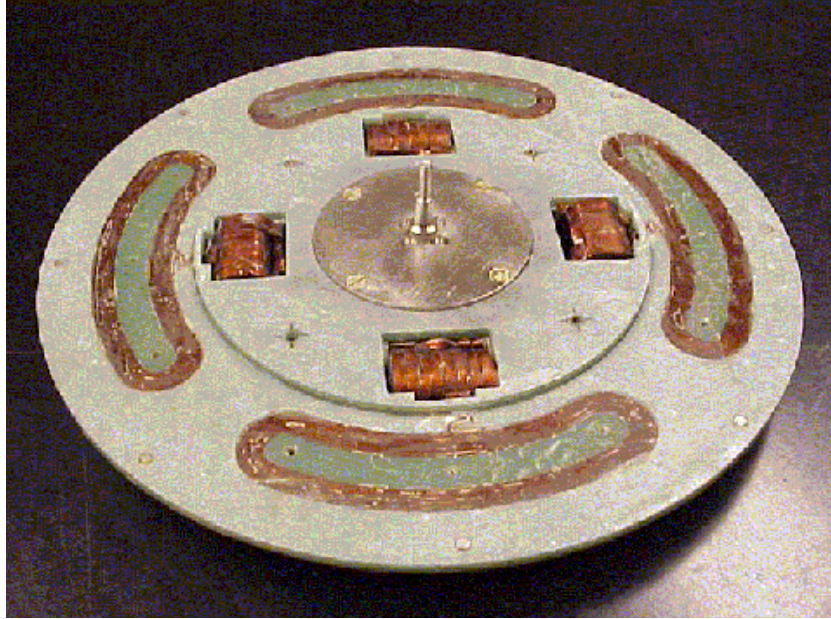


Fig. 2.6 a,b. Filatovs homopolar bearing with rotor windings.

Description:

1	Multi turn loops	11	Series inductor
6	Damping coils	12	Magnetic yoke
7	Outer stator stabilizing magnet	15	Rotor magnet
8	Inner stator stabilizing magnet	16	Lift magnet
9	Steel disc	17	Tilt protection magnets

2.3 Axial flux gyroscope stabilized bearings

Finally a few words will be said about another homopolar bearing, which is spread around the world in a toy called the “Levitron”.

The Levitron, Fig. 2.7, consists of two concentrically, but axially displaced, permanent ring magnets. The larger one is mounted in a fundament and the smaller one is rotating mounted to the spinning top.

There are no eddy currents involved in stabilizing the top. Instead gyroscopic forces and gravity stabilizes the bearing. However, stability is only achieved within a very narrow speed range. At low speed when gyroscopic forces are negligible, the Earnshaw stability criterion is applicable and the top tips around and is attracted to the other ring magnet.

At high speed the rotor is stiff compared to the available magnetic forces, so it can't tip, and thus there is no possible cross coupling that can stabilize the bearing. The problem can be said to be two dimensional, and the two dimensional form of the theorem is still applicable.

The speed range depends on the size of the magnets, but lies for the most common size between 20 and 30 rps, revolutions per second. This limits the use of the bearing, and until now the invention has not found any other use than in this fascinating toy.



Fig. 2.7. The Levitron.

3 General on eddy currents and losses in homopolar electrodynamic bearings

In Chapter 2 an overview of different methods of reducing eddy current losses in electrodynamic bearings was given. It was found that recent research on different homopolar designs represents a technological breakthrough for this kind of bearings. By introducing a rotationally symmetric magnetic flux, similar to that used in homopolar electric motors, these inventors have all shown that it is possible to reduce the induced eddy currents to a minimum, virtually to zero.

In this chapter the focus lies on general principles that will gain understanding on how heavy rotors can levitate at high speed, almost without the induction of any eddy currents. It will be shown that eddy currents can be divided into two groups; necessary and unnecessary ones. With the homopolar bearing it is possible to exclude almost all currents of the second category.

Expressed in a more scientific, almost philosophic way, the subject of this chapter is “to explain why bearing stability, due to the Earnshaw stability criterion, requires the *possibility* for eddy currents to be induced, rather than the induction of these currents itself”.

Important keys to understand are:

- why eddy currents are neither required, nor possible in concentric operation
- how eddy currents are induced in eccentric bearing operation
- how to separate bearing stiffness from bearing lift force with permanent magnets

3.1 Concentric operation

A conducting body of arbitrary shape, rotating in a rotationally symmetric magnetic field around an arbitrarily chosen pivot point, will not experience any change of flux anywhere in the body. Thus no voltage and no eddy currents are induced, since

3 General on eddy currents and losses in homopolar electrodynamic bearings

$$E = \frac{d\phi}{dt} = 0 \quad (3.1)$$

for all arbitrary closed current paths in the conducting body. This is illustrated in Fig. 3.1a where a cylindrical body is shown, but again, it should be pointed out that the rotor could have any shape, and there would still be no induced voltage in any part of the rotor.

With no currents being induced, there will be no force as well, as long as the rotor is centered. The situation is the same for fluid film bearings and ball bearings, that there is no lift force in concentric operation. But they still have losses, which the induction bearing does not have.

In concentric operation obviously the rotor position is correct, and it does not need to move away. Thus no force is required to accelerate it to another position. However, stiffness is required in order to keep the rotor concentric. But stiffness does not require force, just a force derivative. So stiffness itself does not require eddy currents to be induced when the bearing is centered. This will be further analyzed later in this chapter.

Should there be static forces involved, like gravity, this force has to be compensated for. It can be done in several ways, for instance by letting the bearing operate at a certain eccentricity, which is the normal thing to do for other bearings like conventional fluid film bearings. In an induction bearing this will induce eddy currents, as will be explained in the section on eccentric operation. Thus, electrodynamic repulsion can be used to compensate for gravity, but it will inevitably cause losses.

There does though exist a better way of compensating for gravity and other static forces than the method described above. By using magnetostatic forces instead of electrodynamic forces, the rotor is allowed to remain centered in the bearing. Magnetostatic forces from permanent magnets have the advantage that they do not require eddy currents, so this is the method to be preferred. Thus it can be concluded that eddy currents related to static forces belong to the category of unnecessary eddy currents.

Until recently it was generally thought that magnetostatic forces would destabilize the bearing and counteract the eddy current stiffness. This is not necessarily true as will be explained in Chapter 3.3, "Separation of lift force and stiffness".

There are two kinds of eddy currents that actually can be induced even when the rotor is centered. One concerns unnecessary eddy currents due to space harmonics caused by inhomogeneous magnetic materials and badly machined stator parts. The other kind of eddy currents, which is not strictly necessary,

3.2 Eccentric operation and comparison with induction generators

but highly advantageous, is damping currents that occur when the radial speed is not zero. They will be offered a special section.

3.2 Eccentric operation and comparison with induction generators

In eccentric operation, the flux as experienced by the rotor, is no longer circumferentially uniform. Thus the rotor will see a change of flux, and corresponding eddy currents will be induced. To understand the physics behind these currents it is convenient to compare the bearing with an induction generator.

Consider the bearing in Fig. 3.1b. It shows a cut through the middle pole shoe in which the axial flux from the magnets is concentrated and radially directed. The radial flux is homopolar, with the flux density B_h . When the rotor is not centered, the flux, as seen from the rotor surface, is not homogenous any more, and eddy currents are induced that repel the flux lines so that there seem to be a mirror image of the stator magnets inside the conducting cylinder. However, the imaging is very complex and phase delayed, so a 3D-FEM program to visualize and optimize the eddy current paths is required. The results from these simulations are shown in several illustrations and diagrams in Chapter 6. A simplified eddy current path is illustrated and viewed from different angles in Fig. 3.1b and Fig. 3.2a.

From Fig. 3.1b it is obvious that the homopolar bearing rotor operating in an eccentric position will have many similarities with a two pole induction generator operating at very high slip. This motivates the term induction bearing.

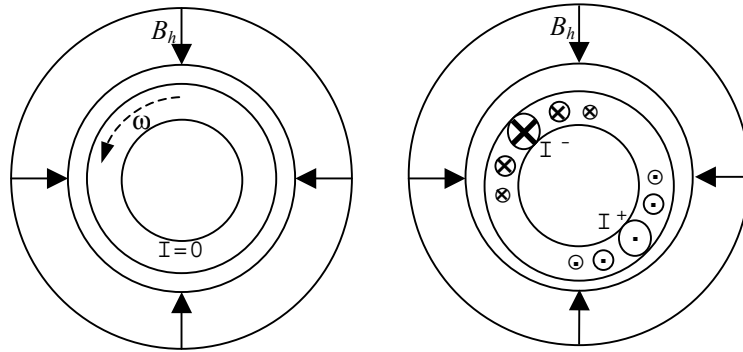


Fig. 3.1a, b. Principle of the homopolar induction bearing.

3 General on eddy currents and losses in homopolar electrodynamic bearings

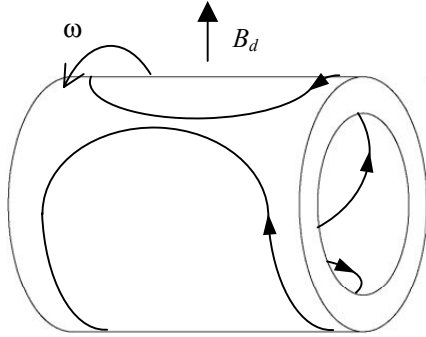


Fig. 3.2a. Perspective of the conducting cylinder in Fig. 3.1b.

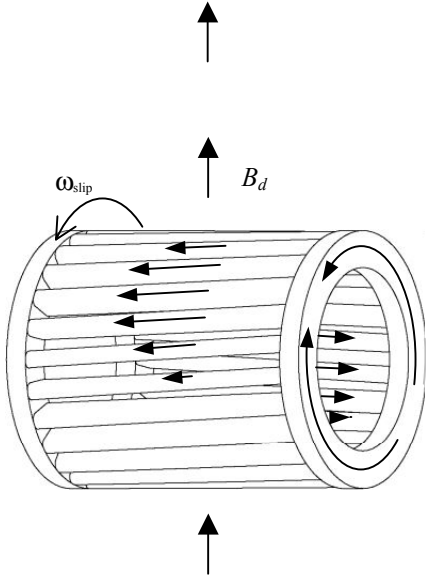


Fig. 3.2b. Comparison with an induction generator rotor cage with slip.

In Fig. 3.2a a perspective view of the conducting rotor cylinder is shown, and in Fig. 3.2b the corresponding rotor cage from an induction machine. In both Fig. 3.2a and Fig. 3.2b the rotor has been displaced downwards as in Fig. 3.1b, so that the rotor will see a diametrical two-pole flux component B_d . In Fig. 3.2a,b the homopolar flux component is removed for clarity, since it does not contribute to any eddy currents.

In induction generators the forces from the currents have two force components, one tangential drag force component F_t producing torque, and one normal component F_n producing radial force. In the cage the conductors are optimized to produce the largest possible braking torque. In the induction bearing we optimize for largest possible relation between normal force and drag force. This is illustrated in Fig. 3.3.

3.2 Eccentric operation and comparison with induction generators

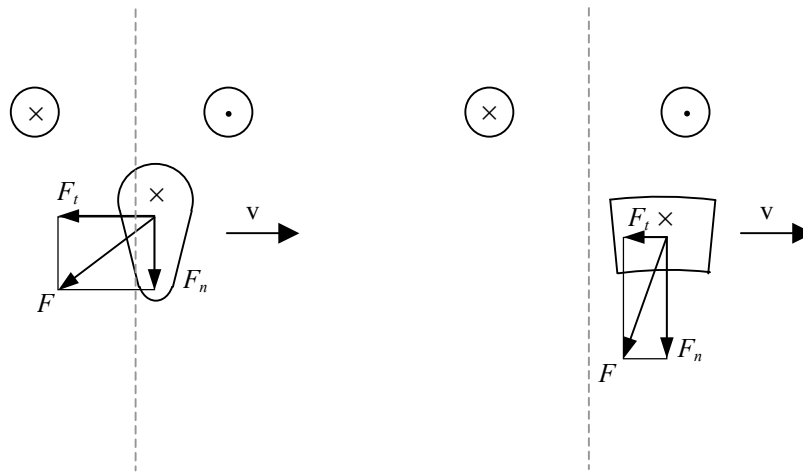


Fig. 3.3. Comparison between Lorentz's forces in an induction generator, left, and an induction bearing, right.

A few words about normal forces has to be said in this context. Fig. 3.3 left shows the normal and tangential components of the Lorentz force in an induction generator with many poles. It could as well be a linear generator. The Lorentz force is produced from the current in the rotor bar, the so-called active part of the electric circuit. To the right the same is shown for an induction bearing with many poles.

In the homopolar bearing the rotor will see only one pole, or two poles when it is not centered, as described above. The curvature of these poles is so high that the bearing is far from linear, and the direction of the forces becomes less obvious. A thorough analysis will be performed in Chapter 5.

Within the scope of this chapter, it is not necessary to understand the details about the induced currents and corresponding forces. It is only required to understand that

- Currents are not induced in concentric operation
- Currents are induced in eccentric operation and are related to the displacement
- Bearing forces are proportional to the currents
- Bearing forces consist of a normal and a perpendicular force component, where the latter is related to the bearing losses.

3.3 Separation of lift force and stiffness

There are two very important aspects of the Earnshaw theorem. The first one is referred to as the “Earnshaw stability criterion” and explains why three-dimensional stability in a magnetically suspended system requires some means of stabilization, as we have described earlier.

The second aspect is a special case of the normal formulation of the theorem, and to the knowledge of the author it has seldom or never before been referred to. Thus we will call it the “Earnshaw separation criterion”. It makes it possible to separate the stiffness from the lift force in a permanent magnet bearing, PMB.

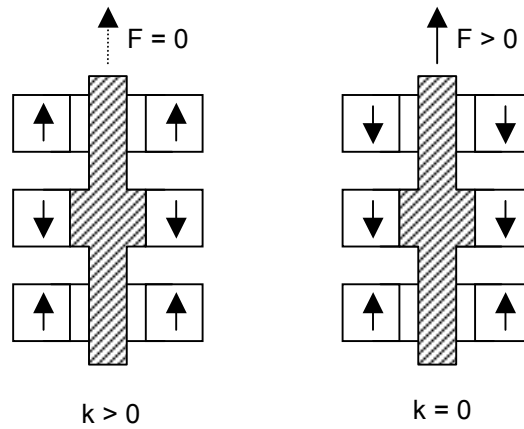


Fig. 3.4. Axial bearing to the left, and axial unloader to the right.

Fig. 3.4 shows how this can be applied to axial bearings. To the left a preloaded axial bearing is shown, and to the right a bearing with large lift force, but with no stiffness in any direction is illustrated. The bearing to the right will be denoted an unloader. Unloaders can be used to improve the load capacity of any bearing type without hazarding the stability. Thus the separation criterion can be predicted to be of great importance in the design of new machines.

If Eq. (1.1) is reduced to

$$\frac{d^2V}{dx^2} = \frac{d^2V}{dy^2} = \frac{d^2V}{dz^2} = 0 \tag{3.2}$$

3.3 Separation of lift force and stiffness

it means that we have no stiffness, neither stabilizing nor destabilizing, in any direction as long as we stay close to the working point. But we can still have a large force, that is

$$\frac{dV}{dx} \neq 0 \quad \text{or} \quad \frac{dV}{dy} \neq 0 \quad \text{or} \quad \frac{dV}{dz} \neq 0 \quad (3.3)$$

where by definition

$$\frac{dV}{dx} = -F_x \quad (3.4)$$

and

$$\frac{d^2V}{dx^2} = -k_x, \quad (3.5)$$

where F and k denotes the force and the stiffness respectively.

It is to be observed, that the stiffness is zero, while the force is non-zero. This is the opposite compared to the stability criterion where the force is zero and the stiffness in at least two directions can be chosen at will.

Thus, by combining one bearing of each kind, freely choosing the size of each, it is possible to achieve any desired combination of stiffness and lift force. In other bearing types like ball bearings this cannot be done, as in these bearings the lift force is the product of the stiffness and the eccentricity.

Take a careful look at Fig. 3.4. The two lower magnets are the same in the bearing and in the unloader. The only difference lies in the upper magnet. Thus instead of taking one bearing of each kind, as proposed above, only the upper magnet needs to be changed in order to achieve any combination of lift force and stiffness.

3 General on eddy currents and losses in homopolar electrodynamic bearings

3.4 *The principle behind zero loss bearing operation*

Based on the Earnshaw theorem and some basic knowledge on eddy current induction, it is now possible to formulate a simple but powerful principle. It explains in general words how it is possible to suspend a heavy rotor in eddy current bearings without the induction of any eddy currents at all.

§1

For any given operating point it is possible, according to the separation criterion, to compensate a static load in any direction with a counter-acting force from permanent magnets alone without the introduction of any instability.

§2

According to the Earnshaw stability criterion permanent magnets can also be used to achieve stability in all but one degree of freedom.

§3

Thus, according to the same stability criterion, a stabilizing second derivative of the magnetic energy potential is required in at least one direction, and it has to be of non- magnetostatic nature.

§4

A second derivative of an energy potential is a force derivative.

§5

Eddy currents can provide stiffness, which is a force derivative of electrodynamic nature.

§6

A force derivative does not require a non-zero force.

§7

Without force there is no need for eddy currents.

§8

Without eddy currents there are no losses.

When designing a magnetic bearing according to this principle, the bearing will not produce eddy currents until some disturbance of the system takes place that causes the rotor to move outside its operating position. All that is

3.5 A bearing without losses – is it realistic?

required is to choose an eddy current bearing that does not produce eddy currents when they are not needed. Due to the rotational symmetry of the homopolar bearing this is the ideal choice, as it cannot produce eddy currents when center positioned.

3.5 A bearing without losses – is it realistic?

In Section 3.4 it was concluded that neither stiffness nor load requires losses. It is not too far fetched to assume that a bearing without losses has been invented. However, this is unfortunately not true. There will always be some stray losses from magnet imperfections and air drag. Even in ultra high vacuum there are some air drag losses that can't be eliminated.

Furthermore the rotation of the earth will cause gyroscopic effects that have to be dealt with, most methods causing small but nonzero losses.

Nevertheless, the invention of different kinds of homopolar bearings definitely contributes to a large scientific step towards the ultimate lossless bearing. It is very difficult to imagine a bearing principle with less losses at high speed than the homopolar bearing, even worse to make an industrial product of it. Reports with superconducting bearings for example, sometimes show impressive spin down curves, but one has to remember that cooling of the bearings is rather energy demanding.

4 Design of the radial flux homopolar induction bearing

Magnetic bearings differ much from conventional bearings like ball bearings, and it is important to define the purpose of the bearing before dimensioning it, otherwise heavily over dimensioned bearing designs may result. As was found from the previous chapter, an optimal combination of magnetostatic forces and electrodynamic forces can be achieved in every load situation. Since the calculation of magnetostatic forces in permanent magnet bearings has been described by Lang [25] and others, the following sections will be devoted entirely to the induction bearing and to electrodynamic forces.

4.1 General comments on electrodynamic bearing design

Suppose that the passive bearings and unloaders have already been designed. Then the purpose of the induction bearing is to:

- provide enough radial stiffness and damping to achieve rotor-dynamic stability within a certain and predefined speed range,
- provide enough radial restoring forces when not centered to compensate for dynamic load.

The bearing does generally NOT need to:

- provide any static force when centered, since the permanent magnet unloader is better suited for this purpose,
- compensate for any unbalance force, since it is often better to let the rotor rotate around its mass center than to compensate with large radial forces to keep it in its geometric center,
- provide axial stiffness.

In Appendix 1 some simple hands on rules are given that are useful when designing a new induction bearing. These rules are based on the analysis in Chapters 5 and 6.

4 Design of the radial flux homopolar induction bearing

4.2 Bearing description and drawings

The geometry of an induction bearing is comparatively simple. All parts are rotationally symmetric, including the magnets. Fig. 4.1 shows a cut through a “real” induction bearing for spindles. The picture is a photo realistic image generated using 3D-CAD.

The four axially oriented magnets generate the magnetic flux. The number of magnets can be optimized for the appropriate stiffness. Between the magnets iron washers, which we will denote intermediate pole shoes, are placed to concentrate the flux and change the direction so as to create a radial flux penetrating the conducting cylinder.

The radial flux causes eddy currents to be induced in the conducting and nonmagnetic rotor when it rotates in a non-centered position. Also the shaft, which is inserted into the conducting cylinder, is preferably made from a conducting and non-magnetic material, but it is not a demand.

The ferromagnetic end plates have a slightly different shape than the intermediate pole shoes, but in the analysis a somewhat simplified shape will be used, as in Fig. 4.2. Their purpose is to avoid leakage flux and to increase the inductance of the magnetic circuit.

The housing is made of non-magnetic material in order not to short circuit the magnetic flux.

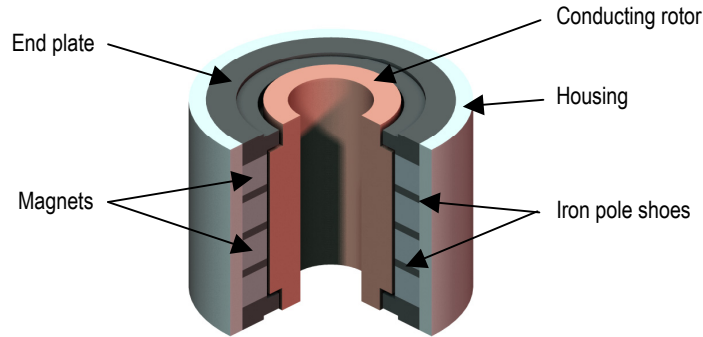


Fig. 4.1. Description of the homopolar induction bearing.

4.2.1 Inner rotor bearing for spindles and turbines

Fig. 4.2 shows a principle drawing of an inner rotor induction bearing with two magnets. Compare with the bearing in Fig. 4.1 that has four magnets. The term inner rotor is used when the rotor spins inside the bearing stator. Other rotor alternatives are found in the following subsections.

One difference from Fig. 4.1 is the shape of the end plates. Fig. 4.2 shows how they are normally modeled in the FEM software. The thickness of the end plate is l_w while the thickness of the intermediate pole shoes, or washers, is $2l_w$. Note also that the outer diameter of the washers normally is less than the diameter of the magnets. This is to prevent too much leakage flux penetrating the housing, where it does not contribute to bearing stiffness.

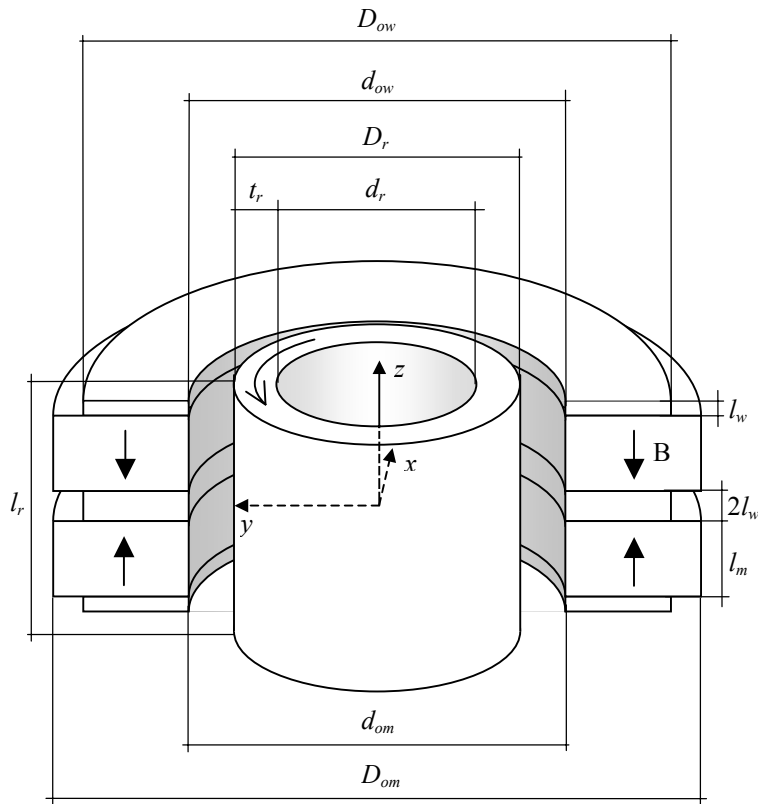


Fig. 4.2. Spindle bearing nomenclature.

4 Design of the radial flux homopolar induction bearing

The thickness of the copper tube is chosen with regard to the skin depth. Once the speed range has been determined, the thickness t_r has to be at least one skin depth calculated for the lowest operating speed, ω_{\min} .

$$t_r \equiv \frac{D_r - d_r}{2} \geq \delta_{skin}^{\max}$$

where

$$\delta_{skin}^{\max} = \sqrt{\frac{2}{\omega_{\min} \sigma \mu_0}}$$

The length of the cylinder, l_r , has a large influence on the end effect currents and is analyzed in Chapter 6. It turns out that there are two good solutions; either the rotor should be slightly shorter, or much longer than the stator.

The magnetic length, or thickness, of the magnets, l_m , affects the speed range of the bearing. Thick magnets are used for low speed operation, as will be shown in the analysis.

Magnet width, w_m , defined by $w_m = (D_{om} - d_{om}) / 2$, influences the radial flux density in the airgap which in turn has a quadratic effect on stiffness. Since magnets are expensive, an important task in Chapter 6 will be to optimize stiffness with regard to the amount of magnet material.

If the shaft is hollow, magnets can be placed inside the rotor as well. In the following subsections we will describe two other types of induction bearings, both using magnets on the inside of the shaft.

To distinguish magnets outside the rotor from magnets inside, the index “*om*” will be used for outer magnets, while the index “*im*” will be used for inner magnets.

Outer rotor bearings are used with outer rotor motors and are specially suited for flywheel applications, Fig. 1.3. Thus henceforth they will be referred to as flywheel bearings. In an outer rotor design the rotor spins outside the stator, which has several rotor dynamic advantages. Also the leakage flux from the bearing magnets is reduced, making the bearing cheaper since less material is required.

The most powerful bearing is a combination of the above. Placing magnets both on the inside and on the outside of the rotor cylinder approximately doubles the bearing stiffness. Such bearings are denoted intermediate bearings.

4.2.2 Outer rotor bearing for flywheels

Applications like the flywheel in Fig. 1.3 and the double flow expander in Fig. 1.4 require an inside out motor/generator concept. Fig. 7.2a,b shows the motor developed during the project. It is referred to as an outer rotor motor. An outer rotor bearing, or flywheel bearing, designed for this purpose is shown in Fig. 4.3.

The main difference compared to the spindle bearing in Fig. 4.2 is that the diameters of the iron washers between the magnets are changed to reduce the leakage flux on the inside of the stator magnets.

A mechanical advantage with outer rotor arrangements is that the carbon fiber bandage required to prevent the conducting cylinder from exploding at very high speed does not interfere with the magnetic flux in the air gap.

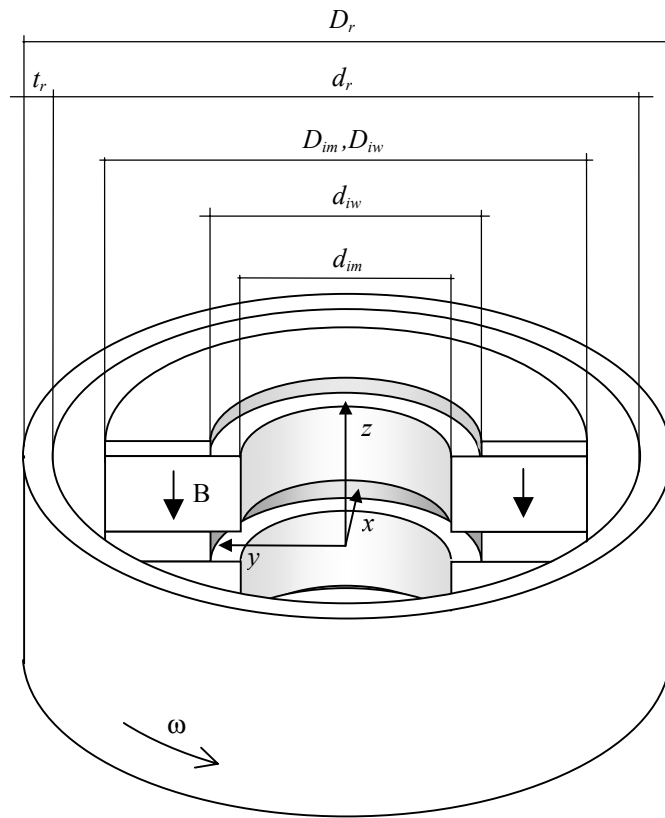


Fig. 4.3. Flywheel bearing nomenclature.

4 Design of the radial flux homopolar induction bearing

4.2.3 Intermediate rotor bearing for hollow shafts and pumps

In some applications like turbomolecular pumps it is advantageous to use a thin walled hollow shaft. Such a shaft enables fast acceleration, large pumping surface and small gyroscopic effects.

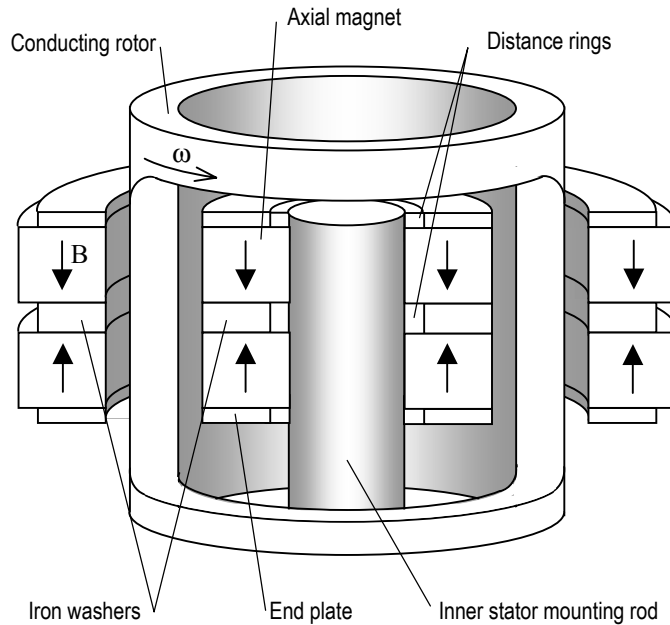


Fig. 4.4. Description of the intermediate rotor bearing.

The bearing is shown in Fig. 4.4. It should be noted that the nomenclature is the same as for the previous two bearing types. This bearing comprises both bearings, contains twice as many magnets and has approximately double the stiffness.

An interesting aspect is the inductance, which is about twice as large as for the other bearing types. This means that losses are not twice as high as the other bearings, as will be seen in the analyses presented in the following chapters. Thus, this bearing is clearly the best choice, if the design permits this kind of rotor.

4.3 Auxiliary bearings

During start up and landing induction bearings does not provide enough restoring forces to keep the rotor centered. Thus some form of auxiliary bearings are needed, sometimes called “landing bearings” or “touch down bearings”.

Normally the induction bearing have integrated unloading bearings, so the resulting force acting on the landing bearings is virtually zero. However, in all kinds of magnetic bearings there is always a risk for whirl whenever a touch down bearing contact occurs. A fully developed whirl will cause very large radial forces. Thus careful considerations must be taken in order to adjust damping and geometry of the landing bearings so as to prevent this motion.

The author [5] has, during earlier tests of heteropolar induction bearings, successfully used rubber mounted PTFE bushings as landing bearings. Correctly tuned no whirl is introduced, and thus no radial forces are apparent. As wear is proportional to the product of surface speed and the normal component of force, this means that wear is very low.

An interesting alternative to landing bearings is to have bearings in continuous operation, like airfoil bearings. They can provide damping and shock absorption and contribute to rotordynamics in a better way than seldomly used landing bearings. At the same time the induction bearings reduces the take off speed of the foil bearing, the latter normally referred to as a great drawback when foil bearings are used alone. This bearing combination is ideal for applications where vibrations and heavy shocks are likely to occur like in vacuum cleaners. When airfoil bearings are mounted in the airgap of an induction bearing [27], there are two benefits: firstly they gain damping, since they operate in a strong stationary magnetic field, and secondly they add positioning accuracy to the rotor since it is mounted concentrically to the bearing.

The induction bearing can also be used in a vacuum environment, thus allowing for very high-speed operation like in flywheels and gyroscopes. In this case air bearings are not used. Instead coated plain bearings, with or without a centrifugal clutch, are more appropriate.

5 Bearing analysis

In the following sections analytical expressions for bearing forces and losses, as well as stiffness- and damping coefficients, will be derived, and will be compared to results from the computer simulations in Chapter 6. Finally the equations of motion will be derived, in order to study system dynamics and stability. The analysis is applicable to bearings with at least two rows of magnets, and to bearings with, as well as without, pole shoes.

5.1 Purpose of the analysis

A magnetic bearing is an advanced machine element and is to be applied by machine engineers. However, the analysis of the bearing is more like the analysis of an electrical machine. Thus an important goal of this analysis is to convert the electromagnetic properties of the bearing into useful mechanical and rotordynamic data.

Table 5.1. List of electrical bearing properties and their related mechanical ones.

Electrical properties	Mechanical properties
Induced voltage	Speed, rotational and lateral
Current	Force
Current space gradient	Stiffness, damping
Resistance	Losses
Phase lag	Force angle, cross coupling
Demagnetization	Lifetime

5.2 Analytical method

The analysis will be performed in the following way:

1. First the magnetic circuit is investigated, without any rotating electric conductor, to find an expression for the space gradient of the flux density, $\partial B_r / \partial \rho$, for the three different bearing types described in Chapter 4.
2. Then the conducting cylinder, to which one rotating and one translating coordinate system are fixed, is introduced into the airgap,

5 Bearing analysis

and the flux density time derivative in the rotating frame, $\partial\tilde{B}_r/\partial t$, is calculated around the rotor surface.

3. Now the shapes of the eddy current paths have to be found. From the flux density change, the induced voltage $\tilde{E}(t)$ around an arbitrary eddy current path of area A can be calculated by integration as

$$\tilde{E}(t) = \frac{\partial\tilde{\Phi}_r(t)}{\partial t} = \iint_A \frac{\partial\tilde{B}_r(t)}{\partial t} dA.$$

Finding the areas A that maximizes the amplitude of the induced voltage, to a great extent facilitates the search for the main eddy current circuits. However, since an infinite number of paths are possible, some initial help from 3D-FEM simulations will help to find the main pattern.

4. Once the shape of the eddy current paths are known, the resistance R can be calculated. This also requires an estimation of the skin depth, which has to be analyzed separately.
5. When the shapes of the eddy current paths are known, the magnetic circuits and their corresponding reluctance models have to be found in order to calculate the inductance L .
6. Using the resistance and the inductance, the currents in the rotating frame can be found from the induced voltage $\tilde{E}(t)$ as

$$\tilde{i}(t) = \hat{i} \sin(\omega t - \varphi) = \frac{\tilde{E}(t)}{R + j\omega L}$$

7. The currents can now be transformed to the non-rotating frame, where they appear to be fixed in space and constant, for each given set of eccentricity and lateral velocity. Using the phasor notation [22] one can write

$$\tilde{i}(t) \rightarrow \vec{I}(\varphi)$$

8. The bearing force is achieved by calculating the Lorenz force, which can be found by integration in the non-rotating frame over the conducting cylinder volume V_{cyl} ,

$$\bar{F} = \iiint_{V_{cyl}} (\bar{J} \times \bar{B}) dV$$

9. The bearing losses equal the Ohmic losses, which can be calculated from the currents and the resistance.
10. From the bearing force derivatives, the stiffness and damping coefficients can be derived.
11. A stability analysis can now be performed using the coefficients above.
12. Finally, the equations of motion have been formulated in a general way so that engineers can simulate the dynamic behavior of their own different applications.

In Chapter 6 the 3D-FEM analysis has been performed, and in Chapter 8 experimental data are obtained. These values are compared to the analytical results, and possible deviations are discussed.

5.3 Magnetic circuit

The magnetic circuit from the permanent magnet rings is illustrated in Fig. 5.1, where the stator magnets and pole shoes are shown for an inner rotor bearing. The rotor, which is non-magnetic, is not shown. Since the bearing is homopolar, it is convenient to introduce cylindrical coordinates. In Fig. 5.2 the radial flux component is plotted schematically versus cylinder coordinate ρ_0 at $z=0$, where the subscript 0 indicates that it is a stator fixed coordinate system.

The axial magnetic flux density B from the magnets is concentrated in the pole shoes and leaves the pole shoe inner and outer surface in radial direction. To avoid too much leakage on the outside, the diameter of the iron pole shoe can be reduced as in Fig. 5.1. For the analysis the radial flux B_r will be defined positive in positive ρ_0 -direction. The analysis will first be performed for an inner rotor bearing, and then for the other two types of bearings.

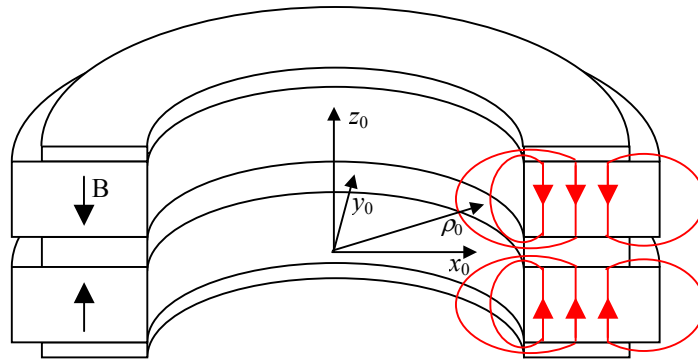


Fig. 5.1. Magnetic circuit.

5.3.1 Magnetic circuit of an inner rotor bearing

Consider Fig. 5.2a. The radial air gap flux density B_r has its maximum absolute value $B_0 = |B_r|$ at the inner surface of the pole shoe at $\rho_0 = d_{om}/2$,

and it approaches zero towards the center of the stator, where it finally vanishes.

Since the cylinder has a limited wall thickness t_r we can only use a limited volume of the magnetic flux. The operating interval $\Delta\rho_{op}$ is defined by

$$\Delta\rho_{op} = t_r + 2g_a \quad (5.1)$$

where g_a is the available airgap defined by

$$g_a = g - g_e. \quad (5.2)$$

Here g_e is the emergency airgap required by the emergency bearing. Normally the emergency bearing clearance is set to half the airgap, thus Eq. (5.1) becomes

$$\Delta\rho_{op} = t_r + g$$

One of the most important quantities when calculating eddy currents is the radial flux gradient $\delta B_r / \delta\rho_0$.

Since $\Delta\rho_{op}$ is small compared to the inner diameter of the magnet, d_{om} , we will assume that the flux gradient is linear in this region. Thus the expression becomes

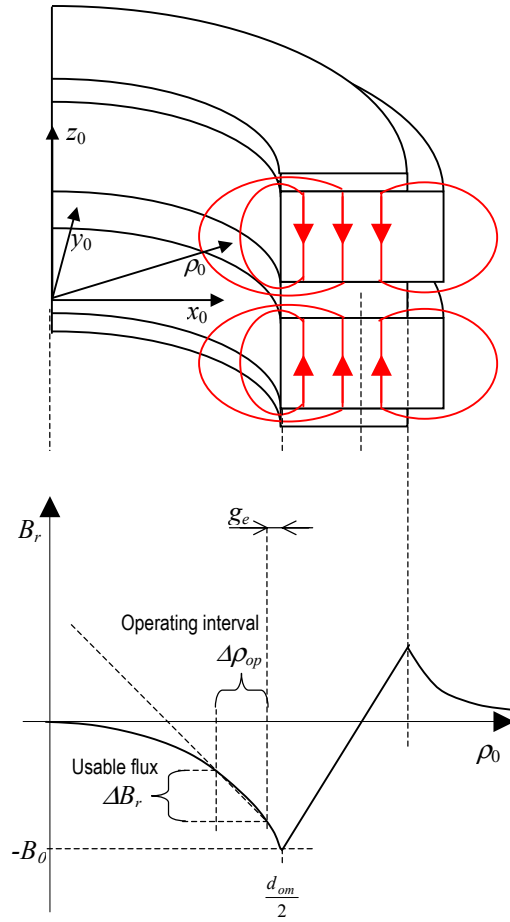


Fig. 5.2a. Radial flux density distribution. Inner rotor bearing.

5 Bearing analysis

$$\frac{\delta B_r(\rho_0)}{\delta \rho_0} \approx \frac{\Delta B_r(\rho_0)}{\Delta \rho_{op}} = \frac{B_r\left(\frac{d_{om}}{2} - \Delta \rho_{op} - g_e\right) - B_r\left(\frac{d_{om}}{2} - g_e\right)}{t_r + 2g_a}. \quad (5.3)$$

5.3.2 Magnetic circuit of an outer rotor bearing

The analysis of an outer rotor bearing is basically identical to an inner rotor bearing, with the difference that the rotor is on the outside of the magnet, and that the flux in that region is positive, given the magnets having the same orientation. There is another difference as well. The leakage flux this time occurs at the inner diameter of the magnet. Thus the utilization of the total flux, and thus also of the magnets, is better in the outer rotor case.

However, since the value of the flux density, $B_r(\rho_0)$, is either measured or taken from the FEM software rather than from a reluctance model, there is no real difference in the analytical part between the bearing types. Thus the flux density change becomes

$$\frac{\delta B_r(\rho_0)}{\delta \rho_0} \approx \frac{\Delta B_r(\rho_0)}{\Delta \rho_{op}} = \frac{B_r\left(\frac{D_{im}}{2} + g_e\right) - B_r\left(\frac{D_{im}}{2} + \Delta \rho_{op} + g_e\right)}{t_r + 2g_a}. \quad (5.4)$$

Concerning leakage flux it is worth noting that it is possible to eliminate leakage flux almost completely, as described in Chapter 6, using radial magnets. But such magnets are still considerably more expensive than axially magnetized ones, and their use is not yet to be regarded as a viable solution for mass production.

5.3.3 Magnetic circuit of an intermediate rotor bearing

For the intermediate bearing described in Fig. 4.4, any of Eq. (5.3) and (5.4) can be used, since an intermediate rotor bearing can be said to consist of both an outer and an inner rotor bearing. However, due to symmetry it is possible to simplify the analysis for the case of the intermediate rotor bearing.

Consider Fig. 5.2b where the radial flux density of the bearing is shown. The inner and outer magnets help each other to linearize the flux in the whole airgap. The flux gradient can be derived directly from Fig. 5.2b, and is found to be

$$\frac{\delta B_r(\rho_0)}{\delta \rho_0} \approx \frac{\Delta B_r(\rho_0)}{\Delta \rho_0} = \frac{-2B_0}{t_r + 2g}, \quad (5.5)$$

where the total airgap g has been used instead of the available airgap used in Eq. (5.3) and (5.4). Whenever in doubt though, on whether the flux really is linear or not, the latter equations should be used.

The gradient is higher for this bearing than for the other bearings, since the null radial flux limit lies approximately in the middle between the magnets. However, it should be noted that for the intermediate bearing, B_0 is lower than for the other two bearing types, because the repulsive poles weaken the flux to some extent, so the flux gradient is not double as high as one might think.

Until now the radial flux and its gradients have been studied. They are of importance in determining the induced voltages. The axial flux plays a different role, and is of importance to the bearing forces. To generalize, the flux is axial in the magnets, and in the airgap besides the magnets.

In the intermediate bearing the flux lines are compressed between the magnets so that the axial flux is basically parallel to the magnets, but for the inner and outer rotor bearings, the flux more resembles the shape of half circles, as shown in Fig. 5.2a.

The axial flux will be studied later in more detail when it comes to bearing forces.

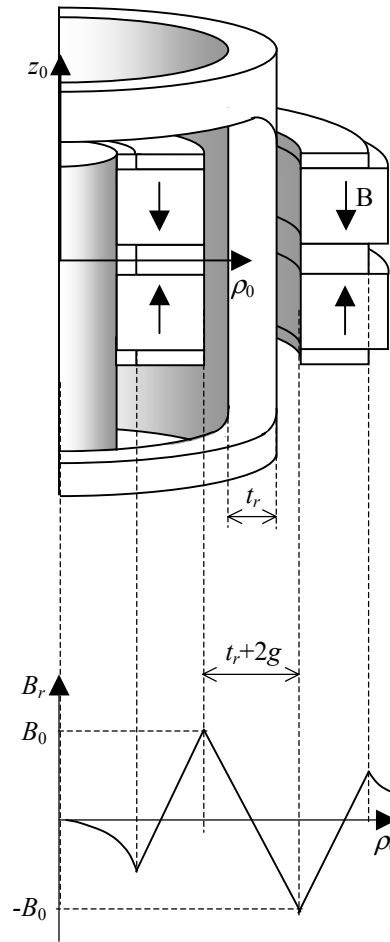


Fig.5.2b. Radial flux density. Intermediate rotor bearing.

5.4 Eddy current circuits

Previously the magnetic circuit has been analyzed with special emphasis on the radial flux gradients in the airgap. The conducting rotor will now be introduced into the airgap, and the eddy current paths will be identified and analyzed. As already stated, eddy currents are induced in a conductor only when an arbitrary conductor area experiences a change of flux. Thus for a conductor rotating or moving in a homopolar stationary field, a necessary but not sufficient condition for such a change of flux to exist, is that at least one of the following sub conditions are met:

- 1 The conductor spins about an axis, which is not concentric with the center of the homopolar flux.
- 2 The conductor moves about any of its remaining five degrees of freedom.

In reality, perfectly homopolar magnets cannot be manufactured, so it is apt to add a third sub condition to the list:

- 3 The magnets experience various kinds of mechanical or magnetic inhomogeneities.

It may seem unclear why this is not sufficient for a change of flux to appear, but as will be shown below, sub condition 1 and 2 may interact in such a way as to produce no net change of flux.

In the following paragraphs, eddy currents resulting from these flux changes will be analyzed in detail.

5.4.1 Eddy currents induced due to eccentricity

In this chapter eddy currents induced by eccentric operation will be studied. These currents are related to the bearing load, and are responsible for bearing properties like stiffness and cross coupling stiffness.

For the analysis it will be assumed that the center of the homopolar flux coincides with the bearing center, and that the lateral motion of the rotor is zero. Further, the magnets will be assumed to be homogenous and perfectly circular.

Let's first study the case when the rotor is centered, as in Fig. 5.4a. On the conducting cylinder surface there are no points that can see any change in flux density as it rotates in the homogenous magnetic field. Thus according to

5.4 Eddy current circuits

Lenz’s law no voltage is induced in the conductor anywhere. Consequently no eddy current path exists over which there is any induced EMF, and so no currents will be induced. This is true regardless of rotor shape. It does not need to be circular, but in the analysis it will be assumed to be so in order to find simple expression for the resistance.

Now consider sub condition 1 above. In Fig. 5.4b the rotor is displaced downwards in the negative y-direction and the corresponding eddy currents are shown in Fig. 5.4d. A perspective view is given in Fig. 5.3. In order to improve the viewing angle the coordinate system has been turned so that the y-axis points to the left. Accordingly, the rotor is displaced to the right. A perspective view of the bearing and the currents are shown in Fig. 5.6a,b.

Since the shape of the eddy currents by no means is obvious, we shall analyze them a bit further. Before doing so we need to introduce a coordinate frame $x_l y_l z_l$ translated in the xy plane by the vector $\Delta \vec{r}_0$, Fig. 5.3. We also need a rotating coordinate frame $x_r y_r z_r$ fixed to the rotor in which we will calculate the eddy currents. The angle between x_l and x_r is ωt . For convenience we introduce a second cylindrical coordinate frame $\rho \phi z_l$ where ϕ is defined as the positive angle between x_l and $\bar{\rho}$.

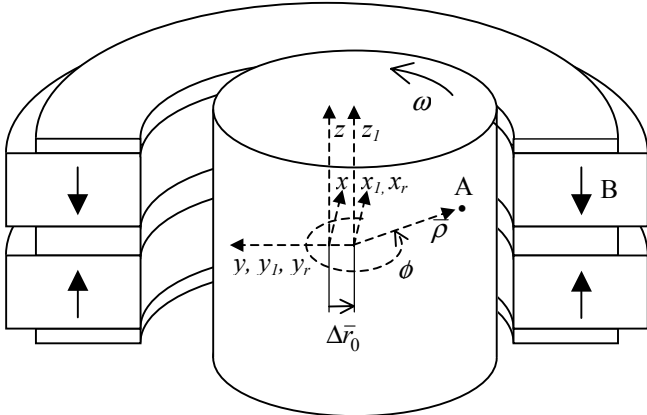


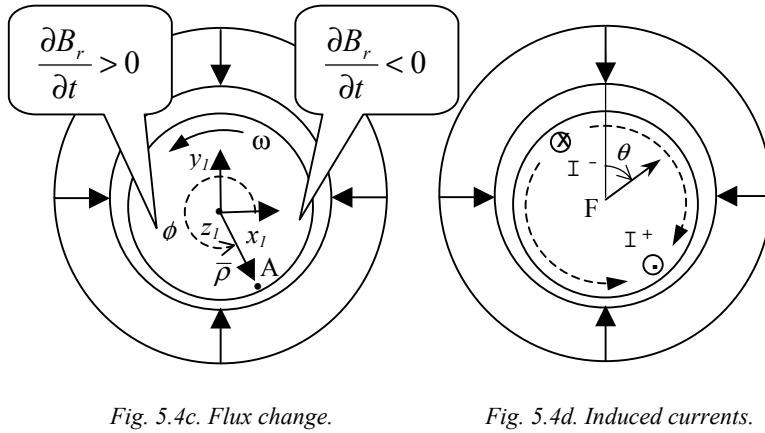
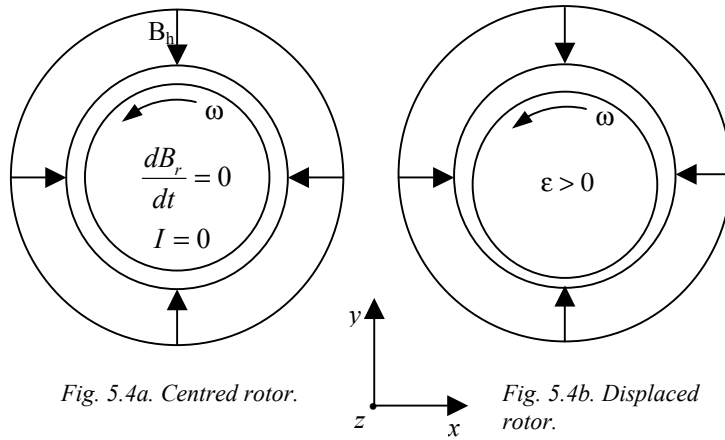
Fig. 5.3. Definition of coordinate systems at time $\omega t=0$.

5 Bearing analysis

Now let us focus on point A in Fig. 5.4c, which is spinning around axis z_1 at speed ω . When the rotor is not centered, point A on the rotor surface will experience not only the homopolar flux, but also a superposed diametrical two-pole flux. Point A will thus see an almost sinusoidal flux with a constant bias.

To find the eddy current amplitude and phase we need to know the time derivatives of the normal flux penetrating the surface. Let us first make a few simplifications concerning the eccentric motion of point A.

Assume a position for point A so that $\phi = 0$ at time $t = 0$. Also assume a certain displacement Δr_o in the negative y-direction. At this instance of time the position of A expressed in the stator coordinate system xyz is $(\rho, -\Delta r_o, 0)$.



Since $|\Delta\bar{r}_0| \ll |\bar{\rho}|$ we can assume that $|\bar{r}| \approx |\bar{\rho}|$ for $\omega t = 0$ and $\omega t = \pi$.

With the simplification above we can write the radial position for point A as it spins around axis z_l as

$$|\bar{r}| \approx |\bar{\rho}| - |\Delta\bar{r}_0| \sin(\omega t) \quad (5.6)$$

or

$$r \approx \rho - \Delta r_0 \sin(\omega t) \quad (5.7)$$

Now the time derivative in point A of the flux from an intermediate bearing, using Eq. (5.5) and (5.7) is

$$\frac{\partial B_r}{\partial t} = \frac{\partial B_r}{\partial r} \cdot \frac{\partial r}{\partial t} \approx \frac{-2B_0}{t_r + 2g} \cdot \frac{\partial(\rho - \Delta r_0 \sin(\omega t))}{\partial t} = \omega \Delta r_0 \frac{2B_0}{t_r + 2g} \cos(\omega t) \quad (5.8)$$

For a given time t_0 the radial speed $\partial r / \partial t$ varies sinusoidally around the rotor perimeter of the cylinder, so an expression valid for all points around the rotor has the form

$$\frac{\partial B_r}{\partial t} \approx \omega \Delta r_0 \frac{2B_0}{t_r + 2g} \cos(\omega t_0 + \psi) \quad (5.9)$$

where ψ is the angle in the rotating coordinate frame between axis x_r and the point in question. Fig. 5.5 shows the radial (normal) flux versus ψ around the

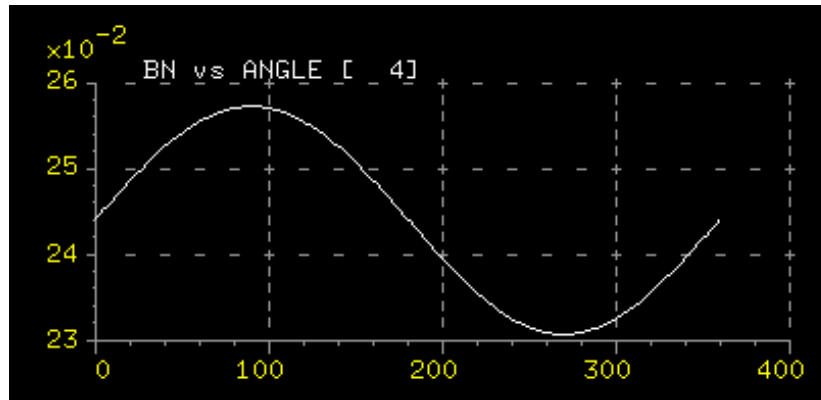


Fig. 5.5. Air gap radial flux density penetrating the rotor surface.

5 Bearing analysis

rotor surface for a given time $t_0 = 0$. It is calculated using the 3D-FEM software Mega, a program that will be used frequently in Chapter 6. The normal flux B_n in Fig. 5.5 penetrating the inner rotor surface can be found by integrating (5.9) and setting the integration constant equal to the homopolar flux component, B_h , which in this case is 244 mT. Thus

$$B_n = B_r = \int \frac{\partial B_r(t)}{\partial t} dt = \Delta r_0 \frac{2B_0}{t_r + 2g} \sin(\omega t_0 + \psi) + B_h.$$

Where the homopolar flux component on the surface of the rotor is given by

$$|B_h| = B_0 \left(1 - \frac{2g}{t_r + 2g}\right)$$

where the sign is positive for the inner surface of the rotor, and negative for the outer. These two equations are shown for a general understanding only, and will not be used more. For the induced voltage only the time derivative in (5.9) is important. The flux itself is significant only for the generation of forces, and then particularly the axial flux, not so much the radial one.

In Chapter 3 the induction bearing was compared to the induction generator due to their obvious geometrical similarities. Thus the induction bearing rotor will behave as a 2-pole induction rotor made up of an infinite number of bars (see Fig. 3.2a,b) with a dc-current applied to the stator winding. For simplicity, the calculation of the axial eddy current i_z (rotor bar currents) can be performed assuming that the current paths is concentrated to four rotor bars, (two for each eddy current circuit,) connected at each end to short-circuit rings. Since the model is reduced to 4 bars, this simplification means that the axial bar currents i_z equals the tangential short circuit current i_{sc} , which will also be denoted i_r . Thus

$$i = i_z = i_{sc}.$$

To confirm that this model is appropriate, several 3D-FEM models were made, some of them shown in Chapter 6. Generally, the current paths, specially the bar currents, are more rounded than is possible in a squirrel cage. The rounded “real” current paths are shown in Fig. 5.6a,b, and in the analysis a compromise will be used, which is shown in detail in Fig.5.10a,b, in which the short circuit rings, region 1 and 2_s, and the bars, region 3, are straight, while the corners are rounded, region 2_c.

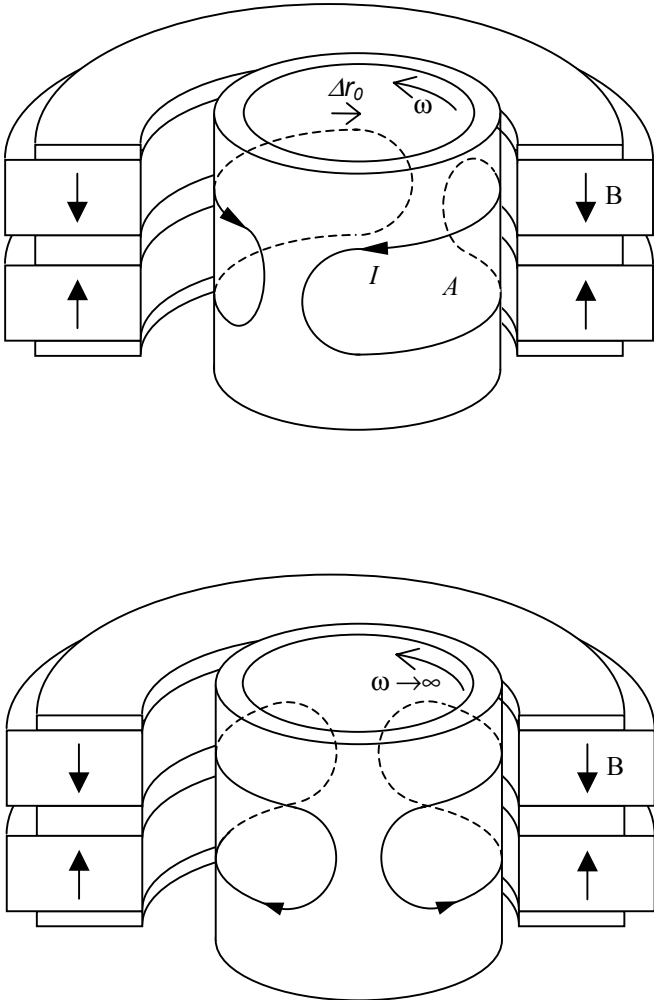


Fig. 5.6a,b. Restoring eddy current circuits.

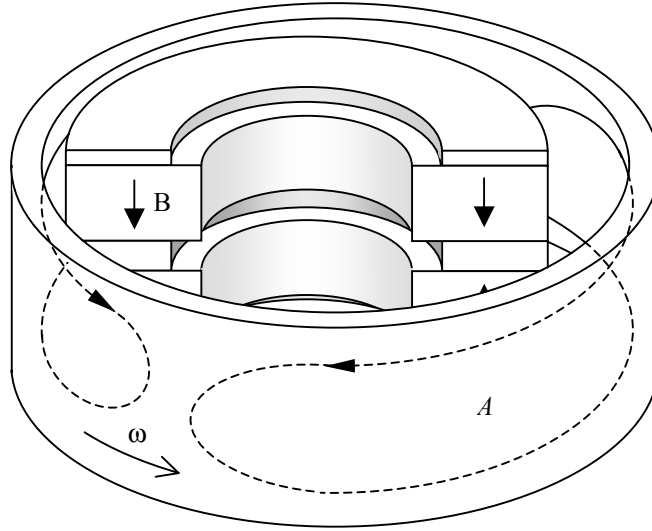


Fig. 5.7. Eddy currents in a flywheel bearing.

The eddy current paths encircle the area A , Fig. 5.6a and 5.7 above, and the current amplitude i depends on the flux change across this area as

$$i = \frac{E}{R + j\omega L} = \frac{\partial \Phi_r / \partial t}{R + j\omega L} = \frac{1}{R + j\omega L} \iint_A \frac{\partial B_r}{\partial t} dA \quad (5.10)$$

where E is the induced voltage, and R and L are the resistance and the inductance of the whole eddy current circuit. The influence on these variables will now be analyzed one by one in the following subchapters. However, since these chapters are very interdependent, and since the shape of the eddy current paths depend on all of these variables, there will be a lot of cross references between the chapters. To make things even more complicated, there are many different cases. The bearings have different numbers and configurations of magnets, and they are analyzed with or without pole shoes.

5.4.1.1 Induced voltage

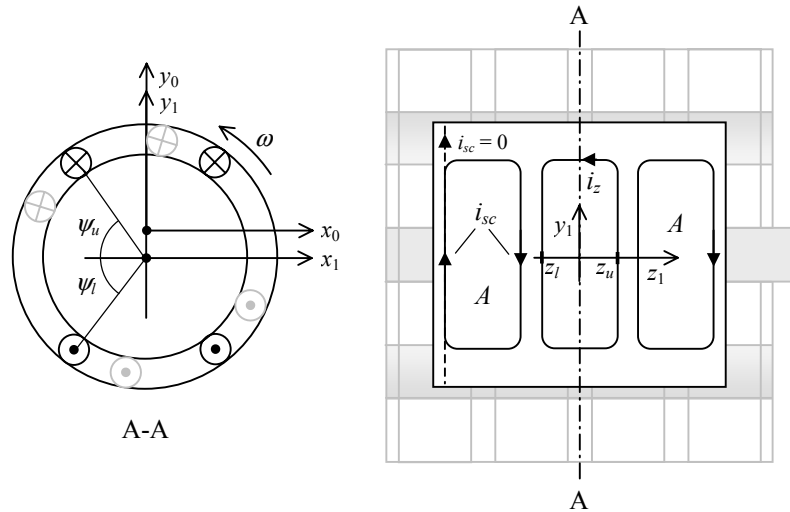


Fig. 5.8. Definition of integration limits for the calculation of flux change within the area A . The black currents to the left shows the bar position for maximum voltage, and the grey currents show the position for maximum current.

To calculate the induced voltage, the eddy current path has to be defined. Since they are not yet known in detail, they have to be defined in terms of variables to be determined later. The variables are defined in Fig. 5.8, where a 4-row intermediate rotor bearing with three identical eddy current paths is shown. The rotor is rotating and is displaced in the negative y -direction, giving rise to induced voltages and currents. To the right the short-circuit currents and bar currents are displayed. To the left the four bars in the model are displayed for two different positions. The black bars show the position for maximum induced voltage, and the bars in gray show the same bars in the position for maximum current. Since the voltage is to be studied, the focus will be on the black bars and the area A .

The area A is defined inside each circuit, and it is limited in axial direction by the upper and lower integration variables z_u and z_l , shown to the right, and in tangential direction by the upper and lower angular integration variables ψ_u and ψ_l . The latter are shown to the left.

Using the expression from Eq. (5.9) for the flux density change, the integral for the time t_0 is found to be

5 Bearing analysis

$$\begin{aligned}
 E &= \iint_A \frac{\partial B_r}{\partial t} dA = \int_{z_l}^{z_u} \int_{\psi_l}^{\psi_u} \frac{\partial B_r}{\partial t} r d\psi dz = 2l_w \int_{\psi_l}^{\psi_u} \frac{\partial B_r}{\partial t} r d\psi = \\
 &= 2\omega\Delta r_0 \frac{2l_w}{t_r + 2g} \int_{\psi_l}^{\psi_u} B_0 \cos(\omega t_0 + \psi) r d\psi
 \end{aligned} \tag{5.11}$$

where the integration boundaries comes from the eddy current path shown in Fig. 5.8a,b. Observe that the result from the integration of the z-coordinate equals the pole width $2l_w$, which is less than the integration boundaries $z_u - z_l$ since there is no radial flux outside the pole.

The upper and lower angular integration limits ψ_u and ψ_l depend on the width of the axial eddy current path, the rotor bars. The latter is investigated in the next section, and is illustrated in Fig. 5.10a,b, in which the bars are referred to as "region 3" and the width of the bars is denoted w_3 .

Using w_3 the integration limits ψ_u and ψ_l can be derived from Fig. 5.8 left. The width w_3 [m] expressed in angular coordinates is w_3/r [rad]. Thus

$$\psi_u = \frac{\pi}{2} - \frac{w_3/2}{r} = \frac{\pi}{2} - \frac{r/\pi}{r} = \frac{\pi}{2} - \frac{1}{\pi}$$

and

$$\psi_l = -\frac{\pi}{2} + \frac{w_3/2}{r} = \dots = -\frac{\pi}{2} + \frac{1}{\pi}.$$

The integral in Eq. (5.11) has its maximum value for $t_0 = 0$, so evaluating the integral for $t_0 = 0$, using the integration limits above results in the amplitude of the induced voltage

$$\hat{E} = \omega\Delta r_0 \frac{8l_w r B_0 \cos\left(\frac{1}{\pi}\right)}{(t_r + 2g)} \tag{5.12}$$

Inserting it into Eq. (5.10) results in the current amplitude

$$\hat{i}_z = \omega \Delta r_0 \frac{8l_w r B_0 \cos\left(\frac{1}{\pi}\right)}{(t_r + 2g)\sqrt{R^2 + (\omega L)^2}} \quad (5.13)$$

In literature on rotordynamics [17] the radial displacement Δr_0 is often denoted e . It is often expressed in terms of eccentricity ε , which is a dimensionless unit related to the airgap defined by

$$\varepsilon = \frac{e}{g}$$

Expressing Eq. (5.13) in terms of eccentricity results in the final expression for the current amplitude:

$$\hat{i}_z = \hat{i}_t = \omega \varepsilon g \frac{8l_w r B_0 \cos\left(\frac{1}{\pi}\right)}{(t_r + 2g)\sqrt{R^2 + (\omega L)^2}} \quad (5.14)$$

The axial current i_z turns direction into a tangential current i_t at the cylinder ends, or, if many magnets are used, at each symmetry line B-B, see Fig. 5.10 right. The tangential current in the bearing cylinder corresponds to the current in the short circuit ring in an induction generator.

The phase shift φ , and the force angle θ , are then

$$\varphi = \arctan \frac{\omega L}{R}, \quad \theta = \arctan \frac{R}{\omega L} \quad (5.15, 5.16)$$

Equation (5.14) represents a current that initially increases linearly with frequency ω and then asymptotically reaches its maximum value.

The force angle in Eq. (5.16) starts from $\pi/2$ at low frequency, which then asymptotically reaches zero at high speed. This explains the angle θ in Fig. 5.4d.

An attempt to illustrate the eddy currents is made in Fig. 5.6-5.7. Fig. 5.6a and 6.7 shows the two main eddy current circuits at low speed, and Fig. 5.6b shows the theoretical current distribution at infinitely high speed.

5 Bearing analysis

The pole area A , which is used in Eq. 5.10 to 5.11, refers to the whole area which is enclosed by the eddy currents. But in the integral in Eq. (5.11) only the part of the area where the flux is radial contributes to the induced voltage, as previously described. This effective area A_{eff} will be analyzed further below.

When pole shoes are used, the simple model assuming that all radial flux goes through the pole shoe, gives accurate results. The currents will basically follow the geometry of the magnets, which makes it easy to estimate the shape of the current path, however, one should consider that in reality the current distribution is not discrete as illustrated in Fig. 5.6 and 5.7, but sinusoidally distributed, and the shape is rounded or elliptic. In order to avoid elliptical integrals, and focus more on the understanding of the bearing, a discrete and somewhat simplified current path will be used, which is shown in Fig. 5.10 and 5.11. An expression for the effective pole area A_{eff} based on this current path is

$$A_{eff} \approx 2l_w \left(\frac{\pi d_{rc}}{2} - w_3 \right) \quad (5.17)$$

where $2l_w$ is the pole width and w_3 is defined in Eq. (5.18). Finally d_{rc} is the diameter of the rotor cylinder centerline, defined as

$$d_{rc} = \frac{(D_r + d_r)}{2}$$

where the diameters are defined in Fig. 4.2. Equation (5.17) is valid for inner, outer as well as intermediate bearings, all with iron poles.

This expression for the area is the same for all pole shoes, regardless if they belong to a 2-row bearing or to the additional pole shoe inserted when more magnets are added. For the end plate, or end pole shoe, the pole width is normally the half, that is l_w , instead of $2l_w$, but this is of less interest since the end poles are not enclosed by any currents, unless the rotor is very long.

Now consider a bearing without pole shoes. The magnets are mounted with the poles directly opposing one another, as in Fig. 5.9a,b. Since there are no pole shoes, the area A in which the flux is normal is not that well defined, and the direction of the flux lines have to be carefully studied. There exists no region without radial flux, so there will be no difference between the total area A and the effective area A_{eff} . There is also a more pronounced difference between the area in the 2-row bearing, Fig. 5.9a, and the area for the additional row, Fig. 5.9b, than for the case when pole shoes are used. An estimation would be to exchange l_w in Eq. (5.17) for $l_m/2$ in the 2-row case and $l_m/4$ in the latter case.

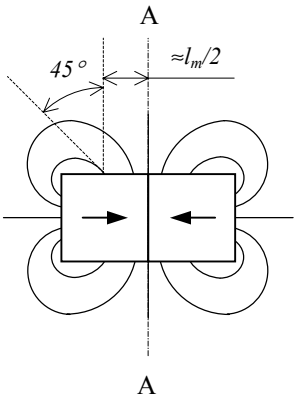


Fig. 5.9a. Expanding flux lines in a 2-row bearing without pole shoes.

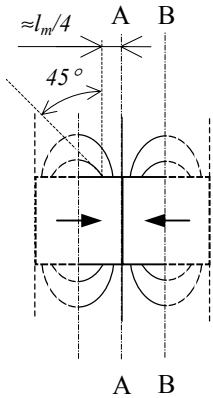


Fig. 5.9b. Compressed flux lines for an additional magnet row without pole shoes.

For the additional row in Fig. 5.9b this approximation is well motivated by the fact that by symmetry the flux lines change direction from upward to downward over the length of one magnet. The flux is parallel with the magnets when crossing symmetry line B-B. Thus there is a change of angle with 180 degrees over the length l_m . If the “pole” is now defined as the area where the flux angle is less than 45 degrees, then the width of this area is $2 \cdot l_m / 4$ which should be compared to the pole width $2l_w$ in Eq. (5.17).

In the 2-row case, Fig. 5.9a, there is only 1 symmetry line A-A, thus allowing the flux lines to expand to the sides, forming a magnetic 4-pole. This allows a wider pole area A . A rough estimation, at least for quadratic magnet cross-sections, is to set the pole width to $2 \cdot l_m / 2$, since this will result in four equal pole areas.

Now having determined the shape and the area of the eddy current circuits, expressions for the resistance R and the inductance L can finally be found. In order to find a formula for the resistance it will also be necessary to study the influence from skin effect.

5 Bearing analysis

5.4.1.2 Resistance

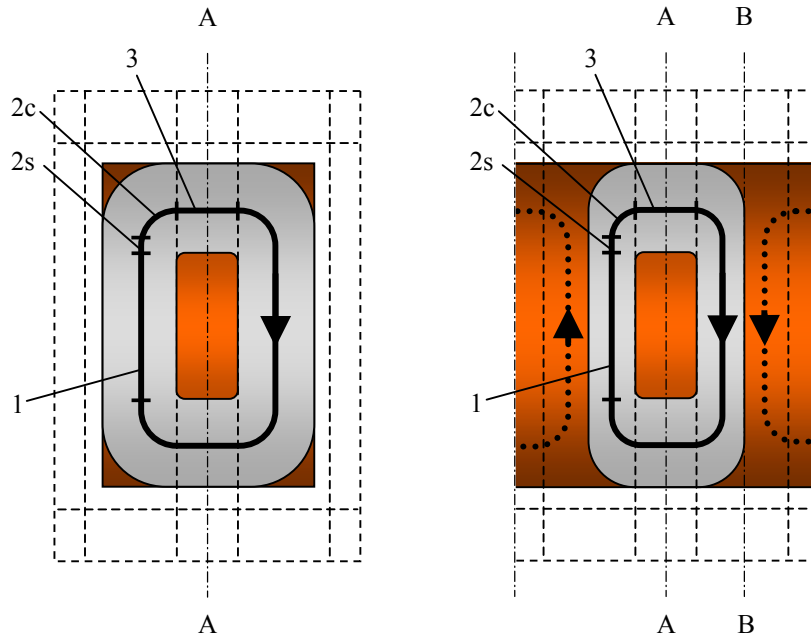


Fig. 5.10a,b. Eddy current path in a 2-row bearing (left) and due to an additional row (right). Both bearings have pole shoes. The short circuit paths (1) are connected both to each other forming a full short circuit ring (the other half not shown), and to the bars (3) via the rounded corner (2c).

The resistance R of the eddy current circuits can be derived using the simplified model shown in Fig. 5.10. Before going into details of the model, one has to bear in mind that in reality the currents are not bound to these discrete paths. For future work, in order to develop more accurate analytical formulas, it might be necessary to solve the diffusion equation with proper boundaries. But at this early stage of the development phase it feels more appropriate to use this simple model and solve it using the generator approach, as it will give a better understanding of the physics than would the typical series expansions resulting from a solution to the diffusion equation.

The model is derived for two cases:

- the 2-row bearing with pole shoes, shown in Fig. 5.10a, and
- the case for additional rows including pole shoes, Fig. 5.10b.

Each of these cases can be recalculated for corresponding bearings without pole shoes by modifying the pole width as described in the previous chapter.

Consider again Fig. 5.10a. The conducting cylinder, here colored red as copper, is somewhat shorter than the stator. The latter has dashed contours and consists of magnets and pole shoes. On the cylinder one of the eddy currents is shown in gray. This current blocks the view of the other current, which is located on the reverse side of the cylinder.

In Fig. 5.10b a part of an infinitely long bearing is shown, in order to study the current induced due to one additional magnet and pole shoe. In this case there is not only the symmetry line A-A, but also the symmetry line B-B, which narrows the available space for the eddy currents. Thus the resistance in this case will be higher than for the circuit in Fig. 5.10a.

The symmetry line B-B exists only in infinitely long bearings. However, in order to reduce the number of possible cases in the model, a bearing with any number of rows will be regarded as consisting of only these two types of currents. This approximation will be best for either 2-row bearings or bearings with many rows. The largest deviation will be found in 3-row bearings.

Now consider Fig. 5.11, which shows a linearized model of the eddy currents in Fig. 5.10, omitting some corner effects. The same linear model can be used for both types of currents, just taking into consideration that the width of region 1, w_1 , is different for the two cases, which also affects the length of region 2, l_2 . The length of each current segment is denoted l_1 to l_3 , and the widths are correspondingly denoted w_1 and w_3 . w_2 is not used since it is not constant. Instead the average $(w_1 + w_3)/2$ is used. Region 2 will be divided into a straight part of length l_{2s} and a circular part of length l_{2c} . The lengths and widths are defined geometrically from Fig. 5.11 and are summed up in Eq. (5.18).

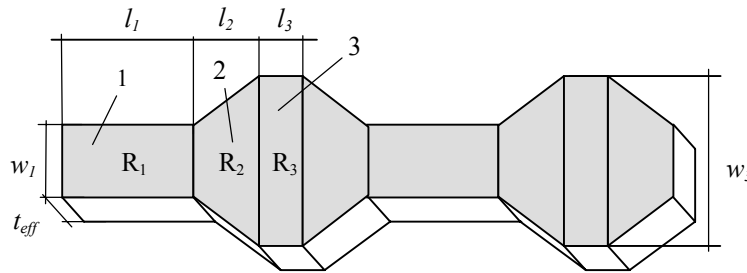


Fig. 5.11. Linear model of the eddy current path shown in Fig. 5.10a,b. Numbers refer to the different regions.

5 Bearing analysis

$$\left\{ \begin{array}{l} l_1 = \pi r - 2w_3 \\ l_2 = l_{2s} + l_{2c} = \frac{w_3}{2} - r_2 + \frac{2\pi r_2}{4} \quad \text{where } r_2 = \frac{w_1}{2} \\ l_3 = 2l_w \\ w_1 = \begin{cases} \frac{l_r}{2} - l_w & \text{for 2-row bearings} \\ \frac{l_m}{2} & \text{for additional rows} \end{cases} \\ w_3 = \frac{2r}{\pi} \end{array} \right. \quad (5.18)$$

In these formulas r refers to the radius of the center of the rotor cylinder,

$$r = r_{rc} = \frac{R_r + r_r}{2}, \quad (5.19)$$

and l_2 is a quarter of the circumference of an ellipse. However, since an ellipse does not have any simple analytical expression for this length, an approximation is used consisting of a straight part l_{2s} and a circular part l_{2c} with the radius r_2 . Of the same reason, the width w_2 is taken as an average as shown in the linearized model in Fig. 5.11.

The width w_3 is by no means obvious and requires an explanation. It could have been set to one quarter of the circumference of the rotor, which is true in that aspect that the whole area actually carries eddy currents. There exists no area inside the current loop as in Fig. 5.10a,b where the current is completely absent. However, in reality the current density is sinusoidally distributed, which means that the main part of the currents in region 3 passes through the upper and the lower part of Fig. 5.10, which will result in higher losses compared to the constant current distribution in the model. To require equal losses for both approaches is a way to define w_3 . Setting the currents equal in both cases results in

$$\begin{aligned} I_z &= \int_A j_z \cdot dA \\ I_z &= t_{eff} \int_0^{\pi/2} \hat{j}_z \sin \alpha r d\alpha \\ I_z &= \hat{j}_z r t_{eff} \end{aligned} \quad (5.20)$$

where α is an integration angle which is zero on top of Fig. 5.10 and follows the circumference of the rotor. This angle is $\pi/2$ turned counterclockwise from the load angle θ . Also the losses shall be equal, thus

$$R_3 I_z^2 = \int_V \rho j_z^2 dV$$

$$\rho \frac{l_3}{t_{eff} w_3} I_z^2 = \rho \int_0^{\pi/2} (\hat{j} \sin \alpha)^2 l_3 t_{eff} r d\alpha \quad (5.21)$$

Solving, using Eq. (5.20), gives

$$w_3 = \frac{2r}{\pi} . \quad (5.22)$$

The total resistance R of the linearized circuit can now be written as

$$R = 2(R_1 + 2R_2 + R_3) =$$

$$= 2 \frac{\rho}{t_{eff}} \left(\frac{l_1}{w_1} + 4 \frac{l_2}{(w_1 + w_3)} + \frac{l_3}{w_3} \right) \quad (5.23)$$

where t_{eff} is the effective thickness of the circuit due to the skin depth. Using the expression from Eq. (5.18), the resistance in each eddy current circuit of a 2-row bearing with pole shoes is found to be

$$R_{2-row} = \frac{\rho}{t_{eff}} \left(4 \frac{r(\pi - \frac{4}{\pi})}{l_r - 2l_w} + \frac{r \frac{8}{\pi} + (l_r - 2l_w)(\pi - 2)}{\frac{2r}{\pi} + \frac{l_r}{2} - l_w} + 2\pi \frac{l_w}{r} \right), \quad (5.24)$$

and the resistance in each additional circuit, which is created when more magnet rows are added to the bearing, to be

$$R_{add} = \frac{\rho}{t_{eff}} \left(4 \frac{r(\pi - \frac{4}{\pi})}{l_m} + \frac{r \frac{8}{\pi} + l_m(\pi - 2)}{\frac{2r}{\pi} + \frac{l_m}{2}} + 2\pi \frac{l_w}{r} \right). \quad (5.25)$$

5.4.1.3 Skin depth

In the previous subsection the effective thickness t_{eff} of the conducting cylinder has been used in the expressions for resistance. At low speed, the effective thickness equals the material thickness t_r of the rotor cylinder, but as speed increases the skin effect decreases the effective thickness of the circuit.

An often-used definition of t_{eff} relates to the skin depth δ_{skin} as

$$t_{eff} = \begin{cases} t_r, & t_r \leq \delta_{skin} \\ \delta_{skin}, & t_r > \delta_{skin} \end{cases} \quad (5.26)$$

where

$$\delta_{skin} = \sqrt{\frac{2}{\omega\sigma\mu_0}}. \quad (5.27)$$

This relation is applicable to outer and inner rotor bearings. For the intermediate rotor bearing, having two airgaps with magnets on both sides of the cylinder, the effective thickness is accordingly

$$t_{eff} = \begin{cases} t_r, & t_r \leq 2\delta_{skin} \\ 2\delta_{skin}, & t_r > 2\delta_{skin} \end{cases}. \quad (5.28)$$

The model above, which is often used in literature, has the clear disadvantage that the function derivative is discontinuous, leading to curves for forces and losses with discontinuous slope. A better estimation for the inner and outer rotor bearing is the gradually increasing t_{eff} according to the exponential function

$$t_{eff} = \delta_{skin} (1 - e^{-t_r / \delta_{skin}}) \quad (5.29)$$

and for the intermediate bearing the function is, of the same reason as above,

$$t_{eff} = 2\delta_{skin} (1 - e^{-t_r / (2\delta_{skin})}). \quad (5.30)$$

Results on bearing stiffness calculated for the intermediate bearing using these two different approximations are shown in Fig. 5.22 where they are compared to results from FEM simulations. Clearly Eq. (5.30) is the most appropriate in this case.

5.4.1.4 Inductance

The inductance L of the eddy current circuit is strongly dependent on whether iron pole shoes are used or not. This factor is sometimes neglected in literature on eddy current devices, probably due to the fact that the pole shoes do not to a great extent affect the air gap flux density, since the magnets are operating in repulsive mode. However, in generator theory it is well known that the magnetizing inductance and the armature inductance can vary a lot. In our case the eddy current circuits should be treated as the armature winding. Normally the phase angle between the armature current and the magnetizing current is of importance, but since the bearing is homopolar and the effective airgap is constant, this does not effect the value of the inductance.

Consider first the case when pole shoes are not used. If the relative permeability of the magnets is close to unity, then the influence of the magnets is negligible. Thus the inductance can be calculated as that from an air wound coil, and it will be the same for as well outer, inner and intermediate bearings. Filatov [10] whose coils are similar and also air wound, uses the formulas for the inductance from two infinitely long conductors, applied to the tangential parts of the current circuits. Thus

$$L = l_t \frac{\mu_0}{\pi} \left(\frac{1}{2} + \ln \frac{l_0}{r_0} \right) \quad (5.31)$$

where l_t is the length of the tangential sections of the coil, which in Fig. 5.10b are the vertical parts of the current paths. If the length $l_1 + 2l_2$ is projected on to the vertical symmetry line A-A the vertical length is found to be $l_1 + w_3$. The radius r_0 of the conductor is approximated to half the width w_1 , thus for the bearing without pole shoes $r_0 = l_m/8$. Finally the distance between the centers of the conductors l_0 is $3l_m/4$, which is found from the model in Fig. 5.10b applied to the magnets without pole shoes in Fig. 5.9b. Thus the inductance of one eddy current circuit from an additional magnet is

$$\begin{aligned} L_{add} &= (l_1 + w_3) \frac{\mu_0}{\pi} \left(\frac{1}{2} + \ln \frac{\frac{3l_m}{4}}{\frac{l_m}{8}} \right) = \\ &= \frac{\mu_0}{\pi} (l_1 + w_3) \left(\frac{1}{2} + \ln 6 \right). \end{aligned} \quad (5.32)$$

Similarly, by applying the model in Fig. 5.10a to the magnets in Fig. 5.9a the corresponding value for the 2-row bearing with a rotor length l_r the

5 Bearing analysis

inductance of one eddy current circuit in a 2-row bearing without pole shoes is

$$L_{2\text{-row}} = (l_1 + w_3) \frac{\mu_0}{\pi} \left(\frac{1}{2} + \ln \frac{l_r + l_m}{l_r - l_m} \right) \quad (5.33)$$

where the length $w_l = (l_r - l_m)/2$, $l_0 = l_r - w_l$ and finally $r_0 = w_l/2$. These relations can be found explicitly from Fig. 5.12a,b below. Expression 6.33 is valid for rotors approximately equally long as the two magnets, that is

$$l_r \approx (2 \pm 0.5)l_m. \quad (5.34)$$

The important condition is that the flux has to be axial $\pm 45^\circ$ within the circuit region 1 of width w_l .

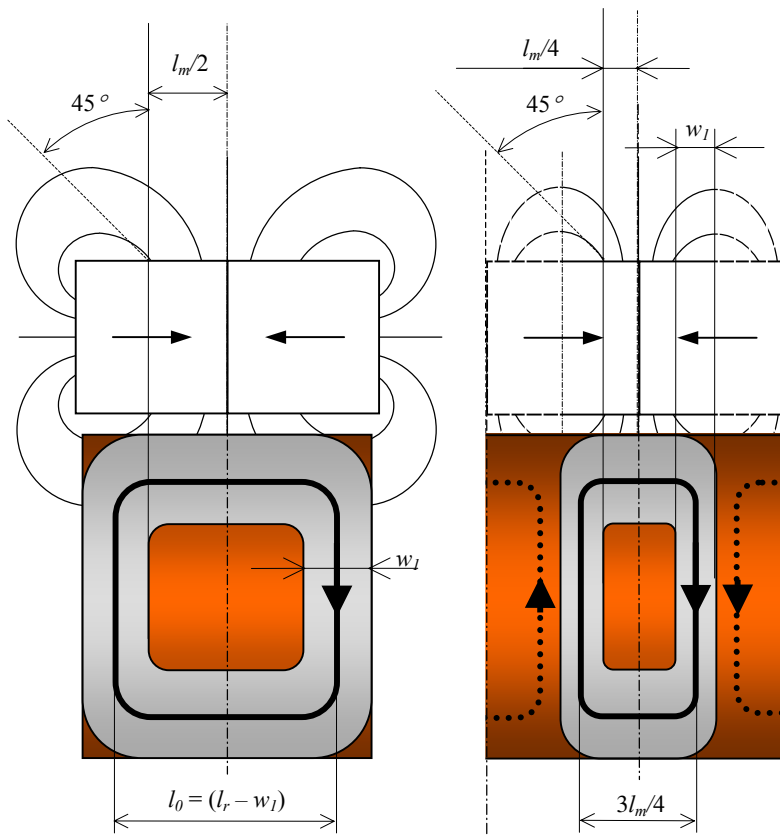


Fig. 5.12a,b. Eddy current paths in bearings without pole shoes. Compare with Fig. 5.10a,b showing bearings with pole shoes.

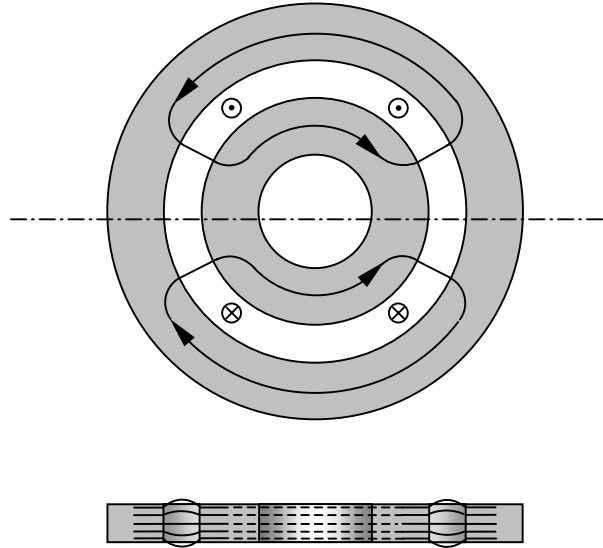


Fig. 5.13a,b. Enhanced 2D-model of the inductance. For clarity the copper cylinder is not shown. a) Main flux in one pair of pole shoes in an intermediate bearing. b) Fringing between poles.

If pole shoes are used, the inductance is dramatically increased. A 2D-model of the inductance can be established as follows:

Consider Fig. 5.13 above in which an intermediate bearing is shown. The magnetic flux (arrows) from the two opposite eddy current loops (currents perpendicular to the picture) is shown. The flux follows the iron outer disc, penetrates the effective airgap including the copper cylinder twice (cylinder not shown for clarity), and uses the inner iron pole as a return path.

Since it is a 2D model, it does not take leakage between adjacent poles in the axial direction into account, and there is also some stray inductance between adjacent iron poles that is neglected.

The inductance depends on the number of turns, n , and the reluctance R_m as

$$L = \frac{n^2}{R_m} = \frac{n^2}{R_{Fe,o} + R_{Fe,i} + 2R_{g,eff}} \approx \frac{n^2}{2R_{g,eff}} \quad (5.35)$$

5 Bearing analysis

where the reluctance in the outer and inner pole shoes, $R_{fe,o}$ and $R_{fe,i}$, have been considered to be small in comparison with the effective airgap reluctance $R_{g,eff}$, which is

$$R_{g,eff} = \frac{l_{g,eff}}{\mu_0 A} = \frac{2g + t_r}{2\mu_0 l_w (l_1 + w_3)}, \quad (5.36)$$

where $l_{g,eff}$ is the effective airgap including two mechanical airgaps each of length g and the copper rotor thickness t_r .

Using the fact that the winding has two turns in parallel, one in each airgap, the inductance will be:

$$L = 4\mu_0 l_w \frac{l_1 + w_3}{2g + t_r} \quad (5.37)$$

This far the model is a pure 2D model, but by modifying the airgap width in the axial direction it is possible to compensate for fringing, which in this case is a 3D effect. The washers have a thickness l_w or $2l_w$, and in Eq. (5.37) the same values are also used for the axial length of the airgap. In reality the flux lines have shapes more like arcs as illustrated in Fig. 5.13b. By exchanging l_w for the average effective airgap width $l_{w,eff}$ fringing can be accounted for in the model. Typically fringing increases the effective airgap width with approximately 10%, so

$$l_{w,eff} = 1.1 \cdot l_w. \quad (5.38)$$

Naturally, fringing can be calculated more accurately, which might be necessary in future work. Then leakage inductance between the poles should also be taken into account.

Using the simplification in Eq. (5.38), the final expression for the inductance is found to be

$$L = 4\mu_0 l_{w,eff} \frac{l_1 + w_3}{2g + t_r} \quad (5.39)$$

A drawback of this 2D model is that the inductance lack a speed dependance. At high speed the skin effect will prevent some of the flux penetration. Thus the inductance will decrease at high speed, which this model does not take into consideration. In Fig. 5.22 where the analytical model is compared to the

FEM model, it can be seen that the slope of the stiffness curve is slightly higher for the FEM model, which indicates that the inductance is decreasing somewhat at very high speed. On the other hand, when applying a model of a variable inductance, it is also important to reduce the flux change, since this is also related to the skin effect. For future research one of the aims would be to implement these two effects into the model.

Below in Fig. 5.14 the total impedance and its components are shown for a 2-row bearing with pole shoes. It is evident that the reactance ωL is the dominant part at high speed. For this particular bearing the resistance and the reactance equals at about 30.000 rpm. The increase in resistance is due to the reduced effective thickness caused by skin effect at high speed. The continuous model from Eq. (5.30) has been used here and throughout the report.

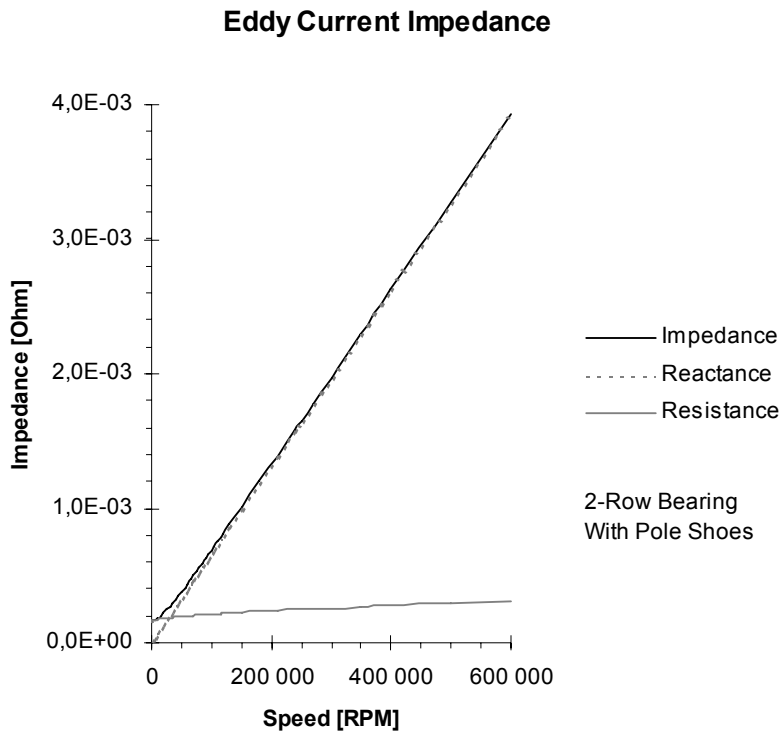


Fig. 5.14. Analytical model of rotor impedance. Above 30.000 rpm the reactance ωL is the dominant part.

5.4.2 Eddy currents induced by lateral motion

Previously eddy currents induced due to eccentric operation have been studied in Chapter 5.4.1. The second condition during which eddy currents can be induced is when the conductor moves about any of its remaining five degrees of freedom in such a way that the conductor surface experiences a varying magnetic flux density. It can be axial movements in the z-direction, tilting movements or lateral movements in the x-y plane. The latter category is of particular interest in rotordynamics, and will be studied below in more detail.

The types of lateral motion that will be studied are

- Constant speed
- Vibrations
- Low frequency whirl
- High frequency whirl
- Synchronous whirl

5.4.2.1 Constant speed

To understand the rotors different motions, and their effect on the eddy currents, consider first the simplest case when the rotor moves with constant velocity. Clearly, the practical use of this example is very limited, since the rotor will quickly reach to the bearing boundaries, normally the emergency bearing, and bounce back.

Fig. 5.15a shows a rotor, which is not rotating, but moving in the bearing with constant radial velocity v . A point on the surface of the rotor, heading in the direction of motion, will experience a flux density change

$$\frac{\partial B_r}{\partial t} = \frac{\partial B_r}{\partial r} \cdot \frac{\partial r}{\partial t}, \quad (5.8)$$

where the radial flux derivative is already determined in Eq. (5.5)

$$\frac{\partial B_r}{\partial r} = \frac{-2B_0}{t_r + 2g}, \quad (5.5)$$

and the radial velocity has a maximum value equal to v in the direction of motion and then varies around the perimeter according to

$$\frac{\partial r}{\partial t} = v \cos(\phi - \phi_0) \quad (5.40)$$

where ϕ_0 is the angle along the direction of motion. For coordinate references see Fig. 5.3.

Inserting Eq. (5.5) and (5.40) into Eq. (5.8) gives the final expression for the flux density change:

$$\frac{\partial B_r}{\partial t} = \frac{\partial B_r}{\partial r} \cdot \frac{\partial r}{\partial t} = \frac{-2B_0}{t_r + 2g} \cdot v \cos(\phi - \phi_0). \quad (5.41)$$

Integrating the flux density change over the area A results in the flux change

$$\begin{aligned} \frac{\partial \Phi_r}{\partial t} &= \int_A \frac{\partial B_r}{\partial t} dA = \frac{2B_0 \cdot v}{t_r + 2g} \int_{\psi_l}^{\psi_u} 2l_w \cos(\phi) r d\phi = \\ &= v \frac{8l_w r B_0}{t_r + 2g} \cos\left(\frac{1}{\pi}\right) \end{aligned} \quad (5.42)$$

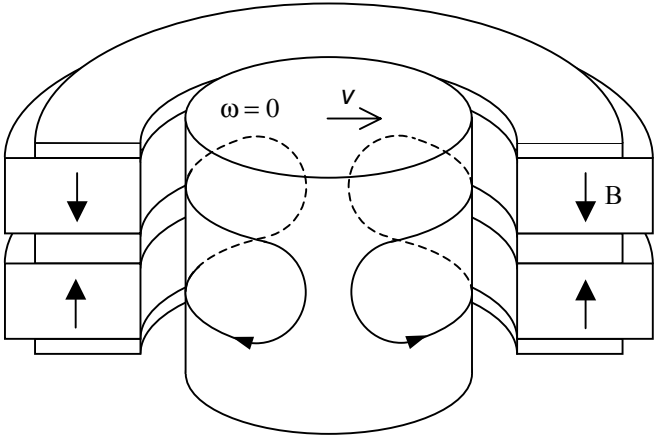
where the integration limits are the same as in Eq. (5.12). Inserting into Eq. (5.10) gives the expression for the velocity-induced current.

$$\hat{i}_{z,v} = v \cdot \frac{8l_w r B_0 \cos\left(\frac{1}{\pi}\right)}{(t_r + 2g) \sqrt{R^2 + (\omega L)^2}} \quad (5.43)$$

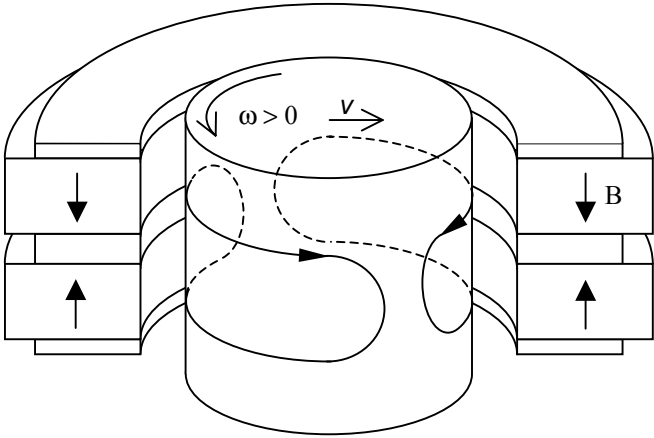
This current is a pure damping current, and will be used later when calculating the damping coefficient for this particular case when the rotor is not rotating, and having constant velocity v .

The resistance R and the inductance L are identical to the ones calculated previously concerning the eccentric rotation. Comparing Eq. (5.43) and (5.13) shows that

$$\hat{i}_{z,v} = \frac{v}{\omega \Delta r_0} \hat{i}_{z,e} \quad (5.44)$$



(a)



(b)

Fig. 5.15. Internal damping circuit when rotor moves with speed v .
a) Zero rotational speed. b) Non-zero rotational speed ω .

Since the frequency ω is zero, Eq. (5.43) can be simplified to

$$\hat{i}_{z,v} = v \cdot \frac{8l_w r B_0 \cos\left(\frac{1}{\pi}\right)}{(t_r + 2g) \cdot R} \quad (5.45)$$

This is the only expression in which the inductance is of no importance for the induced currents and forces.

5.4.2.2 Vibrations

With rotor vibrations will be understood a reciprocating motion along any vector in the x-y plane. For instance a vibration with frequency ω_t parallel to the y-axis passing through the origin will cause the rotor axis z_l to move according to

$$\Delta \bar{r}_0 = a_v \sin(\omega_v t) \hat{y}, \quad (5.46)$$

where a_v is the amplitude of the vibration. The velocity v_0 is found by derivation to be

$$\bar{v}_0 = a_v \omega_v \cos(\omega_v t) \hat{y} \quad (5.47)$$

Zero rotational speed

At zero rotational speed the damping currents are directed so as to produce a force directed oppositely towards the direction of motion. If the inductance is negligible, which is the case for low enough frequencies, the damping force is proportional to the lateral speed v_0 , and Eq. (5.45) from the previous subsection can be used as a good low frequency approximation. A mechanical interpretation of this damping effect resembles that of a perfect viscous one.

At higher frequencies the inductance is not negligible. This delays the current and the damping force. From control theory it is well known that a delayed damping action produces stiffness. Thus the damping effect of these eddy currents will gradually turn into stiffness when the frequency increases. This can be shown by inserting the speed v_0 in Eq. (5.43). It results in the delayed damping current $i_{z,f}$ due to vibration of frequency ω_v , which is

$$\hat{i}_{z,f} = a_v \omega_v \cdot \frac{8l_w r B_0 \cos\left(\frac{1}{\pi}\right)}{(t_r + 2g) \sqrt{R^2 + (\omega L)^2}}. \quad (5.48)$$

5 Bearing analysis

The phase lag with respect to velocity is

$$\phi = \arctan \frac{\omega L}{R}, \quad (5.15)$$

and since velocity v_0 comes $\pi/2$ ahead of the displacement, it is clear that the phase lag with respect to displacement is 0 at very high frequencies. Forces produced by this current will be in phase with, and proportional to, the displacement, properties which define bearing stiffness.

Important conclusions from this section are that a non-rotating bearing

- has certain high-frequency stiffness, and
- has certain damping at all frequencies.

Non-zero rotational speed

At non-zero speed currents induced by vibrations will be dragged along with the rotor surface due to the phase delay which occurs in the now rotating coordinate system. Thus the damping force will have a tangential component like the restoring force. We can call it a “phase delayed internal eddy current damping”. (It should be noted that this damping is not identical to the term “rotating damping” used in rotordynamics. There is a confusion in literature on how to apply the term “rotating damping” to eddy current devices, and in Chapter 5.8 the author tries to straighten out some misunderstandings.)

The directions of the velocity dependent force F_v is shown in Fig. 5.16b, and is compared to the eccentricity induced force F_r shown in Fig. 5.16a. It is to be noted that the damping eddy current circuit has a forward shift compared to the restoring circuit. This comes from the fact that speed is a displacement derivative and lies $\pi/2$ ahead of the displacement itself. The flux change in the rotating frame due to lateral velocity $\bar{v}_0 = (v_{0x}, v_{0y})$ is

$$\frac{\partial B_r}{\partial t} = \frac{\partial B_r}{\partial r} \cdot \left| \frac{\partial \bar{r}}{\partial t} \right| = \frac{\partial B_r}{\partial r} \cdot \left| (v_{0x} \cos(\omega t) \hat{x} + v_{0y} \sin(\omega t) \hat{y}) \right| \quad (5.49)$$

where Eq. (5.47) has been used and applied to both the x - and y - directions,

and where

$$\frac{\partial B_r}{dr} = \frac{-2B_0}{t_r + 2g}. \quad (5.15)$$

Assuming movements only in the y-direction, the velocity function becomes

$$\bar{v}_{0x} = 0 \quad \text{and} \quad \bar{v}_{0y} = a_v \omega_v \cos(\omega_v t) \hat{y}. \quad (5.47)$$

Inserting this into Eq. (5.49) results in the expression for the flux density change due to velocity,

$$\frac{\partial B_r}{\partial t} = \frac{-2B_0}{t_r + 2g} \cdot a_v \omega_v \cos(\omega_v t) \sin(\alpha t). \quad (5.50)$$

Since the vibration is always combined with displacement $\Delta y_0 = a_v \sin(\omega_v t)$, another term needs to be added to the final expression. This term is the speed $\Delta r_0 \alpha \cos(\alpha t)$ from Eq. (5.8) where Δr_0 in this case is Δy_0 . Inserting into Eq. (5.50) gives

$$\frac{\partial B_r}{\partial t} = \frac{-2B_0}{t_r + 2g} \cdot (\alpha a_v \sin(\omega_v t) \cos(\alpha t) + a_v \omega_v \cos(\omega_v t) \sin(\alpha t)) \quad (5.51)$$

In Eq. (5.51) above the vibrations and displacements are limited to the y-axis. Note that there are two frequencies involved, vibrational frequency ω_v and rotational frequency ω and simple expressions can only be achieved when they are either equal, or one of them can be neglected.

In the following subsections these special cases will be studied more in detail.

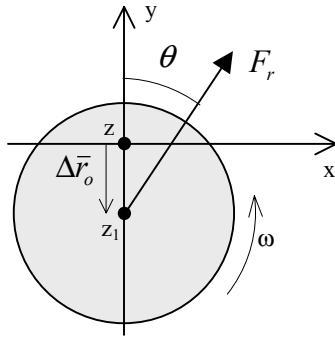


Fig. 5.16a. Force due to eccentricity.

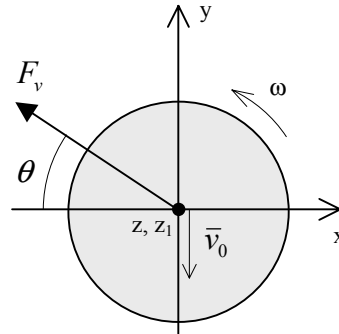


Fig. 5.16b. Force due to lateral speed.

5.4.2.3 Low frequency whirl

Rotor vibrations normally have the shape of elliptical or circular orbits, a superposition of two perpendicular vibrations with equal frequency ω_w but not necessarily equal amplitude. The rotor is said to whirl, and this motion can be either forward or backward with respect to the direction of rotation. Thus the whirl frequency ω_w will induce damping eddy currents in the rotor similar to the time delayed damping currents described in the previous section. The magnetic circuits of these damping eddy currents are the same as the ones shown in Fig. 5.15, where two cases are shown. The first case above shows the rotor having no rotational speed, and the second case shows an example where the rotor is spinning at velocity ω . One just needs to consider that the velocity is no longer parallel to the displacement as in the previous case, also illustrated in Fig. 5.17a. If the orbits are circular, the speed and displacement are perpendicular, as shown in Fig. 5.17b.

Calculating the currents and forces from this damping is not trivial. However, Filatov [10] has done a study on the dynamics of slow lateral motion of a conductor superimposed on high-speed rotation. Applying his results to the phase shift and the force angle in the special case when the whirl frequency ω_w is much lower than the rotational frequency ω , results in damping forces F_v that are perpendicular to the force F_r induced by eccentricity when displacement and velocity have the same direction, which is illustrated in Fig. 5.17a. Applied to the case of low frequency whirl, they turn out to be oppositely directed, Fig. 5.17b.

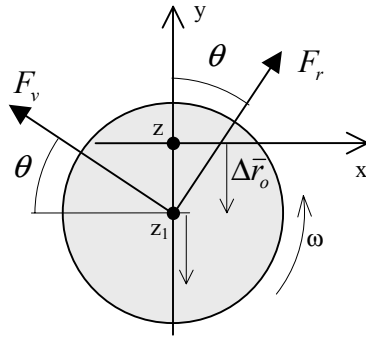


Fig. 5.17a. Forces due to eccentricity and velocity.

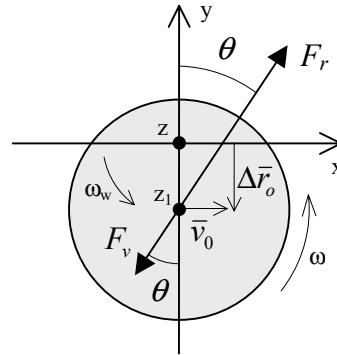


Fig. 5.17b. Forces due to low frequency whirl.

5.4.2.4 High frequency whirl

If the vibrational frequency ω_f is much higher than the rotational speed ω , then there is not much time for the currents to be dragged around by the rotation. The situation is more similar to the first case with a non-rotating but vibrating rotor.

Causes for high frequency vibration can be interaction with turbine blades, disturbances from cutting or grinding tools in machine spindles, motor cogging if applicable and inverter switching. The motion patterns from these disturbances have no simple shapes, but are more stochastic to their nature. They usually excite harmonics related to the bending critical frequencies of the shaft or turbine blades, and at least the ones belonging to the shaft will have orbital shapes, which might be referred to as high frequency whirl.

When active magnetic bearings are used, it has proven to be quite difficult to damp these vibrations, since a high frequency cut off filter is normally used before the damping algorithm to prevent the controller from saturating the amplifiers. The sensor position is also critical, since it is axially displaced with respect to the bearing, and thus may not see the vibration modes that are present in the bearing.

The induction bearing provides both damping and high frequency stiffness, and has potential to complement active magnetic bearings in these kinds of applications.

5 Bearing analysis

5.4.2.5 Synchronous whirl

The term synchronous whirl will be used when the whirl frequency ω_w equals the rotational frequency ω .

Reviewing Eq. (5.51) which is valid for a one-dimensional vibration along the y-axis, and remembering that whirl is a superposition of two perpendicular vibrations,

$$\begin{aligned} \frac{\partial B_r}{\partial t} = \frac{-2B_0}{t_r + 2g} \cdot (\omega \alpha_v \sin(\omega_v t) \cos(\omega t) + \\ + a_v \omega_v \cos(\omega_v t) \sin(\omega t)). \end{aligned} \quad (5.52)$$

Observe that

$$\omega_w = \omega \Rightarrow \frac{\partial B_r}{\partial t} = \frac{-2B_0}{t_r + 2g} \cdot 0 = 0, \quad (5.53)$$

which means that during synchronous whirl no flux change occurs on the rotor surface in the rotating coordinate frame. Thus no forces, no losses and no damping occur, and these rotor vibrations cannot be transmitted to the stator via the induction bearing. Instead they are transmitted via the external damper, which is not described in this dissertation since there are several available concepts to choose among, some of them having nothing to do with eddy currents.

Important types of synchronous whirl occur due to

- unbalance
- rigid body critical speeds
- bending critical speeds.

The inability to transfer forces from synchronous whirl has advantages and disadvantages. A great advantage is of course reduced costs of rotor balancing, and quiet operation. When for instance active magnetic bearings are used on unbalanced rotors it is often important to filter away the synchronous frequency from the controller. This can be done using either a variable notch filter, or by using a feed forward algorithm. With induction bearings this filtering is done automatically.

A disadvantage is that passing the bending critical speed is impossible without additional damping, so the requirements regarding the external damper might be quite high. However, passing the rigid body modes is not a problem, as will be explained in Chapter 5.7.

5.4.3 Stray eddy currents

Any inhomogeneities in the permanent magnets, it may come from sintering or from magnetization, will most likely cause a non-rotationally symmetric magnetic field, which in turn will induce stray eddy currents. These currents will have a shape depending on the inhomogeneity. The most common one is misalignment between the geometric and the magnetic axis. Local flux dips, or random change of magnetic orientation around the perimeter of the magnet rings are also common.

Stray eddy currents may also result from inhomogeneities or remanent magnetic flux in the iron pole shoes. Iron screws and pins close to the airgap can also alter the flux so as to induce unwanted eddy currents.

Many FEM simulations on different kinds of inhomogeneities have been performed. Some of them are shown in Chapter 6, and they all show that the influence on restoring forces is very limited, whereas the influence on losses is large.

When ordering magnets it is very important to specify the maximum allowed misalignments and local flux dips depending on application loss requirements. Today not many magnet manufacturers undertake such considerations.

Though, even in the case of not perfectly manufactured magnets, the induction bearing still produce very low losses compared to many other magnetic bearing types.

5.5 Bearing forces

This far we have analyzed the magnetic flux and the eddy current circuits. By forming the product $J \times B$ along the eddy current circuit in Fig. 5.10a,b, the Lorenz force distribution is achieved. In Fig. 5.10a,b it is important to note that the magnetic flux is radial in cut A-A while it is axial in cut B-B. This comes automatically from the flux lines in Fig. 5.1. In Fig. 5.18a,b this is illustrated from another viewing angle. Thus, in the linear model of the current path in Fig. 5.11, the current is tangential and the flux is axial in region 1. In region 3 the flux is radial and the current is axial. Since the length l_1 normally is much longer than the length l_3 , the main force is generated in region 1. In Fig. 5.18c below the force distribution from region 1 is illustrated.

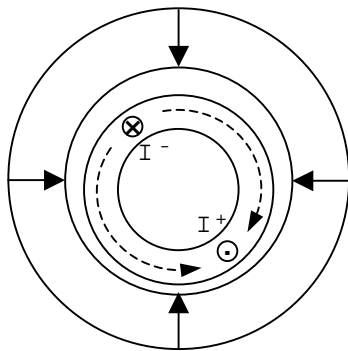


Fig. 5.18a. Same as Fig. 5.4a. Cut A-A, radial flux.

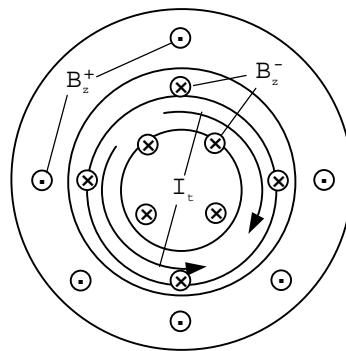


Fig. 5.18b. Cut B-B, axial flux.

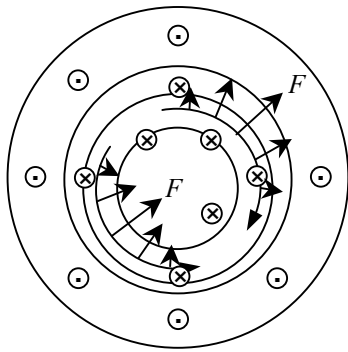


Fig. 5.18c. $J \times B$ force distribution.

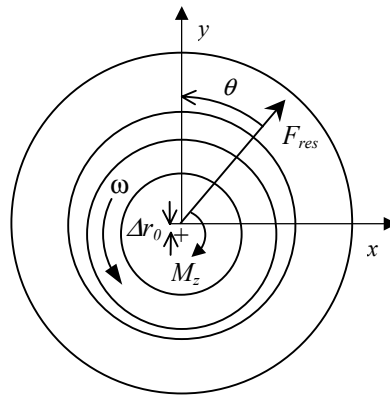


Fig. 5.18d. Resultant force and brake torque.

Region 1 would in an induction generator refer to the short circuit ring, and region 3 would refer to the active part or the rotor bars. For an electrical engineer it might be a little bit confusing that the short circuit ring plays such an important role in the induction bearing.

The resultant force F_{res} in Fig. 5.18d is obtained by integrating the force contributions over the whole cylinder. The force angle θ is the same as the one defined in Eq. (5.16), and depends on speed, resistance and inductance.

If we know the point of attack, or any other point on the line defined by the vector \vec{F}_{res} , the brake torque M_z can be calculated. Due to symmetry this line has to pass the center of the homopolar flux, which is the origin of the stator. Filatov [10] has in his Lemma no. 1 shown that this is always true for an axial homopolar bearing, and in a similar way it can be shown for radial flux bearings as well.

If the rotor is displaced in the negative y -direction the torque can easily be calculated as the product of the x -component of the force, F_x with the displacement Δr_θ .

If the bearing is not strictly homopolar, like for instance if the magnets are not perfectly axially magnetized, the point of attack is somewhere else and the brake torque will be larger.

In Fig. 5.6a, b the currents are plotted for different speeds and thus different force angle. In Fig. 5.6a the speed is low and the load angle is large. See also Fig. 5.19. Thus the force angle is also large and the bearing force has a large tangential force component, which has a strongly destabilizing effect on the rotor. In Fig. 5.6b the speed is infinitely high, and the force angle is 0 so that no tangential force component is present. Thus the force is totally restoring.

Unfortunately infinite speed is out of reach, so there will always be a certain tangential force component. However, by using iron pole shoes, or washers, between the magnets, the inductance is increased and thus the relationship between restoring force and tangential force is increased. This reduces the requirements for the external damper that has to be added due to stability considerations.

In the following the force from one magnet will be calculated using the simplification that the force contribution comes solely from the tangential currents and that the flux is axial in this region.

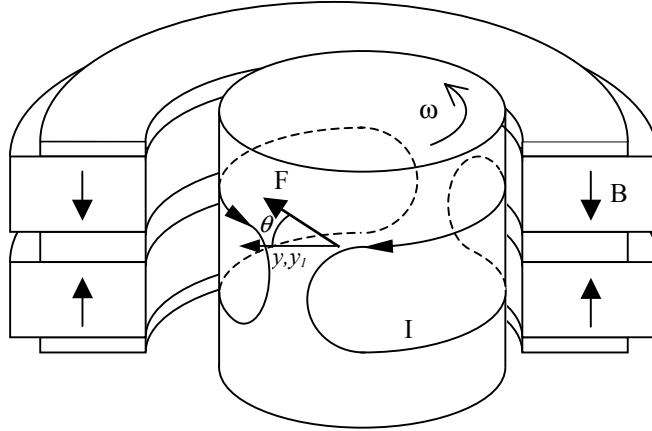


Fig. 5.19. Resulting force between eddy currents and magnets.

The force acting on the rotor can be calculated as the volume integral of the Lorenz forces. Starting with the intermediate magnet rows, each such row induces 2 eddy current circuits, each consisting of two identical tangential parts. Thus the tangential parts can be integrated separately. Using the current I , the resistance R and the inductance L from Eq. (5.25) and (5.39) the force contribution from one tangential current part can now be calculated as

$$\bar{F}_t = \int_V \bar{J} \times \bar{B} dV. \quad (5.54)$$

The integral can be simplified using the fact that we know the force angle. Thus an angle α can be introduced measured from the force angle and integrated from $-\pi/2$ to $\pi/2$. Projecting the force to this line by multiplying with $\cos \alpha$ gives the integral

$$F_t = \int_{-\pi/2}^{\pi/2} \hat{j}_t \cos \alpha \cdot B_z \cos \alpha \cdot \frac{l_m}{2} t_{eff} r d\alpha \quad (5.55)$$

where j_t is the tangential current density which has its maximum at $\alpha = 0$. At this point the total current I equals

$$I_t = \hat{j}_t t_{eff} \frac{l_m}{2} \quad (5.56)$$

which should be the same current as in Eq. (5.20). Thus Eq. (5.55) can be written as

$$F_t = I_t B_z \int_{-\pi/2}^{\pi/2} \cos^2 \alpha \cdot r \, d\alpha = \frac{\pi}{2} I_t B_z r. \quad (5.57)$$

Remembering that the total force F_{add} from one added intermediate magnet row comprises the sum of four tangential current parts, results in

$$F_{add} = 4F_t = 2\pi I_t B_z r. \quad (5.58)$$

The force direction is along the force angle, which is given by Eq. (5.16).

$$\theta_{add} = \arctan \frac{R}{\omega L} \quad (5.16)$$

For 2-row bearings, and for the two end magnets when the bearing consists of more than two rows, the total force from these two magnets F_{2-row} and the force angle θ_{2-row} can be calculated in the same way. One only has to remember that the resistance R and the inductance L has to be taken from Eq. (5.24) and (5.33) instead.

Thus the total bearing force F_B for an intermediate rotor bearing with n rows, is

$$\bar{F}_B = \bar{F}_{2-row} + (n-2)\bar{F}_{add}, \quad n \geq 2, \quad (5.59)$$

where vector notation has been used since the forces F_{2-row} and F_{add} are not acting in the same direction. It has a restoring force component $F_{R,B}$, directed oppositely towards the eccentricity

$$F_{R,B} = F_{2-row} \cos \theta_{2-row} + (n-2)F_{add} \cos \theta_{add} \quad (5.60)$$

and a tangential force component $F_{T,B}$ which is

$$F_{T,B} = F_{2-row} \sin \theta_{2-row} + (n-2)F_{add} \sin \theta_{add}. \quad (5.61)$$

5 Bearing analysis

In Chapter 6 which covers FEM simulations the eccentricity will always be assumed to be in the negative y-direction, so in the diagrams these force components will be denoted F_y and F_x respectively.

Finally the force angle θ_B of the total bearing can be calculated as

$$\theta_B = \arctan \frac{F_{T,B}}{F_{R,B}} \quad (5.62)$$

which is illustrated in Fig. 5.20 below.

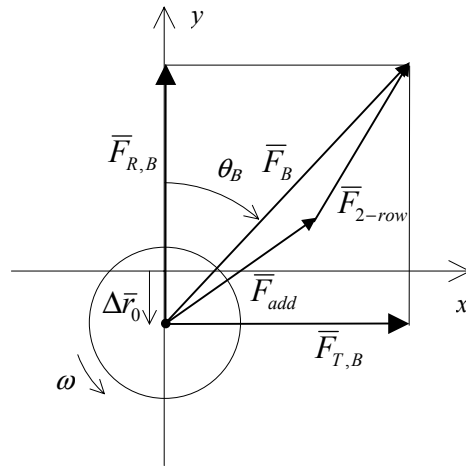


Fig. 5.20. Force components from a 3-row bearing.

5.6 Losses

Bearing losses P_B are composed of eddy current losses P_B^e and fluid film losses P_B^f . Often magnetic bearings are used in high vacuum, where losses from the gas are very low, while they may be high when used in a high viscosity process fluid. The experimental data in Chapter 8 are obtained from measurements at ambient atmosphere. Thus

$$P_B = P_B^e + P_B^f. \quad (5.63)$$

These losses are to some degree connected, since the cooling of the rotor is related to the fluid film losses. However, the thermal analysis shown in Fig. 8.28 clearly shows that the temperature rise is very limited, and thus will be neglected in the loss calculation.

The eddy current losses consist of contributions from all different currents described in the preceding sections, and before adding their contributions, it is important to find out if the currents overlap each other, and what phase angle they have, otherwise it is not possible to know if they increase linearly or quadratically when added, or if they maybe cancel each other out. The synchronous whirl described earlier is an interesting example where losses due to imbalance are completely cancelled out.

Losses due to eccentricity

Losses due to eccentricity is the most important loss component, since it is related to the bearing load and cannot be reduced by manufacturing magnets with higher precision. Contributions from the different magnets do not interact in this case since they are geometrically separated. The currents might interact due to mutual inductance though. However, once they are determined, the losses can be added.

For a 2-row bearing there are two eddy currents, and the losses due to eccentricity is

$$P_{2-row}^l = 2 R_{2-row} I_{2-row}^2 \quad (5.64)$$

where the index l stands for load, and where the current I_{2-row} and the resistance R_{2-row} have to be calculated according to Eq. (5.20) and (5.24).

Similarly, the losses from an additional intermediate row P_{add}^l can be calculated using the resistance and current for this particular case.

5 Bearing analysis

$$P_{add}^l = 2R_{add}I_{add}^2 \quad (5.65)$$

Altogether, the losses due to eccentricity for a bearing with n magnet rows is then

$$P_B^l = P_{2-row}^l + (n-2)P_{add}^l, \quad n \geq 2 \quad (5.66)$$

Losses due to eccentricity can be alternatively calculated using the mechanical power from the torque produced by the tangential force $F_{T,B}$.

$$P_B^l = M\omega = \Delta r_0 F_{T,B} \cdot \omega \quad (5.67)$$

Losses defined in this way are sometimes referred to as “rotating damping losses”. However, it is important to remember that the tangential force is not a constant, but a function of the impedance ωL , so the traditional usage of this term is not applicable in the stability analysis of eddy current devices, without taking special notice.

Losses due to lateral velocity

Eddy currents induced due to lateral velocity can be calculated in the same way as above, using the currents from Eq. (5.43) or (5.48) instead. Like previously, the current do not overlap each other from different magnets, since their shape are identical to the ones above, so they can be calculated as

$$P_B^v = P_{2-row}^v + (n-2)P_{add}^v. \quad n \geq 2 \quad (5.68)$$

These currents always overlap the currents from eccentricity, so they can not be simply added, they have to be integrated. They can help to completely eliminate the losses from eccentricity, as in the case mentioned earlier regarding synchronous whirl, but they can also add quadratically. The worst case would be that of synchronous backward whirl, where the losses would be

$$P_B = 2(P_B^l + P_B^v), \quad (5.69)$$

which is a very unlikely situation. Backward whirl may happen during a severe emergency bearing touch down, but even in this case it is not synchronous. Thus Eq. (5.69) may be used as an upper limit for bearing losses caused by load and lateral velocity.

Losses due to magnet inhomogeneity

Eddy currents induced due magnet inhomogeneity may have any shape depending on the type of magnet imperfection that is studied. Below some of them will be listed.

- Angular misalignment
- Mechanical eccentricity
- Surface roughness
- Varying density.

Angular misalignment is a severe type of imperfection. It causes a radial two-pole flux superimposed on the expected flux, which should be a homopolar axial flux diverging into a radial flux. These eddy currents are similar to the ones caused by eccentricity, and cause bearing forces and losses as if there actually were some radial displacement of the rotor. Some 3D-FEM calculations were performed, and show that a misalignment of 3 degrees equals approximately a bearing operating at maximum eccentricity. The bearings used in the experiments have a misalignment of less than 0.5 degree.

Mechanical eccentricity occurs when the magnets are mounted on one surface, and the other surface is facing the airgap, that is the inner and outer diameters are not concentric. The best mechanical tolerances available today are ± 0.05 mm for ring magnets in mass production, which is surprisingly bad. For the prototypes used in the experiments shown in Chapter 8, the tolerances are specified to ± 0.02 mm, which required extreme efforts from the manufacturer. Neither losses due to angular misalignments nor due to mechanical eccentricity can be simply added to the other losses, since the currents are very similar and might be overlapping.

Surface roughness and locally varying density causes high frequency small eddy currents, very unlike the ones caused by a two-pole flux. These losses add very well to the other losses, since most of the currents are not overlapping. The high frequency currents are bound to the surface of the conducting cylinder, due to smaller skin depth. The losses might also be quite large due to the frequency. Surface roughness is primarily caused by diamond thread cutting or by the modern water cutting method. For use in magnetic bearings this method should be followed by grinding, which unfortunately is quite expensive.

Since it is very difficult to know from one measurement which of the above mentioned magnet imperfections that cause the losses, the sum of these losses will be denoted P^i , where “ i ” stands for inhomogeneity. The total bearing losses P_B have to be found by integration using Eq. (5.70) below:

5 Bearing analysis

$$P_B = \iiint_V \rho (I^l + I^v + I^i)^2 dV \quad (5.70)$$

Likely, the current distribution I^i is not known, but instead P^i might have been measured. Then the value of the integral has to be within the boundaries

$$0 \leq P_B \leq 3(P_B^l + P_B^v + P_B^i). \quad (5.71)$$

where the upper limit comes from the worst case when all currents have the same frequency, phase and geometric shape. As before, the subscripts B , *2-row* or *add* tells what part of the bearing the losses belong to.

P^i may unfortunately be a function of as well eccentricity as lateral velocity. Thus this function has to be found by several measurements, which is a tedious job. However, during the experimental phase of the project, a more practical definition of the losses due to inhomogeneity was found.

Magnetic offset

The first two magnet flaws, angular misalignment and mechanical non-concentricity, acts as an eccentricity and causes a magnetic offset. That is, the mechanical center of the bearing may be offset a certain distance from the magnetic center of the bearing, where the magnetic center is defined as the point where the radial forces are zero, regardless of rotational speed. This point is easy to find experimentally, and at this point, or at least close to it, the losses also have a minimum. These losses will be denoted the “no load losses”, or “residual losses”, P^r . If the bearing eccentricity is redefined to be measured from the magnetic center, the residual losses do not include eccentricity terms, and may be added to the load losses. The losses measured in Chapter 8 thus consist of load losses and residual losses

$$P_B \cong P_B^l + P_B^r. \quad (5.72)$$

A few words on eccentricity. When many magnets are used, the magnetic center may differ between all magnets. The magnetic center for the whole bearing is the point where the total radial forces are zero. At this point all individual eccentricities and their loss contributions are treated as a part of the total bearing residual loss, P_B^r .

The velocity losses P_B^v are kept zero during the experiments. They may still not be added to the other losses, but have to be integrated. Thus the upper limit for the total losses in Eq. (5.71) can be rewritten

$$0 \leq P_B \leq 3(P_B^l + P_B^v + P_B^r). \quad (5.73)$$

5.7 Stiffness

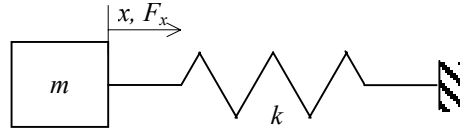


Fig. 5.21. Simple mass-spring system.

Stiffness is defined as the negative derivative of the force and its components with regard to displacement. For a simple one degree of freedom mass and spring system, as the one shown in Fig. 5.21, a displacement x results in a spring force F_x , and the spring constant or spring stiffness k is then defined as

$$k = -\frac{F_x}{x}. \quad (5.74)$$

If the mass is released, it will oscillate with the natural frequency ω_n ,

$$\omega_n = \sqrt{\frac{k}{m}}. \quad (5.75)$$

For a two degree of freedom mass and spring system, like for a bearing rotor moving in the x and y directions, where the force is not parallel to the displacement, three different stiffness definitions will be used.

In-plane stiffness, K

The derivative of the total bearing force F_B with respect to displacement Δr_0 is by Filatov [10] defined as the “in-plane” stiffness, K . Though this definition is not used in literature, it has proven to be very useful in the analysis of electrodynamic bearings. It is responsible for the load capability of the bearing.

$$K = -\frac{dF_B}{d(\Delta r_0)} \quad (5.76)$$

5 Bearing analysis

Rotordynamic stiffness, k

In rotordynamics usually the restoring force component is regarded in the definition of stiffness, k . It can be expressed in several ways,

$$k = -\frac{dF_{R,B}}{d(\Delta r_0)} = -\frac{dF_B}{d(\Delta r_0)} \cos \phi = K \cos \phi \quad (5.77)$$

The rotordynamic stiffness determines the natural frequencies of the system. The first critical speed, provided a rigid shaft and symmetric bearing arrangement, occurs at

$$\omega_n = \sqrt{\frac{2k}{m}} \quad (5.78)$$

where 2 identical bearings each having stiffness k are assumed.

Cross coupling stiffness, k_c

In the same way as above, stiffness can also be defined using the tangential force component. This is referred to as the cross coupling stiffness, k_c , and it plays an important role in the stability analysis of the bearing. Thus

$$k_c = -\frac{dF_{T,B}}{d(\Delta r_0)} = -\frac{dF_B}{d(\Delta r_0)} \sin \phi = K \sin \phi . \quad (5.79)$$

Fig. 5.22 shows the in-plane stiffness calculated using the two different skin depth approximations from Eq. (5.28) and (5.30) respectively. The data are compared with FEM results from Chapter 6.

Fig. 5.23 to 5.24 shows the calculated in-plane stiffness for bearings with different number of rows, (Fig. 5.23) and for bearings with and without pole shoes (Fig. 5.24). In Fig. 5.25 the corresponding force angle is calculated. All calculated data are compared with FEM results from Chapter 6.

Fig. 5.26 shows a comparison of the three different stiffness concepts defined above. Observe that both the in-plane stiffness K and the rotordynamic stiffness k goes asymptotically towards an upper limit when speed increases, while the destabilizing cross-coupling stiffness k_c has a local maximum, and then decreases with speed. This is one of the reasons why it is so easy to establish stable levitation using electrodynamic systems.

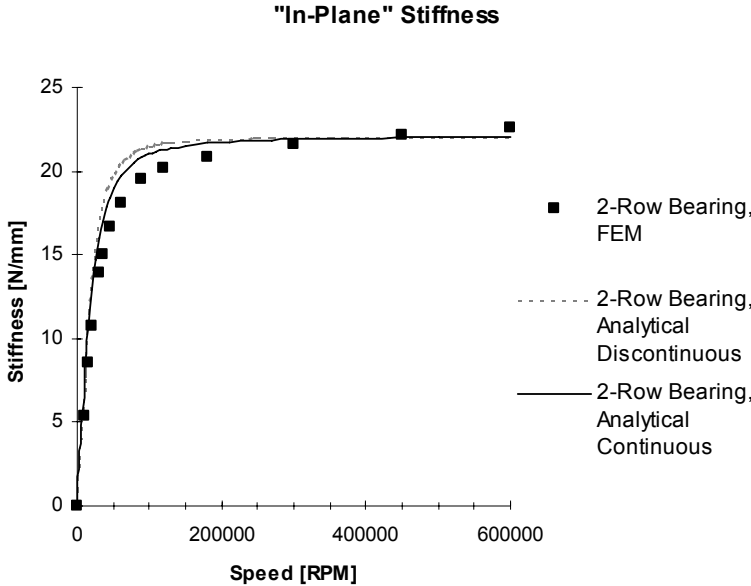


Fig. 5.22. Stiffness calculated using Eq. (5.28) and (5.30). FEM-results shown as reference.

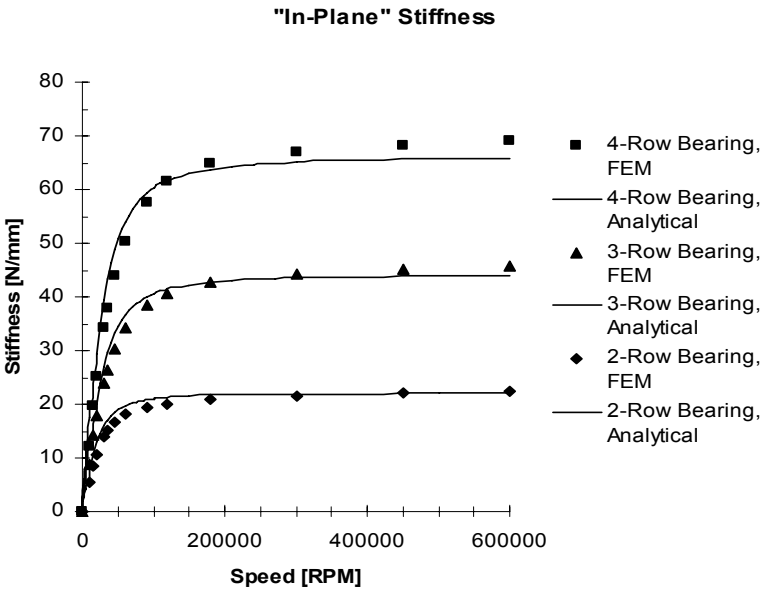


Fig. 5.23. In-plane stiffness versus speed for different intermediate rotor bearings.

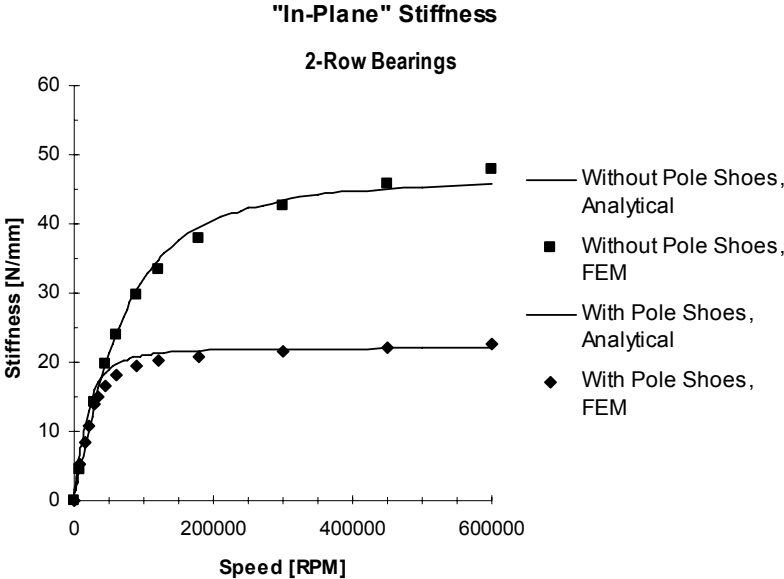


Fig. 5.24. In-plane stiffness versus speed for intermediate rotor bearings with and without pole shoes.

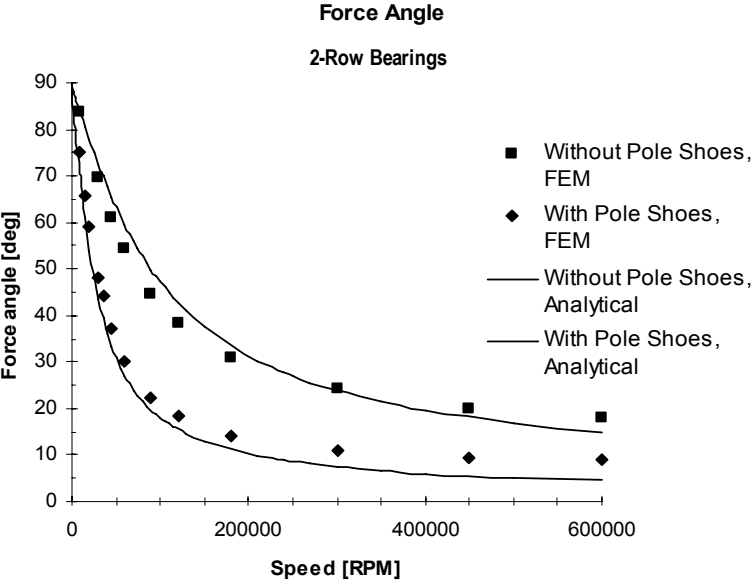


Fig. 5.25. Corresponding force angle for the bearings in Fig. 5.24.

5.8 Damping

In the same way as for the definition of stiffness, the damping coefficient can be defined in different ways, since it does not act parallel and opposite to the velocity.

In-plane damping, C

The derivative of the total bearing force F_B with respect to lateral velocity v is a damping coefficient C taking the total damping force into consideration. It acts in the same plane, but not parallel to, the velocity, and will be denoted “In-plane damping coefficient”.

$$C = -\frac{dF_B}{dv} \quad (5.80)$$

Recalling that

$$\hat{i}_{z,v} = \frac{v}{\omega \Delta r_0} \hat{i}_{z,e} \quad (5.44)$$

means that the damping coefficient can be written

$$C = \frac{K}{\omega} \quad (5.81)$$

Rotordynamic damping coefficient, c

In rotordynamics usually the oppositely directed force component is regarded in the definition of damping, c . It can be expressed in several ways,

$$c = -\frac{dF_B}{dv} \sin \phi = \frac{K}{\omega} \sin \phi \quad (5.82)$$

Cross coupling damping coefficient, c_c

In the same way as above, stiffness can also be defined using the tangential force component. This is referred to as the cross coupling damping coefficient, c_c , where

5 Bearing analysis

$$c_c = -\frac{dF_B}{dv} \cos \phi = \frac{K}{\omega} \cos \phi. \quad (5.83)$$

The cross coupling damping force is directed outward in forward whirl and inward, that is centering, in backward whirl.

Internal and external damping

In literature [17] damping is often referred to as either internal or external, with the coefficients d_i and d_a . Some writers prefer the notation rotating and non-rotating damping and use the coefficients c_r and c_n . A complete theory is built up around these terms. The induction bearing has a rotating conductor, and thus the damping according to this nomenclature is rotating, or internal. Assuming that the induction bearing stator is non-conducting and does not have any hysteresis, then the external or non-rotating damping is zero. It is easy to build in some non-rotating damping in the bearing, but in the analysis it will be assumed that this has not been done.

Below is an attempt to clarify the different damping notations being used.

$$\begin{cases} c_n = d_a \approx 0 \\ c = \frac{K}{\omega} \sin \theta = (c_n + c_r) \approx c_r = d_i \\ c_c = \frac{K}{\omega} \cos \theta \end{cases} \quad (5.84)$$

According to the rather extensive and dominant theory on rotating damping, it is also possible to explain the cross coupling stiffness using the rotating damping. Thus

$$k_c = \omega d_i = \omega d_r = \omega c \quad (5.85)$$

and the tangential force can be expressed as

$$F_T = k_c r = r \omega c. \quad (5.86)$$

However, the theory completely fails to explain the bearing stiffnesses k and K and the restoring force $F_{R,B}$ in Eq. 5.60. The theory also has difficulties to handle the fact that the damping coefficient c decreases with speed. Thus this theory is seldom referred to among researchers in the field of these bearings.

Stiffness Coefficients

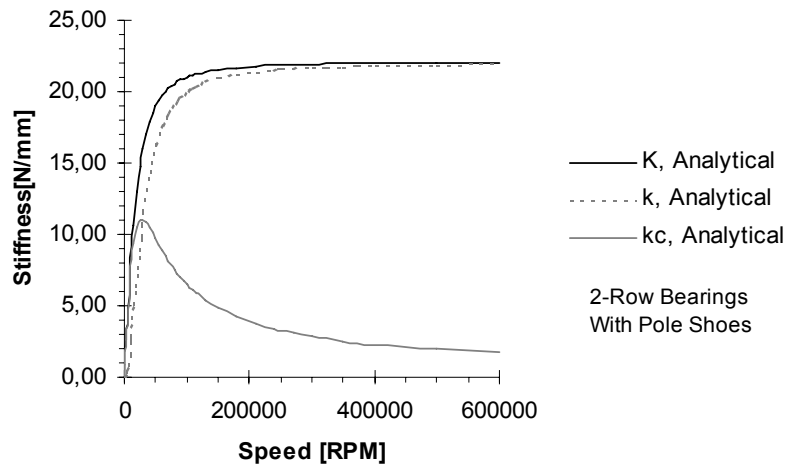


Fig.5.26. Calculated stiffness coefficients for 2-row intermediate bearings with pole shoes.

Damping Coefficients

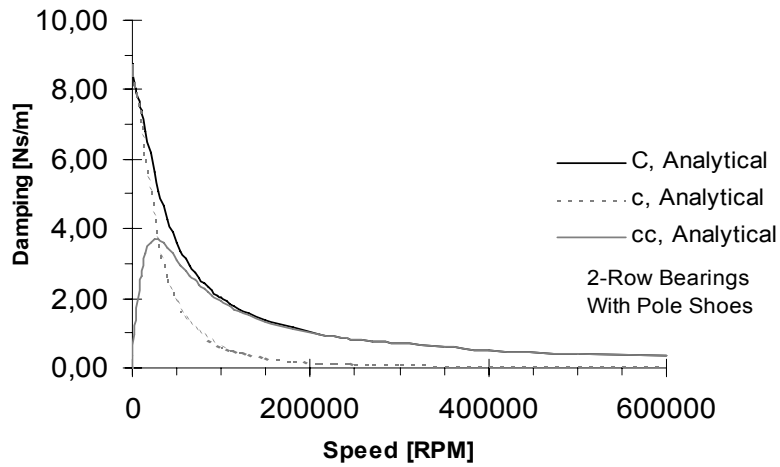


Fig. 5.25. Corresponding damping coefficients for the bearings in Fig. 5.26.

5.9 Rotordynamics

Let us study a few aspects on rotordynamics, to make it easier to compare induction bearings with other bearing types.

A bearing is said to be isotropic if the stiffness is the same in all directions. Tilt pad bearings are for instance not always isotropic. Neither are all active magnetic bearings. Homopolar bearings are.

High stiffness is required in a tool spindle in order to obtain accuracy, while low stiffness is necessary in a centrifuge to avoid vibrations due to imbalance forces. Basically a shaft rotating at a certain speed rotates about its geometric center if the stiffness is high, while at low stiffness it rotates about its center of gravity. A rotor accelerating from stand still to high speed will pass through the first rigid body critical speed, which is the speed where the rotor changes from rotating about the geometrical axis to rotating about its center of gravity. Below the critical speed the rotor is said to run subcritically, and above that speed it runs supercritically.

The first critical speed ω for a rigid rotor with two flexible radial bearings equally distributed from the center of gravity, the bearings not sitting too close to each other, can be calculated from

$$\omega_n = \sqrt{\frac{2k}{m}} \quad (5.78)$$

where m is the mass of the rotor. At this frequency the rotor vibrates so that the axis of rotation is always parallel to the original direction. This mode is called the cylindrical mode.

If the speed is increased another mode will be introduced, the so-called conical mode. The names of the modes refer to the shape of the volumes that are built up by the vibrating shaft. The vibrational frequency for the conical mode depends not on the mass of the rotor as for the parallel mode, but on the moments of inertia. If this moment is very high the conical mode will appear before the cylindrical mode.

Normally a rotor is not as symmetric as described above. This will most likely result in two conical modes, one for each bearing.

At high speed things get more complicated. The two conical modes are split up into four modes due to gyroscopic effects. Depending on factors like rotor

diameter and stiffness several elastic body modes will also be added. A convenient way to represent the different possible frequencies is to map them in a Campbell diagram like in Fig. 5.28. In this diagram the operating line can be drawn, and each crossing with a line referring to a specific vibration mode will represent a critical speed. Some of these modes are more likely to be introduced than others.

If a mode is introduced, the vibration level is normally very high, unless the damping is very good or the acceleration or retardation is high.

Active magnetic bearings offer a very interesting way to eliminate this problem, as the stiffness can be instantaneously altered, as in Fig. 5.29. It is thus possible to temporarily lower the stiffness before passing through a critical speed so that the critical speed is reduced under the actual speed. When the speed is higher the stiffness is raised again. In addition, with active magnetic bearings the damping can be individually programmed for each bending mode for maximum system performance.

Induction bearings offer another possibility to avoid the problem. As the stiffness gradually increases from zero to an asymptotic value when the speed is increased, it is possible to design a bearing so that the rotor always runs supercritically, even at considerably low speed. We call this “resonant free operation”. Fig. 5.30. shows how this is possible.

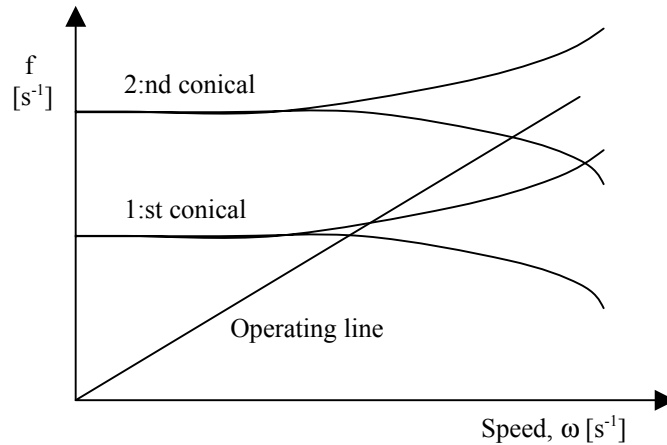


Fig. 5.28. Modal analysis of a rigid unsymmetrical beam.

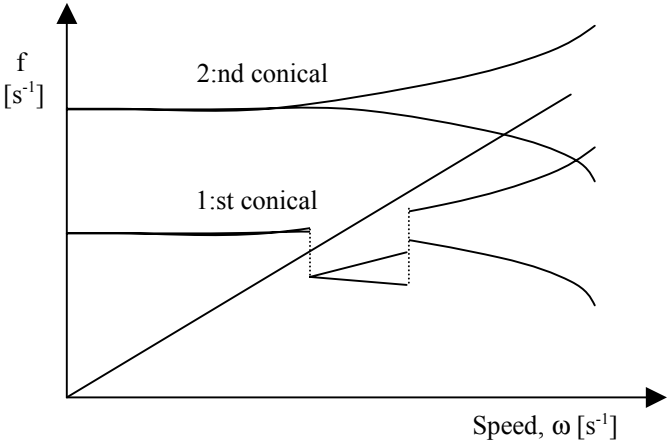


Fig. 5.29. Active control of first conical modes.

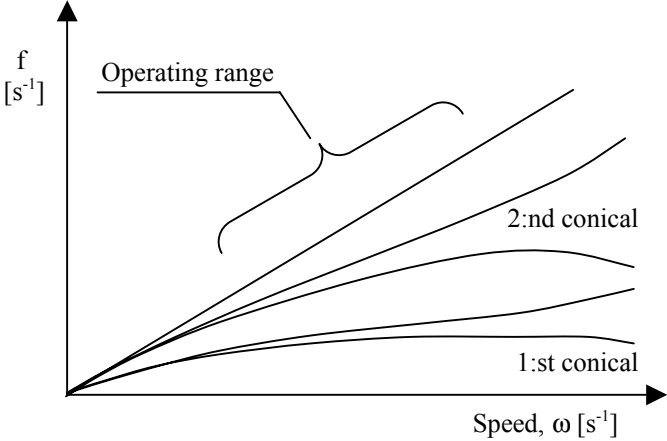


Fig. 5.30. Resonant free operation with induction bearings.

5.9.1 Equations of motion

To study the static equilibrium position of the rotor and its stability, the equations of motion are required. For a two degree of freedom system, thus neglecting gyroscopic effects, and also neglecting effects of imbalance, the system becomes

$$\begin{cases} m\ddot{x} = -kx - d\dot{x} - k_c y + d_c \dot{y} + f_{e,x}(t) \\ m\ddot{y} = k_c x - d_c \dot{x} - ky - d\dot{y} + f_{e,y}(t) \end{cases} \quad (5.87)$$

where $f_e(t)$ represent all external forces acting on the system. The stiffness and damping coefficients k and d and their related cross coupling terms k_c and d_c can be found from the diagrams in Chapter 6 and 8.

These four coefficients can be reduced to two, using the similarities from Eq. (5.77) and (5.79). Thus

$$\begin{cases} m\ddot{x} = (-K \cos \theta)x + \left(-\frac{K}{\omega} \sin \theta\right)\dot{x} + (-K \sin \theta)y + \left(\frac{K}{\omega} \cos \theta\right)\dot{y} \\ m\ddot{y} = (K \sin \theta)x + \left(-\frac{K}{\omega} \cos \theta\right)\dot{x} + (-K \cos \theta)y + \left(-\frac{K}{\omega} \sin \theta\right)\dot{y} \end{cases} \quad (5.88)$$

where the influence from external forces has been neglected. For a certain speed ω , the variables K and θ are fixed, and can also be found from the diagrams in Chapter 6 and 8, or they can be calculated analytically from Eq. (5.77) and (5.79).

Peripheral damping

In all rotating machines, there is always a certain damping from sources that are not always known, like the foundation. Often there are also additional vibration dampers installed. Adding the damping coefficient c_p to the equations of motion will take care of the dynamic effects of this peripheral damping.

Peripheral stiffness

Usually designers of electrodynamic bearings use peripheral bearings as well, providing either positive or negative stiffness k_p . Filatov [10] uses a radial electrodynamic bearing in combination with a passive magnetic axial bearing, which provides negative radial stiffness, and thus has a destabilizing effect on the system. The author has used a passive radial bearing providing positive stiffness in combination with an electrodynamic radial bearing in the

5 Bearing analysis

pump prototype 1, and in prototype 2, the scales, additional stiffness comes from the springs. Thus in order to provide a general system applicable for most types of bearing and damper combinations, the peripheral stiffness as well as the peripheral damping has to be added to the equations of motion, which is done in Eq. (5.89).

$$\begin{cases} m\ddot{x} = (-k_p - K \cos \theta)x + (-c_p - \frac{K}{\omega} \sin \theta)\dot{x} + (-K \sin \theta)y + (\frac{K}{\omega} \cos \theta)\dot{y} \\ m\ddot{y} = (K \sin \theta)x + (-\frac{K}{\omega} \cos \theta)\dot{x} + (-k_p - K \cos \theta)y + (-c_p - \frac{K}{\omega} \sin \theta)\dot{y} \end{cases} \quad (5.89)$$

The equation system above can be rewritten in state space equations and be processed in for instance a software like Matlab to find the bearing dynamics in the time domain for most applications. The external forces $f_e(t)$ may be added to perform harmonic excitations or to find step response and so on.

Auxiliary bearings

Usually some kind of additional bearings are used as a protection for the equipment. They are referred to as auxiliary bearings or emergency bearings. Sometimes also the term landing bearings are used, since most magnetic bearings do not produce any forces when the bearing is at stand still, or is switched off. These bearings normally consist of ball bearings with too large bore, so that they are not in contact with the rotor during normal operation. However, when they do, they provide both stiffness, cross coupling stiffness due to friction, and hopefully also damping. These effects are strongly nonlinear and are usually not treated in the stability analysis above. But their study is important, and simulations can be done in the time domain for specific application setups. During the early days of magnetic bearings, an emergency bearing contact usually resulted in a crash, but today the knowledge has grown in this field, and a contact may not be so devastating. The author [5] has demonstrated plain emergency bearings that can operate for several minutes at bearing contact.

5.9.2 Static Equilibrium

When the rotor is exposed to a static load W , like gravity, the equilibrium position will move to a new equilibrium position. This position is found by setting all time derivatives in Eq. (5.87) or (5.88) to zero and introducing the force

$$f_{e,y} = -W . \quad (5.90)$$

Solving the equations of motion shows that the new equilibrium will move along a line defined by the force angle θ . This line is in fluid film bearing dynamics known as the static load line, and is usually derived for either constant speed or constant load. Fig. 5.31 below shows the static equilibrium and the load line derived for constant speed. The displacement along the static load line is

$$\Delta r_0 = \frac{W}{K} . \quad (5.91)$$

The new equilibrium position (x, y) is, when the load is directed downward as in Fig. 5.31,

$$(x, y) = (\Delta r_0 \sin \theta, -\Delta r_0 \cos \theta) = \left(\frac{W}{K} \sin \theta, -\frac{W}{K} \cos \theta \right) . \quad (5.92)$$

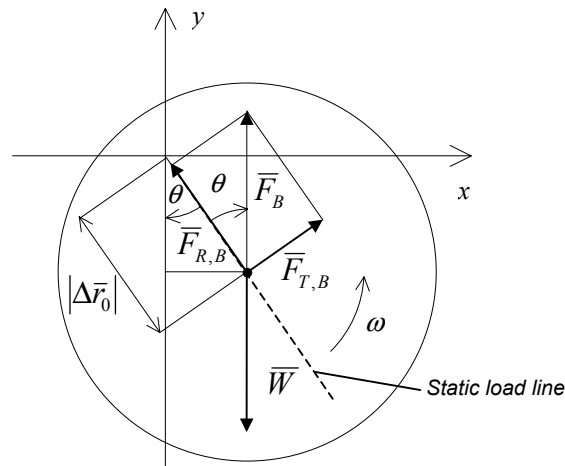


Fig. 5.31. Static load equilibrium.

5.9.3 Load Range

When load is increased, the eccentricity will eventually grow so large that emergency bearing contact will take place. To calculate this force it is convenient to use the “in plane stiffness“ K . The eccentricity takes place along the static load line. The load and the bearing force are identical but oppositely directed in the equilibrium position. Using Eq. (5.91) and replacing the displacement Δr_0 with the available airgap g_a gives the bearing force at emergency bearing contact

$$F_{B,\max} = K \cdot g_a . \quad (5.93)$$

Emergency bearings are normally mounted so as to limit rotor movements to a region within 50% of the total airgap g . Thus

$$g_a = 0.50 \cdot g . \quad (5.94)$$

Note that according to the static equilibrium shown in Fig. 5.31, both the restoring force and the tangential force components are used to carry the load. In Chapter 6 the restoring force is referred to as the lift force, or the y-component of the total force, but this is true only in the case where the displacement is in the negative y-direction, which is always the case in the simulations. Likewise the tangential component is referred to as the side force, or x-component of the force, which is also true only in the particular case of negative y-axis displacements.

Since bearings force is speed dependent, the maximum load should not be applied until the machine has accelerated above the speed for which the maximum load was calculated. If the maximum load is due to the weight of the machine, the load shall be calculated for the highest speed at which safe emergency bearing operation can be guaranteed.

Additional load capability

If higher load is desired, it is possible to add permanent magnets to form a “static unloader” as described in Chapter 4. Such devices can carry very large weights without causing much negative stiffness in any direction. However, no such study has ever been performed to find the maximum levels. Likely, there exists no upper limit for a given maximum allowed negative stiffness. This implicates that very large machines like stationary flywheels can be operated according to this principle.

5.9.4 Stability

The fact that a static equilibrium position exists, as described previously, does not guarantee that this equilibrium is stable.

The standard procedure to analyze the stability of the system defined by the set of equations of motion given in Eq. (5.89), is the Routh-Hurwitz procedure. Filatov [10] has performed a stability analysis according to this procedure, and though his bearing and all coefficients are very unlike the induction bearing presented here, the system of equations is identical. Thus his results can be used.

To solve the Routh-Hurwitz requirements for stability, Filatov made a simplification based on

$$c \gg \frac{K}{\omega m} \quad (5.95)$$

so that the rotational speed dependent terms can be neglected. He also assumed that the lateral velocity v_0 is small compared to the rotational velocity ωr_0 and that the lateral acceleration \dot{v}_0 is small compared to ωv_0 .

If the peripheral stiffness k_p is set to zero, which means that electrodynamic bearing is responsible for all system stiffness, then he was able to show that the system is stable, if the damping coefficient from the peripheral dampers

$$c_e > \sqrt{\frac{K}{m}} \frac{\sin \theta}{\sqrt{\cos \theta}}, \quad (5.96)$$

where it should be pointed out that in his system the mass m is suspended in only one radial bearing of stiffness K .

Since θ decreases with speed, and K increases to an asymptotic value, it means that the system is always stable at high speed, and always unstable at low speed. To improve low speed properties, either more efficient dampers, or a bearing with higher stiffness or lower force angle is required.

Sometimes, like in prototype 1 and 2, it is appropriate to add peripheral stiffness k_p to improve low speed stability. Using this method the author has achieved stability at all speeds, neglecting bending critical speeds.

5.10 Comparison with ball bearing standards

As many parameters are interdependent, data are usually given for certain reference loads. For a ball bearing for instance one reference load is the dynamic load-carrying capacity, which according to ISO 281:1990 is defined so that the probability is 90 % that the bearing lifetime will exceed 1 million revolutions.

Another reference load is the static load-carrying capacity, which according to ISO 76:1987 is defined based on the maximum contact pressure. According to the SKF bearing catalog, this load results in a permanent elastic deformation of the contact surfaces that is approximately 0.0001 of the diameter of the ball.

The static load-carrying capacity is only valid for very low speed applications and thus has no relevance in a high-speed machine.

As a result from the elastic deformation, the inner ring of a ball bearing will rotate in an eccentric position. Also, for other conventional bearing types, there is a certain eccentricity directly proportional to the bearing load and inversely proportional to the stiffness. Thus when heavy load is applied, high stiffness is required in order not to get too large deflections.

This can sometimes be contradictory to results from rotordynamic calculations where lower stiffness may be required for smooth operation.

As was described in Chapter 4 a magnetic bearing offer the unusual possibility to separate the load from the stiffness so that the eccentricity can be chosen at will. Normally the eccentricity is then set to zero during normal operation.

6 FEM -simulations

In Chapter 4 the different bearing topologies were described, and from Chapter 5 we have gained a basic understanding on how the eddy currents are induced and what bearing forces they give rise to. In this chapter, which is the main and most important part of the dissertation, the currents and forces will be analysed using a 3-dimensional finite element method, 3D-FEM.

6.1 Simulation method

The software we will use for the simulations is called MEGA, a 3D-FEM program developed by the University of Bath.

A typical printout from the program is shown in Fig. 6.1, where the current density is represented by coloured areas and the bearing force distribution is represented by arrows.

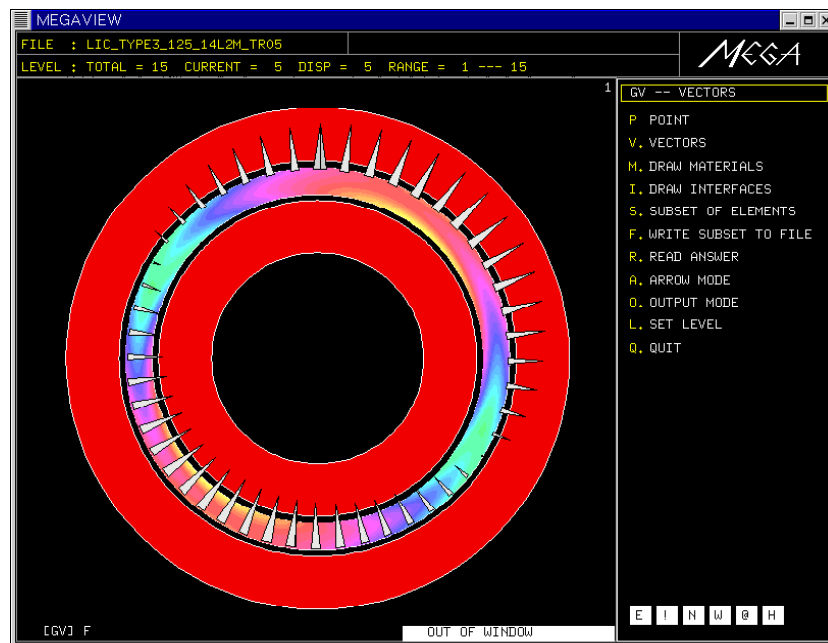


Fig. 6.1. Mega window.

Since 3D-FEM calculations are very time consuming, and this dissertation presents a survey of a vast number of calculations performed during a six year period, much effort was put into selecting the software, and building fast Linux servers.

6.1.1 Software

As this type of bearing configuration represents a true 3-dimensional problem it could not be solved with any of the 2D programs available on the market in 1995 when the project started. Earlier studies by the author on null flux bearings as described in Chapter 2, were performed using the 2D software ACE from ABB, but it could not be used for this task.

The choice fell on Mega, at the time a recently developed 3D FEM program. It was the only identified FEM program that had implemented a velocity solver based on the Minkowsky transform [26].

In 1995, time step solutions was the trend in 2D simulations, but in 3D simulations they turned out to be all too time consuming. The Minkowsky transform makes it possible to solve the rotating field problem in one single calculation.

The Minkowsky transformation increases the number of equations in the eddy current elements by a factor of two. Since about 30% of the elements are used to build up the mesh of the conducting rotor, this means that the total number of equations are increased approximately 30%, which in turn increases the calculation time by 69% compared to the time to solve a single time step. Since a large number of time steps are required, the time saving using the Minkowsky transformation instead of time steps is approximately one day per simulation.

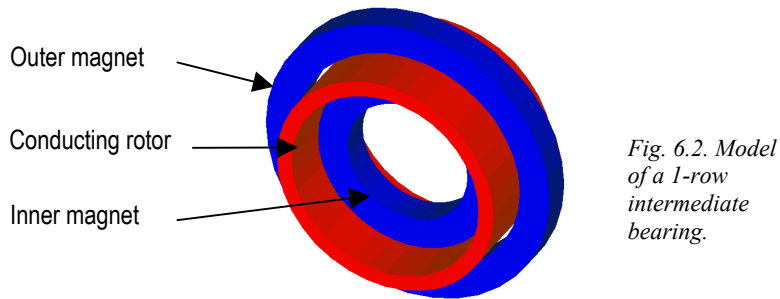
In normal configuration Mega is not optimized for 30% eddy current elements, so the team at Bath had to modify the software used for these calculations.

6.1.2 Platform

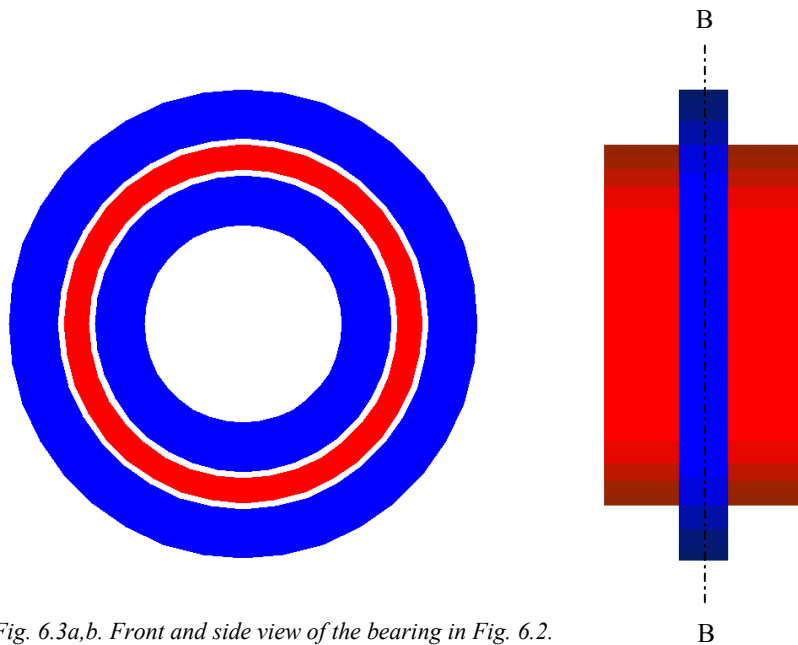
Mega is now run on a 32 bit Linux server using 1 GByte RAM memory, dual 550 MHz pentium processors and 2 parallel fast SCSI hard disc drives. This is the fourth Linux sever built during the project. The maximum allowed number of equations in this configuration is 250,000. To solve more equations a 64 bit processor would be needed. Normally the model size is 150,000 equations which takes about one hour to solve as long as hard disc swapping is not required.

6.2 Model geometry of the studied bearings

All studied bearings have a rotating copper or aluminium cylinder. In the stator there are one or more permanent magnet rings. The stator magnets are located on the outside and/or on the inside of the cylinder as described in Chapter 4. Thus we refer to these bearings as inner rotor or outer rotor bearings. In case there are magnets both inside and outside the conducting cylinder we refer to such bearings as intermediate bearings. Fig. 6.2 shows a



simple intermediate bearing without pole shoes as drawn by the Mega painter subroutine. Due to axial symmetry around plane B-B only one half of the bearing is required to be modeled, Fig. 6.3.



6.3 Symmetry planes and boundaries

In order to reduce the mesh size the following symmetry conditions have been used:

Symmetry plane A-A in Fig. 6.4 divides the bearing axially in two identical halves. The appropriate boundary conditions for this plane are “tangential flux” and “normal currents”. The use of this symmetry should not give rise to any calculation errors.

Symmetry planes B-B and C-C in Fig. 6.4 are used when calculating bearings with more than three poles. They are not “true” symmetry planes and will give rise to minor calculation error. The larger the number of poles the smaller the deviation. For a theoretical bearing with an infinite number of poles the values should be correct as the flux at the planes are not affected by end effect leakage. The boundary conditions in plane C-C are chosen the same as in A-A. In plane B-B the flux lines are perpendicular.

In order to reduce calculation errors for bearings with a limited number of magnets the end effects are calculated separately. Thus for example a bearing with 4 identical magnets as in Fig. 6.4 is calculated as the sum of two ends and four magnet halves. The ends, which are represented by the axial distance between plane C-C and D-D, are calculated in one model, and the magnet halves represented by the distance between A-A and B-B are calculated in a separate model. The first model also includes some levels of air in order to properly deal with the end effects.

Both models are surrounded with air in the radial direction in order to avoid unnatural flux concentration. The side boundaries are “zero A”, that is the field is tangential as above so that no field can escape from the model.

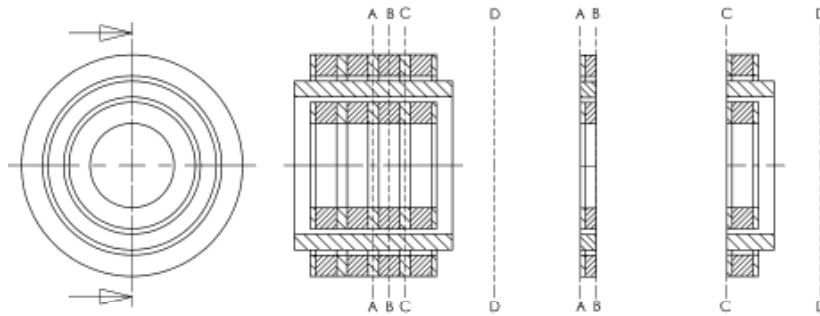


Fig. 6.4. Mega model symmetry planes.

6.4 Mesh generation

A very important aspect of this work is to find a way to create a mesh, which will generate results that are sufficiently accurate. The reason why this is more important for an induction bearing than for a motor or other type of electromagnetic machine is that the losses in the induction bearing are almost zero. Furthermore, post processing of some of the data involves methods leading to cancellation of several significant numbers.

6.4.1 Mesh generation in Mega

Mega differs from many other FEM programs in which the way the mesh is generated. Basically nodes and elements are created to start with, elements being either triangular or quadratic. Initially a two-dimensional mesh is generated, which later is extruded into a three-dimensional mesh. After extrusion the mesh can be modified or skewed to any desired shape. When the mesh is ready, material properties are associated with each element. In Mega materials are denoted regions. A list of the regions used is given in Chapter 6.5.

6.4.2 Comments on automatic mesh generation

It is possible to have the mesh elements generated automatically in Mega. However, as we are designing a bearing with almost zero losses it is utterly important to make a symmetric mesh. When doing parametric changes to the geometry, we want to be sure that the change in the calculated forces is a result from the change in the parameters and not from the change in a newly generated mesh.

6.4.3 Square or triangular elements?

In Mega it is possible to use and combine square and triangular elements. In triangular elements the variables are kept constant, whereas in the square elements they are linearized. We found that we could not use any triangular elements in or close to the eddy current regions, otherwise additional eddy currents would be induced purely related to the bad mesh and with no physical significance.

6.4.4 Structure of the manually generated mesh

In addition to what has been said above, about the importance of the mesh being symmetric, there are some other considerations necessary to be aware of as well. To obtain highest possible accuracy, for a given and limited number of equations possible to solve, it is necessary to find a good compromise between the number of sectors, layers and levels.

6 FEM -simulations

We found an inversely quadratic dependence on stray losses as a function of sector width, while the number of levels had only limited effect on the accuracy. The number of layers on the other hand has to be at least four in the air gap, and in the conducting cylinder there has to be a sufficient number of layers to deal with the penetration depth.

Furthermore the mesh elements, especially in the air gap, shall not be too flat. Mega can handle aspect ratios as high as 80, but it is strongly recommended to use ratios of less than 3. We have tried to keep all elements as close to a quadratic shape as possible, Fig. 6.5 to 6.7.

Close to the airgap it is further recommended that there is a gradually increasing size in mesh elements.

As can be seen from Fig. 6.7, we have not allowed any triangular elements close to the airgap, neither in the magnets nor in the conducting cylinder.

Taking the above discussion into consideration, we estimated that a good compromise was to focus on keeping the sectors narrow, 1.25 degrees each in the airgap, and reducing the number of levels. 15 levels or less were used for most models. We used 4 layers of square elements in each airgap, and between 6 and 10 layers in the conducting cylinder depending on rotor thickness.

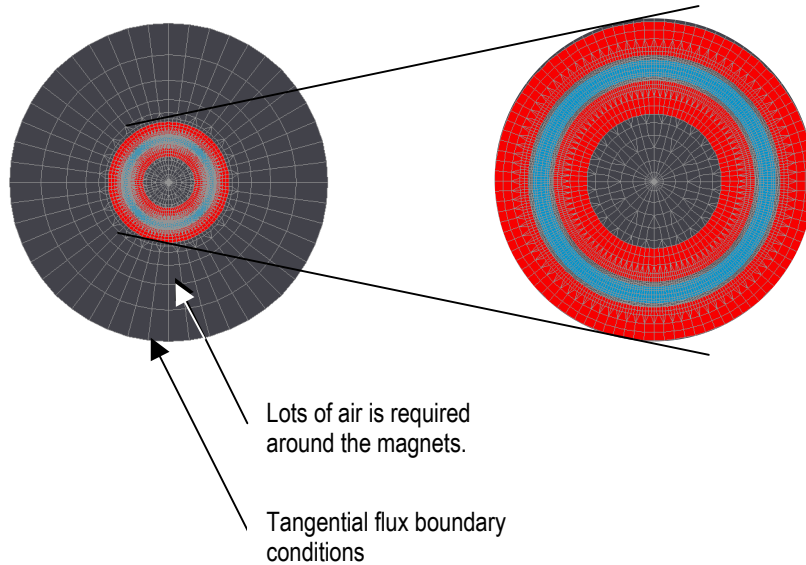


Fig. 6.5. Manually generated symmetric mesh.

The rotor has been translated in the airgap in the negative y -direction when forces due to eccentricity are calculated. Sometimes, as in Fig. 6.7, it has been more convenient to move the stator in the positive y -direction. The result should be the same if the boundaries are far from the rotor, which requires that there is a lot of air outside the magnets, Fig. 6.5. Air is also needed in the z -direction outside the end magnets, which means that we need some levels of air there as well.

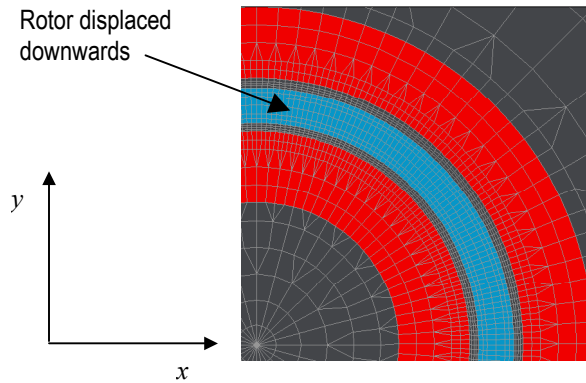


Fig. 6.6. Part of the magnets and the rotor in Fig. 6.5.

Four layers of air, as in Fig. 6.7, are required in the airgap if a proper calculation of maxwell stresses is to be performed. If instead a volume integral of $\mathbf{J} \times \mathbf{B}$ is performed, two layers are enough. With only a few exceptions, we have used four layers for both methods.

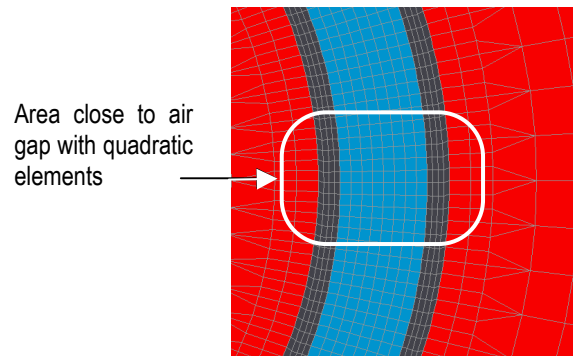


Fig. 6.7. Air-gaps with four layers of elements each.

6.4.5 Influence of mesh size.

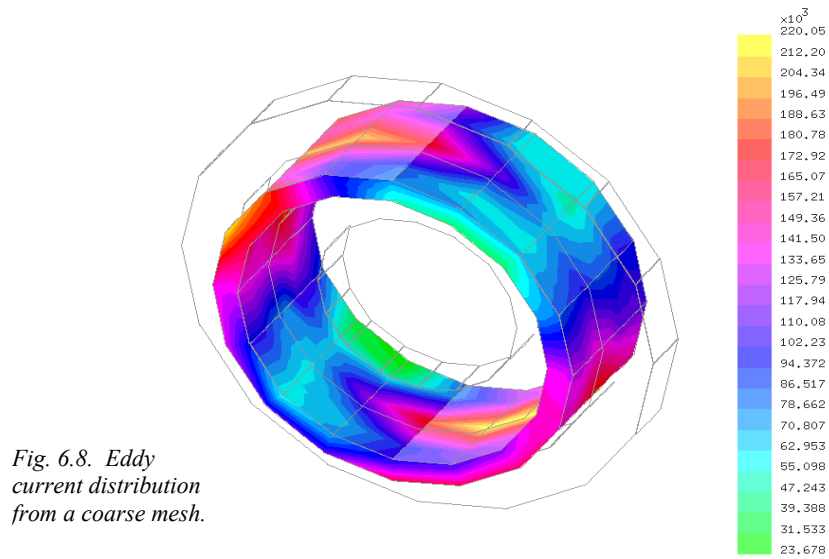


Fig. 6.8. Eddy current distribution from a coarse mesh.

Compare Fig. 6.8 above with Fig. 6.12. The model in Fig. 6.12 has 51,839 equations. All calculations converge and the plotted current distribution is smooth. In Fig. 6.8 the mesh is much too coarse. Throughout this report we have been using between 100,000 and 150,000 equations for end effect calculations and about 50,000 to 60,000 equations for the center magnets. Now consider the coarse mesh in Fig. 6.9. The copper cylinder is rotating with no eccentricity. Thus there can be no induced eddy currents. However, due to the discrete non-circular mesh eddy currents with no physical relevance are induced. Three-dimensional arrows show examples of such currents in Fig. 6.10.

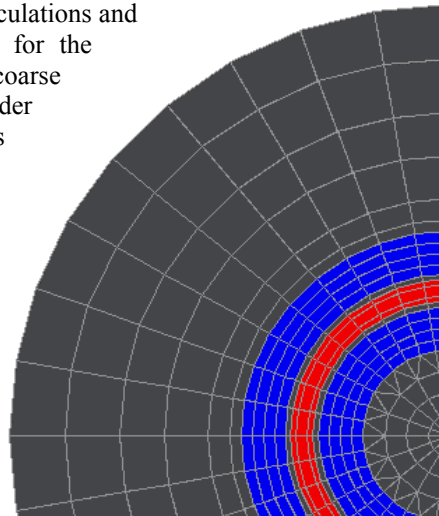


Fig. 6.9. Example of a too coarse mesh.

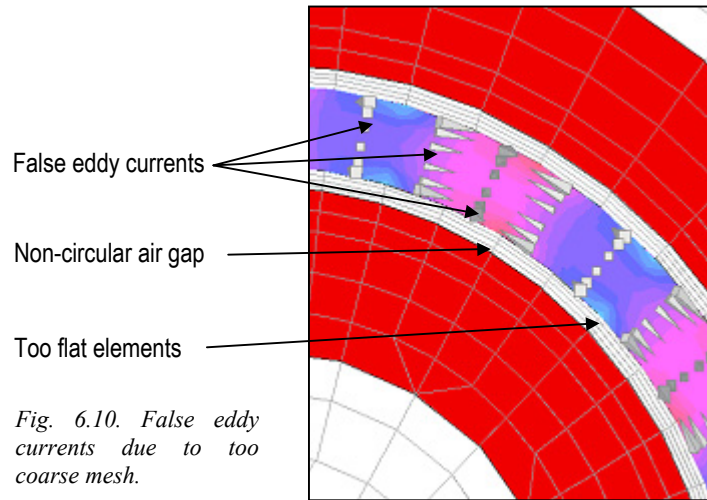
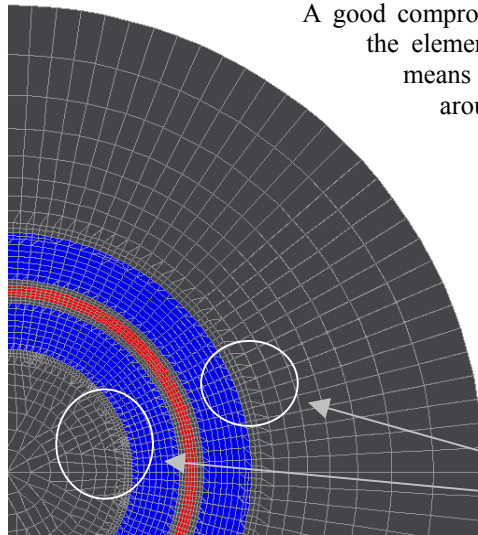


Fig. 6.10 shows the false eddy currents induced solely by the bad mesh. The airgap elements are too wide resulting in a non-circular mesh. In fact the mesh is always non-circular, but by reducing the width of the airgap elements so that the mesh resembles that of circles, these currents can be reduced. It was found that there is a quadratic relationship between the width of the elements and the mesh related fictitious losses.

A good compromise turned out to be to choose the element width to 1.25 degrees, which means that 288 elements are specified around the full circumference.



The triangular elements connecting the arcs of different width have to be made by hand in order to make them symmetric, otherwise results as in Fig. 6.11 can be obtained.

Fig. 6.11. Asymmetric mesh.

6.5 Sources and regions

Each mesh element is given certain material properties like conductivity and permeability. Materials are referred to as regions. Also properties useful for permanent magnets like remanence and direction of magnetization can be applied. Thus there is no need for current sources and surface currents when modelling permanent magnets.

Thanks to the Minkowski transform speed is treated as a region property, so no time step and no sliding interfaces are required.

The following data for the material properties in the different regions have been used:

Copper cylinder

$$\sigma = 60 \cdot 10^6 \text{ (}\Omega\text{m)}^{-1}$$
$$n = 9,000 - 600,000 \text{ rpm}$$

Iron pole shoe

$$\mu_r = 300 \text{ (or nonlinear construction steel)}$$

Powder pole shoe

$$\mu_r = 1 - 500$$

Ferrite pole shoe

$$\mu_r = 1,000 - 40,000$$

Magnets

$\mu_r = 1.0$ or 1.05 (Flywheel bearing)
 $B_r = 1.0$ magnetized in cartesian z- direction. Flywheel radial magnets are radially magnetized.

Distance rings

$$\mu_r = 1.0$$
$$\sigma = 0 \text{ (}\Omega\text{m)}^{-1}$$

6.6 Eddy current distribution

When the bearing is operating in an eccentric mode eddy currents are induced in the conducting cylinder, as has been explained in Chapter 5. However, since the conductor is a homogenous bulk cylinder, the simplified eddy current paths described in Chapter 5 has to be modified to a more continuous current distribution. Fig. 6.12 below shows the modulus of the current densities on the surface of a single row intermediate bearing.

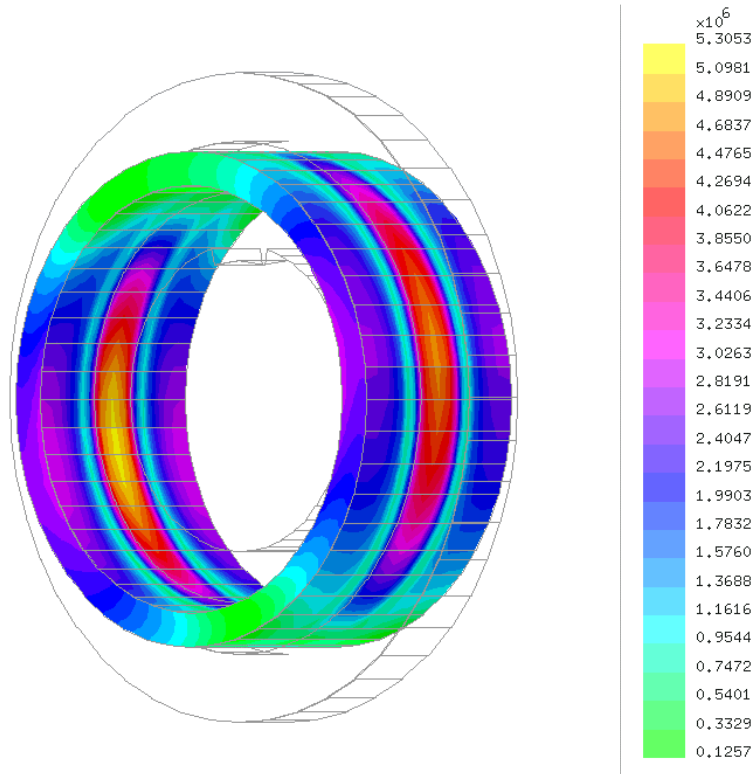


Fig. 6.12. Modulus of the current density [A/m^2] plotted on the surface of a single row intermediate rotor bearing.

The tangential currents in the middle, close to the magnets and colored red and yellow, represents a current density of $4 - 5 A/mm^2$. The return currents on the sides are blue representing approximately half that value.

Inside the cylinder the current density will be highest on the surface close to the magnets and decrease inside the material, Fig.6.13a. This can be even better viewed in the flywheel bearing in Fig. 6.13b.

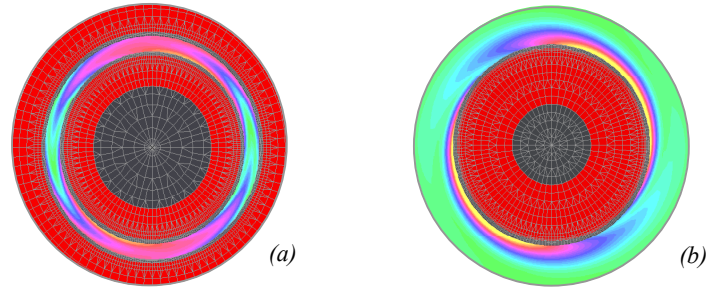


Fig. 6.13. Eddy current density. a) Intermediate rotor bearing.
b) Flywheel bearing.

Especially the flywheel bearing illustrates this since that particular bearing has a rotor cylinder that is very thick. The currents have no chance to penetrate the whole cylinder. There are two reasons for the current decay inside the cylinder:

- Exponential decay of radial flux due to skin effect.
- Geometric decay of radial air gap flux density due to the pole design.

Thus when designing the conducting cylinder there is no meaning in having a cylinder wall that is much thicker than one skin depth. The skin depth should of course be calculated for the lowest operating speed, since the skin depth is larger at low speed. In case both inner and outer magnets are used, the wall thickness may be as high as 2 times the skin depth, since the flux is penetrating from both sides.

In Chapter 5 we derived an expression for the current density based on the flux derivatives. In order to give a complementary and very simple explanation of the direction of the main eddy currents, neglecting the stray ones, we can use Ampere's model of a permanent magnet combined with Lentz law. According to Ampere the magnet can be described as covered with a current sheet around the poles where the surface current density J_s equals the intrinsic remanens of the magnet divided by μ_0 , see Fig. 6.14a. The sheet closest to the conducting surface will have the most influence on the induced currents, and according to Lentz law a voltage will be induced that will drive a current so as to counteract any change of flux. Thus the direction will be opposite, that is repulsive, with respect to this current sheet when that part of the conducting cylinder is closing up to the magnet, and equally directed, that is attractive, when that part of the cylinder is moving away

from the magnet, Fig. 6.14b. Thus the currents will try to simultaneously push and pull the rotor back to the center whenever it is displaced.

To fully explain the current distribution it is necessary to take the phase shift due to the inductance into consideration, which varies from close to zero degrees at low speed and approaches 90 degrees at high speed.

In Fig. 6.14a-c the speed is high, 90,000 rpm, and the force is almost parallel. Using the Ampère surface currents in Fig. 6.14a and comparing it with the real currents in Fig. 6.14b it is easy to understand how repulsive and attractive forces occur in the bearing. This model also helps understand which parameters that are important when optimizing the bearing.

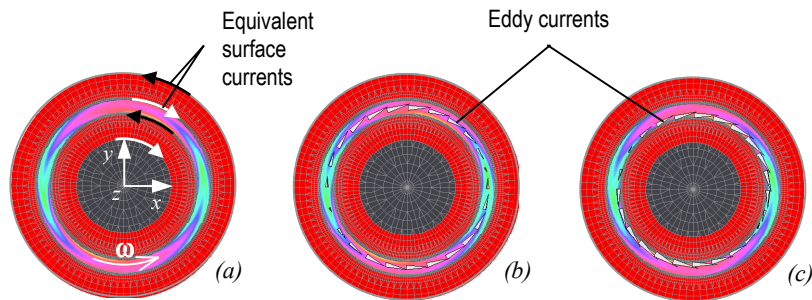


Fig. 6.14a-c. Currents in an intermediate rotor bearing. a) Equivalent surface currents. b) Eddy currents inside the rotor. c) Eddy currents on the surface of the rotor.

6.6.1 Field diffusion

The phase shift is of great importance for the force distribution and for bearing stability. Thus we will perform many parametric studies to see which variables influence the phase shift, and discuss to what extent they can be optimized. But we can make some conclusion directly from Fig. 6.14. Compare Fig. b) and c). The speed and the eddy currents are the same, as can be seen from the colors. But we have chosen two different subset of elements in which we display the current vectors. In Fig. 6.14b the middle of the cylinder is chosen, and in Fig. 6.14c the inner surface has been chosen. There is a clear phase shift between the eddy currents in the middle and the ones on the surface, to the benefit of the former, since we want the phase shift to be as large as possible. This is due to the time it takes for the currents to penetrate the conducting material. Thus it is obvious that in order to decrease the force angle we should use a thick cylinder. However, we concluded above that it is no use to have it much thicker than one skin depth, so from the stability point of view we have already fixed one variable.

6 FEM -simulations

In Fig. 6.15 a flywheel bearing is analyzed at three different speeds. To the left the speed is only 15,000 rpm and the current density is low. In the picture in the middle the speed is increased to 45,000 rpm and the currents are much larger. But there is also a phase delay, which increases with increasing radius. At high speed, 90,000 rpm, this effect is very dominant, as can be seen to the right. This effect is called field diffusion, and these pictures clearly illustrate the well known electrodynamic field diffusion equation.

6.6.2 Importance of flux derivatives

To fully understand the bearing we have to emphasize the importance of flux derivatives. It must be remembered that the eddy currents are generated by time derivatives of the magnetic flux as seen from the rotor, and not by the flux itself. A strong flux does not guarantee large eddy currents, and vice versa there can still be large eddy currents in the center of the cylinder even if this part is operating in a null flux region. Such a region can be generated by counteracting magnets acting on both sides of the cylinder as in the intermediate bearing arrangement presented in Fig. 6.14. The intermediate bearing has the lowest radial flux but as we will see it has the largest stiffness of the three bearing types presented in this report. This is because it has the largest radial flux derivatives.

Finally, a last important aspect will be given before we start calculating the forces and doing some parametric studies: Large time derivatives are caused by large radial space derivatives, which requires large changes over small distances. But above we concluded that for good stability we should use thick walled cylinders to reduce resistance, which is contradictory to the first demand. Thus we can expect that we can never optimize a bearing for both maximum stiffness and maximum stability at the same time.

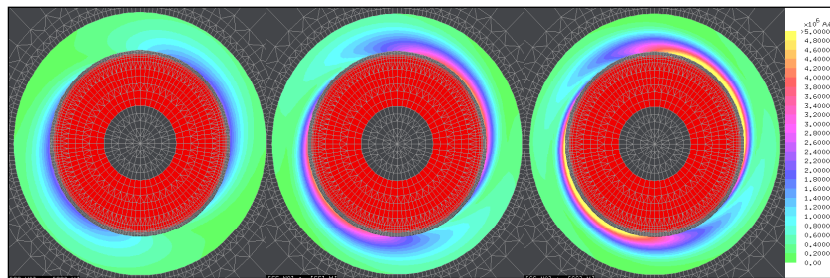


Fig. 6.15. Flywheel bearing. Field diffusion illustrated by the eddy current distribution for different speeds.

6.7 Bearing forces

In Mega there are basically four methods to calculate forces. They all have some advantages and disadvantages. They are:

1. Volume integral of Lorenz forces
2. Surface integral of Maxwell stresses
3. Magnetic potential energy difference
4. Volume integral of Joule heat

The volume integral of Lorenz forces is very accurate since it involves a lot of elements. It does though become less accurate at very high speed due to the fact that the skin effect reduces the number of elements carrying relatively large current, as can be seen in Fig. 6.16a-d where these elements are yellow. The surface integral of Maxwell stresses does not have this problem, since the air gap surface area is constant at all speeds. The disadvantage of Maxwell stress is that for a bearing with more than one air gap, like the intermediate bearing, the surface integral has to be calculated twice in the post processor. The volume integral does only have to be calculated once.

If ferromagnetic materials are used in the rotor, Maxwell stresses have to be used, since Lorenz forces does not take the attractive and destabilizing force between iron and magnets into consideration. Many such calculations were performed, but in this dissertation we will focus on bulk rotors without iron parts.

Energy methods are sometimes useful, but only a few were performed since they require two calculations for each value, and the result obtained is suffering from severe cancellation.

Joule heat can be used to calculate brake torque and bearing losses, and thus equals the mechanical losses in the bearing. Thus

$$\frac{1}{\sigma} \int J^2 dV = M_z \cdot \omega = P_{loss} \quad (6.1)$$

Of the four methods Joule heat is the one most sensitive to mesh accuracy. The reason is that a non-circular mesh will induce additional stray eddy currents. These currents will introduce forces and losses, but the Joule heat losses are squared and thus always positive, while the torque calculated by method 1 and 2 contains both positive and negative contributions, which are summed and thus cancelled. Thus losses calculated using method 4 are always too high. We did not use this method very much, just for comparison. It is though possible to calibrate the result by subtracting the losses calculated

6 FEM -simulations

when the rotor is running in the center position, see Fig. 6.18. But this also requires two calculations, which we want to avoid. The Joule heat method can not be used to calculate the restoring force in the y-direction, F_y , but it can actually be used to calculate the side force in the x-direction F_x , provided that the flux is truly homopolar. In the latter case M_z and F_x are related as:

$$M_z = yF_x = -g\epsilon F_x \quad (6.2)$$

To conclude, all methods were used for comparison until the mesh was sufficiently good and the values converged. During the rest of the study only the Lorenz forces were used, since they provide the fastest method, and yet gave as accurate results as the Maxwell stress method once the mesh was acceptable. Fig. 6.17 and 6.18 show a comparison between the results from 3 of the methods.

To view the forces in Mega, it is possible to select a subset of elements and draw the forces as three-dimensional arrows as in Fig. 6.16a-d. The colors represent the current densities as before. It can be seen that in the areas with largest current densities, yellow areas, the forces are the largest, as expected.

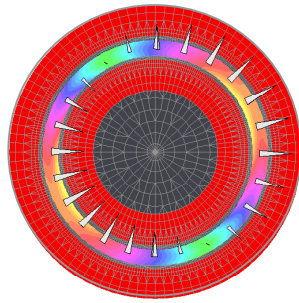


Fig. 6.16a. 30,000 rpm.

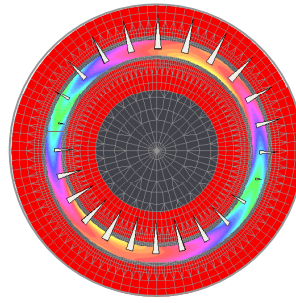


Fig. 6.16b. 60,000 rpm.

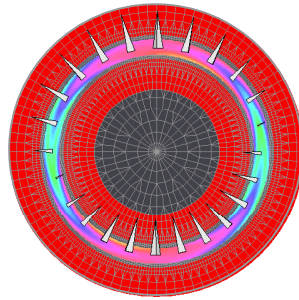


Fig. 6.16c. 90,000 rpm.

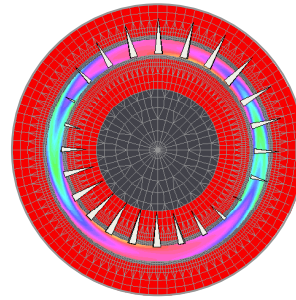


Fig. 6.16d. 90,000 rpm.

Lift and Side Forces

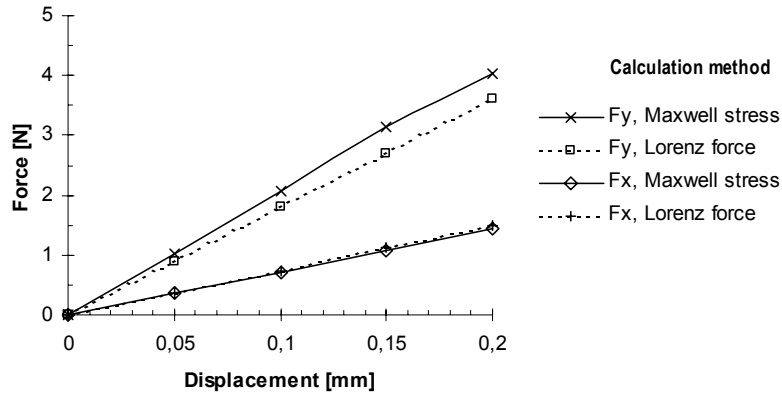


Fig. 6.17. Lift force F_y and side force F_x calculated using different methods. Same bearing as in Fig. 6.16, but without pole shoes. 90,000 rpm.

Brake Torque

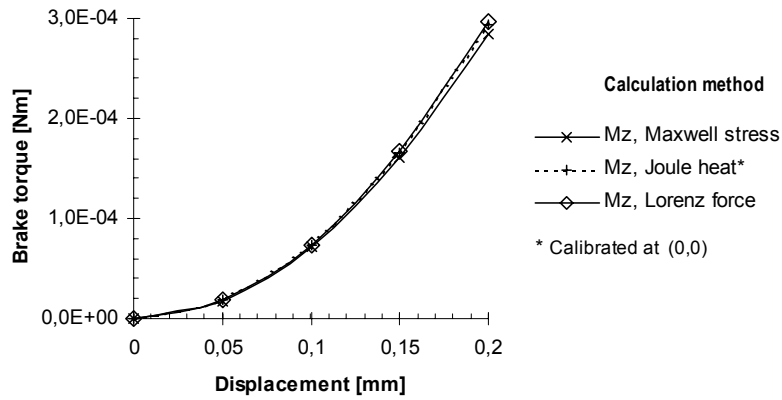


Fig. 6.18. Torque calculated at 90,000 rpm using three methods.

6 FEM -simulations

The forces we want to calculate with Mega are the restoring lift force in the y-direction and the side force in the x-direction. We also simulate the brake torque to cross check it with the force x-component. From these values we then can derive the in plane stiffness, the force angle and finally the losses.

To analyze Fig. 6.16 a little bit closer, consider the direction of the forces, and compare Fig. 6.16c,d with Fig.6.14b,c. It can be seen that the forces in each element are always perpendicular to the currents. Further, the direction changes gradually as speed increases. The x-component is relatively large at low speed and decreases drastically at high speed. (It should be noted that in Fig. 6.16 the colors and arrows are recalibrated for each new picture, so they can't be used to compare the actual values of the forces or current densities between two pictures. However, in Fig. 6.15 the same scaling parameters are used to enable comparison.)

At 90,000 rpm it seems like the force is perfectly restoring and that the force angle is zero, but this is true only for the elements in the middle of the conductor, Fig. 6.16c. In Fig. 6.16d the speed is the same, but the subset of elements is chosen close to the rotor surface where the phase delay is less. Here it is clear that we still have a considerable x-component of the force. The volume integral

$$\bar{F} = \int \bar{J} \times \bar{B} dV \quad (6.3)$$

results in the average of the Lorenz forces over all elements in the cylinder. The average will always contain a certain x-component, which we will try to limit by finding a proper bearing design.

From Fig. 6.16 it is clear that speed is a very important variable in determining the side force. Also restoring forces are speed dependent, as we know from Chapter 5. Let us continue our study by plotting these forces versus speed for the intermediate-bearing model in Fig. 6.16. A principle sketch of this type of bearing can be found in Fig. 4.4. Rotor displacement is 50 μm in the negative y-direction. The results can be found in Fig. 6.19-6.20 and the bearing data are as follows:

Description:	2-row intermediate bearings	
Magnets:	2 outer ring magnets.	38 × 30 × 4 mm
	2 inner ring magnets	24 × 16 × 4 mm
Pole shoes:	1 outer intermediate washer	38 × 30 × 2 mm
(when used)	2 outer end plates	38 × 30 × 1 mm
	1 inner intermediate washer	24 × 16 × 2 mm
	2 inner end plates	24 × 16 × 1 mm
Rotor:	Copper cylinder	29 × 25 × 9 mm

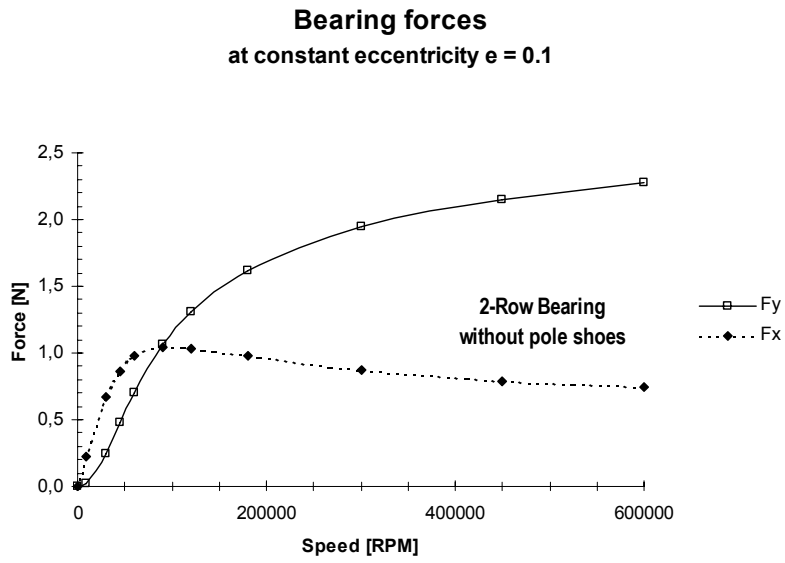


Fig. 6.19. Bearing force components versus speed due to a 10% eccentricity in the negative y -direction.

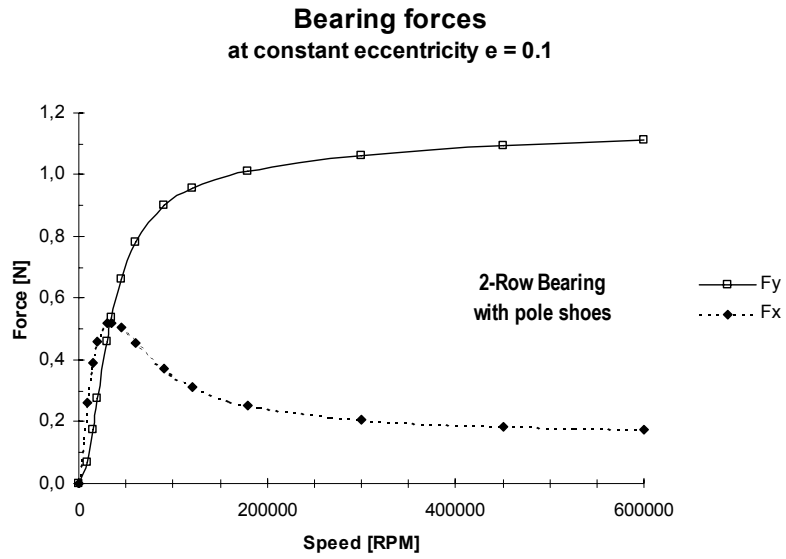


Fig. 6.20. Same bearing as above, but with pole shoes.

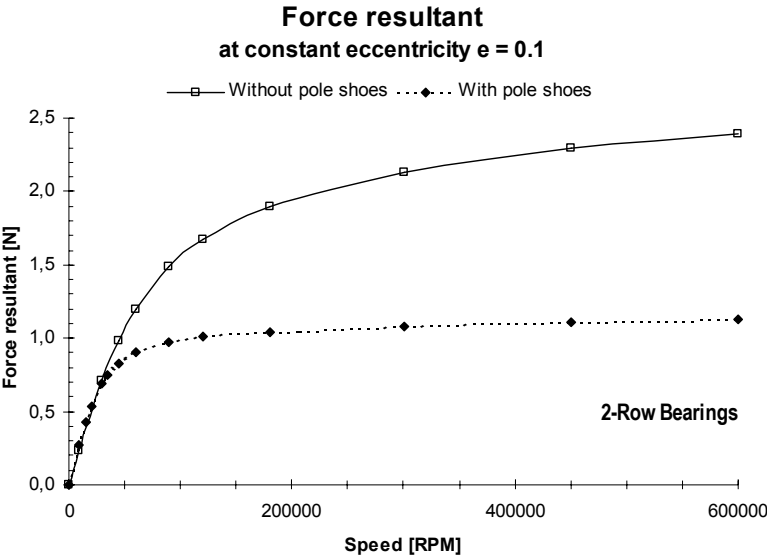


Fig. 6.21. Comparison between resultant bearing forces for the bearings in Fig. 6.19 and Fig. 6.20.

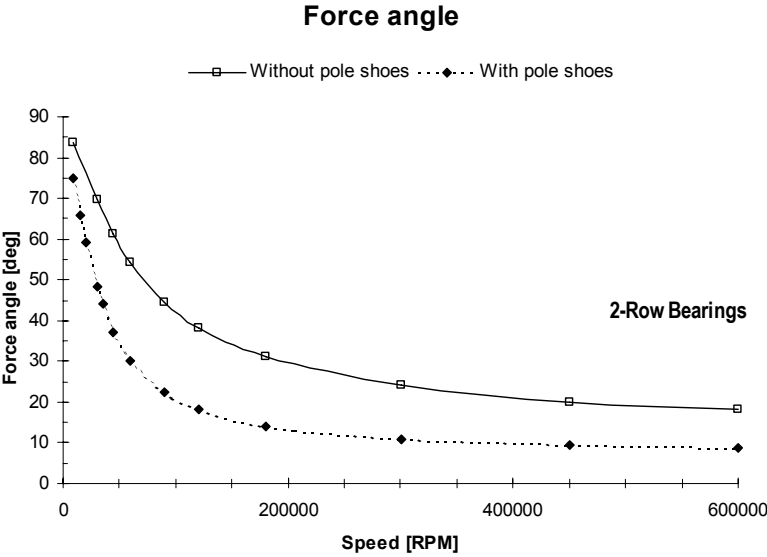


Fig. 6.22. Comparison between force angles for the bearings in Fig. 6.19 and Fig. 6.20.

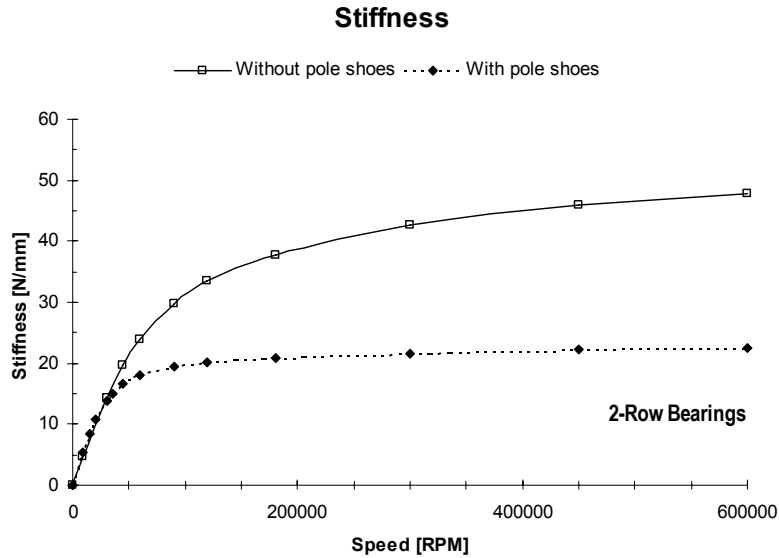


Fig. 6.23. Comparison between stiffness for the bearings in Fig. 6.19 and Fig. 6.20.

In Fig. 6.17-6.20 we have studied how the x and y - components of the bearing force and the losses relates to displacement and to speed. In the speed calculations the displacement was set to 0.05 mm, which corresponds to an eccentricity ε of 10%. We are now able to make some conclusions:

1. F_x and F_y are linear functions of displacement, as predicted.
2. M_z is a quadratic function of displacement.
3. F_x increases linearly at low speed and decreases asymptotically towards zero at high speed.
4. F_y increases asymptotically to a certain finite value at high speed.
5. Iron pole shoes reduce the peak values of F_x and F_y .
6. Iron pole shoes have a positive effect on force angle.

In Fig. 6.21, we have derived the resulting bearing force, using the results from Fig. 6.19 and 6.20. Thus, these values are also valid for an eccentricity of 10%. The corresponding force angle is found in Fig. 6.22.

It is unpractical to use eccentricity dependent quantities. Since the forces are linear with displacement, it means that their relationship expressed as force angle, is constant. Also stiffness is constant since space derivatives of linear functions are constant. Thus neither force angle nor stiffness is dependent on eccentricity. Henceforth we will use these quantities instead of forces. The stiffness curve in Fig. 6.23 is identical to the Fig. 6.21, except for the units.

6.8 Bearing losses

Losses can be calculated directly in the Mega post processor using the volume integral of Joule heat, but due to disadvantages with this method as described earlier losses will instead be calculated from the brake torque. The torque will be calculated as the integral of the Lorenz forces.

In Fig. 6.24 the torque is plotted as a function of speed. The same bearing as in Fig. 6.17 to 6.23 is used, and it is clear that using pole shoes has a large effect on the torque. It not only reduces the torque, it also moves the maximum torque towards lower speeds, which is to be expected with increasing inductance.

Multiplying torque with angular speed is a simple operation, which results in bearing losses for that particular eccentricity, Fig. 6.25. However, we do not have much practical use of this graph. Instead it is much more interesting to study the bearing at constant load, Fig. 6.26. This curve is derived by first dividing the load with the actual stiffness from Fig. 6.23 resulting in the actual eccentricity for that particular speed. Thereafter losses are quadratically extrapolated with respect to eccentricity from the values in Fig. 6.25. The dashed line in Fig. 6.26 represents the emergency bearing, which, according to some often used substandard in magnetic bearing technology, should prevent eccentricity from exceeding 50%.

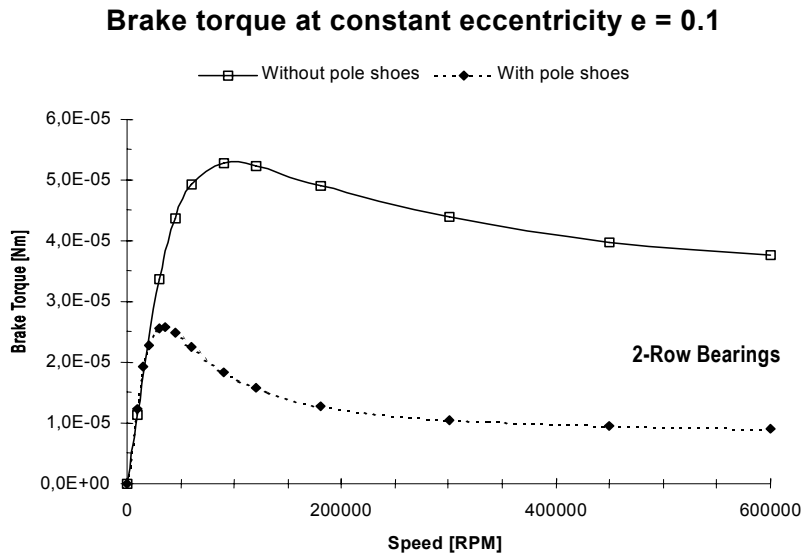


Fig. 6.24. Comparison between brake torque for the bearings in Fig. 6.19 and Fig. 6.20.

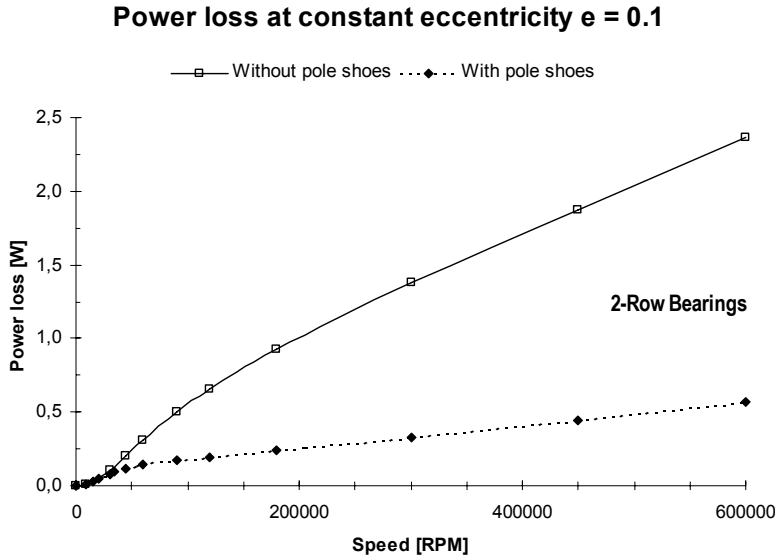


Fig. 6.25. Comparison between power losses at constant eccentricity for the bearings with and without pole shoes in Fig. 6.19 and Fig. 6.20.

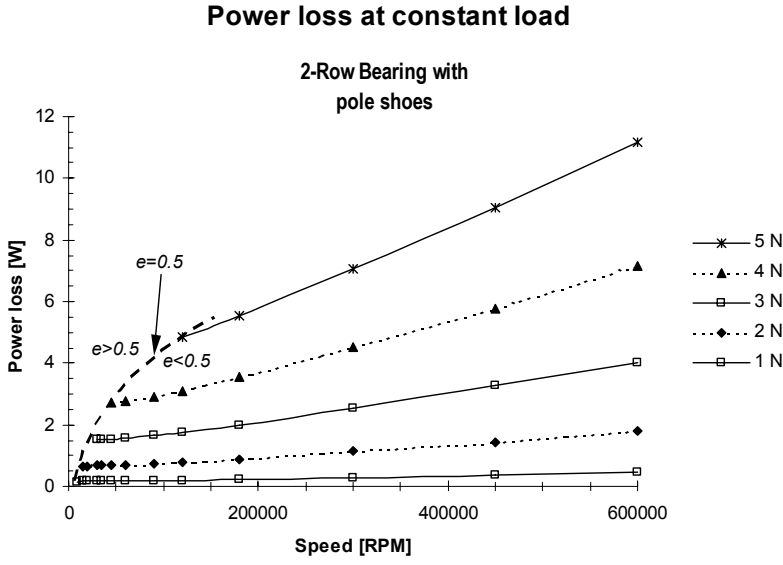


Fig. 6.26. Power loss versus speed at constant load and variable eccentricity. Dashed line shows emergency bearing contact.

6.9 *Parametric optimization of bearing geometry*

The properties of the induction bearing are by nature strongly speed dependent. It is thus important to evaluate all geometric changes at different speed, since the bearing has to be able to operate over a wide speed range. This requires a large number of calculations. In Mega rotational speed can be taken into account either by a time step approach or by using the Minkowski transformation. We have chosen the second alternative since it is the most time saving method.

If high stiffness alone would be the only bearing requirement it could easily be achieved by using large magnets and by always operating the bearing at high speed. Reality is not that simple and we have formulated the following goals for the parametric optimization.

The goal is to find a bearing geometry that

- 1 works well over a wide speed range with regard to stiffness, losses and stability
- 2 reduces the amount of magnet material required for a certain stiffness
- 3 has a design well suited for mass production.

The optimization process will begin with studying how scaling affects bearing properties. After that additional magnets will be added to improve stiffness. The magnets and poles will be optimized with regard to geometric parameters and material properties. Finally leakage flux will be analyzed and prevented.

6.9.1 Influence of scaling

Scaling of magnetic properties is straightforward, and very useful when the operating range has to be moved or extended in any direction. Increasing the bearing size with the linear scaling factor s , affects the bearing properties proportionally to the air gap surface area as follows:

$$\text{Magnetic forces:} \quad F_1 = F_0 s^2 \quad \text{if} \quad \omega_1 = \omega_0 \frac{1}{s^2} \quad (6.4)$$

$$\text{Magnetic torque:} \quad T_1 = T_0 s^2 \quad \text{if} \quad \omega_1 = \omega_0 \frac{1}{s^2} \quad (6.5)$$

$$\text{Stiffness:} \quad K_1 = K_0 s \quad \text{if} \quad \omega_1 = \omega_0 \frac{1}{s^2} \quad (6.6)$$

$$\text{Speed:} \quad \omega_1 = \omega_0 \frac{\sigma_0}{\sigma_1} \cdot \frac{1}{s^2} \quad \text{for a change in conductivity from } \sigma_0 \text{ to } \sigma_1. \quad (6.7)$$

Thus doubling the size will increase the forces a factor of four, if the skin depth has increased proportionally. This in turn requires the speed, (or the conductivity) to be reduced a factor of four.

The magnet material and thus cost, will increase with the volume, which make it a factor of eight.

Temperature affects the remanence of the magnets and the conductivity. For a given bearing that is used in a cryogenic system at a temperature of 77 K instead of at room temperature, the conductivity is roughly 16 times higher and we can expect the same forces at one fourth of the speed due to the conductivity, and some additional force due to the increased properties of the magnets. Thus, this bearing is ideal in cryogenic environments.

Centrifugal forces on a rotor, for instance a flywheel, scales to the square of the peripheral speed. Thus, when scaling a rotor that already is limited by mechanical stress, speed has to be inversely proportional to the scaling factor. Doubling the size requires speed to be one half. But above we have seen that we can reduce speed by a factor of four. Reducing speed by only a factor of two will move us further to the right in the speed diagram, which is advantageous for the stiffness and the force angle. Thus scaling up a machine has a positive effect on bearing performance.

6.9.2 Adding intermediate magnets

Adding an extra magnet to the bearing will of course increase stiffness. However, we have already reached the calculation limit for our FEM program MEGA, so in order to estimate the effect of this additional magnet we have to make a new model of that extra magnet alone, see cut A-A to B-B in Fig. 6.4. This result is then added to our data for the 2-row bearing.

By using proper symmetry conditions as described in Chapter 6.1 we can expect good agreement with reality for bearings with many magnets. However, there will be an error due to the fact that the current normal to plane A-A may not be the same on both sides of the plane, since we are using different models for the two sides. It is likely that the current is less in the 2-row bearing since it has more flux leakage due to end effects. This error will be most accentuated in 3-row bearings, and will not have any significant effect for bearings with large number of magnets.

Now look at Fig. 6.27. The stiffness from the 2-row bearing is recognized from Fig. 6.23. The second curve in Fig. 6.27 is the result from one additional magnet row. Observe that this single row has about the same stiffness as the whole bearing consisting of 2 rows of magnets! This may seem surprising, but comes directly from a comparison between Fig. 5.10a and Fig. 5.10b. Both currents have the same inductance and operates in the same flux density. Only the resistance differs.

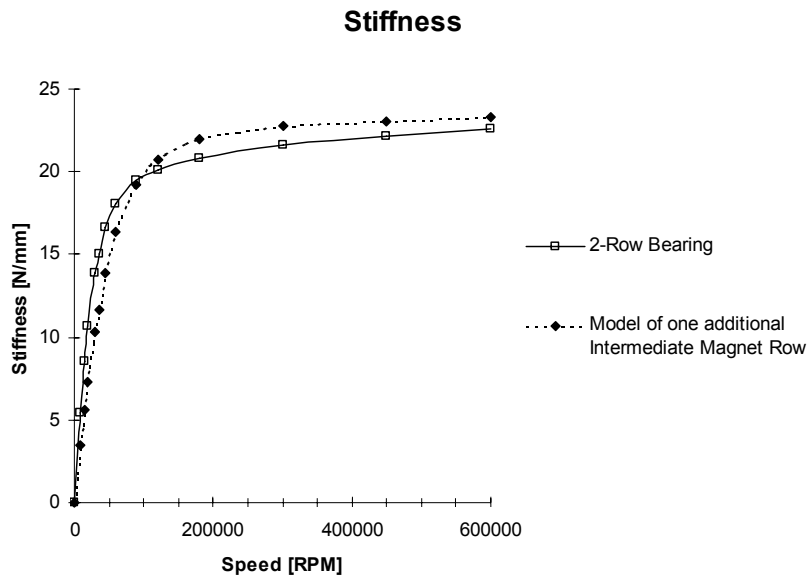


Fig. 6.27. Effect on stiffness by adding more magnet rows.

6.9.3 Optimization of magnet length

In the previous subsection we noted that the intermediate magnets were double as effective as the end magnets. Thus it is obvious that induction bearings shall have many rows and that the optimization work shall mainly focus on these magnets.

A realistic design has to take geometric constraints into consideration. We can't have too many magnets in a high-speed machine since rotor length is critical due to rotor dynamics. Thus we have to choose between either a few axially long magnets, or many shorter magnets to limit the total bearing length.

In Fig. 6.28 stiffness has been plotted versus the axial length of an intermediate magnet pair. The calculations have been performed for two different speeds. There is an optimum around 6 mm at high speed and 9 mm at low speed, when axial constraints are not taken into consideration.

In Fig. 6.29 the results have been divided by the additional bearing length, including the magnet and one additional pole shoe. Here the optimum has changed and the length should be 3 mm at 90,000 rpm and 5 mm at 30,000 rpm, for highest stiffness.

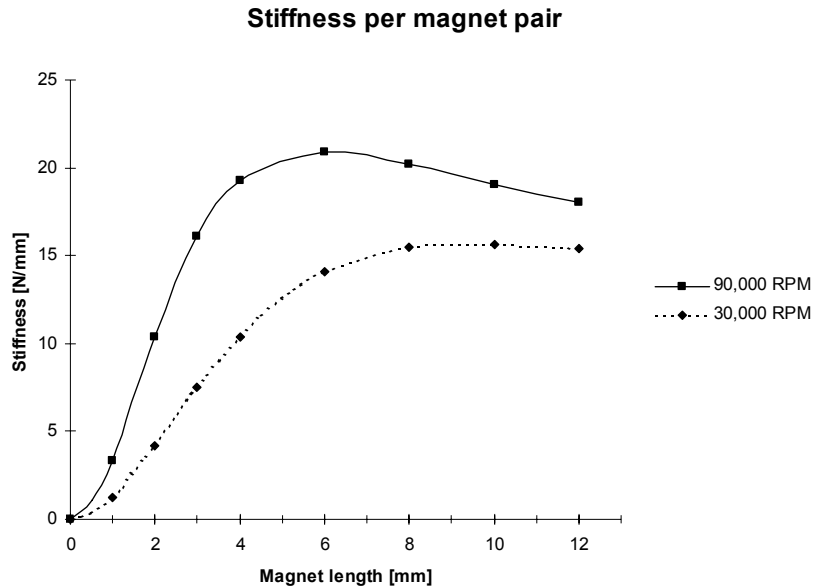


Fig. 6.28. Stiffness as a function of magnet length.

Stiffness per axial length unit

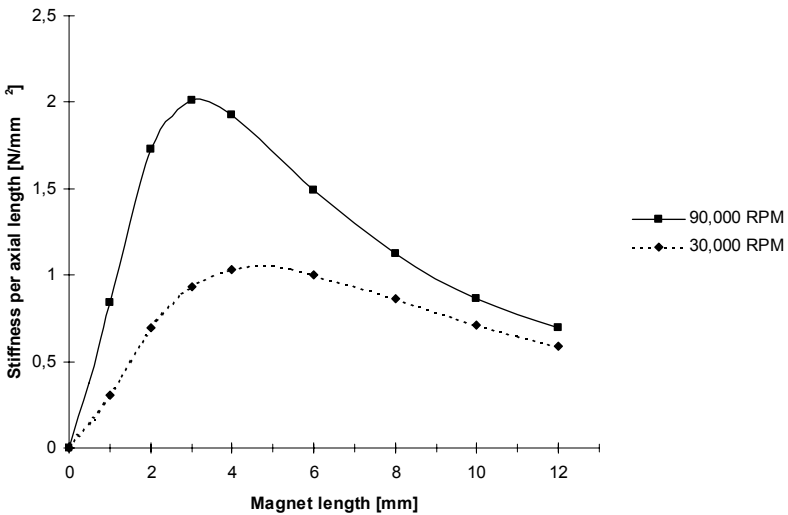


Fig. 6.29. Stiffness per axial length unit versus magnet length.

Force angle

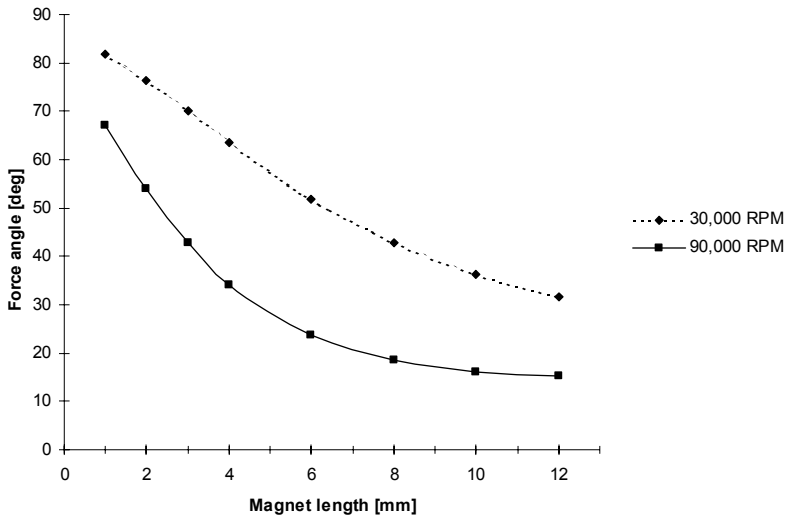


Fig. 6.30. Force angle corresponding to Fig. 6.29.

6.9 Parametric optimization of bearing geometry

In Fig. 6.30 the force angle is shown. If rotordynamic stability is a concern, for instance when damping is difficult to achieve, the force angle is likely the most important parameter to optimize. Long magnets should definitely be used in this case.

For both stiffness and force angle speed is the most important parameter. Thus, it is important to know the operating speed before we can fully optimize the bearing.

In our examples this far we have chosen magnets that are 4 mm long, which is a good compromise between low- and high-speed stiffness. It also has a fairly good force angle at high speed.

With this magnet in mind, we are ready to sum our results and study the properties of magnets with many rows, Fig. 6.31-6.34. All bearings are equipped with pole shoes to decrease the force angle.

In these diagrams, bearings with up to 4 pairs of magnets are plotted. It is trivial to estimate the stiffness for bearings with more magnets simply by summing, and the force angle does not change very much when more magnets are added.

Constant load curves like Fig. 6.26 can be derived for any number of magnets by using the results in Fig. 6.31 and 6.34, as explained earlier.

A little note should be given to the 1-row bearing. Especially from Fig. 6.31- Fig. 6.32 it is clear that it does not quite seem to follow the pattern. The one row bearing is calculated using a separate model. It differs from the other models in that the rotor is considerably longer than the stator. If not, there would be no room in the conducting rotor for eddy current return paths.

In the next subsection we shall study the somewhat complicated effects of the conductor return paths of 2-row bearings.

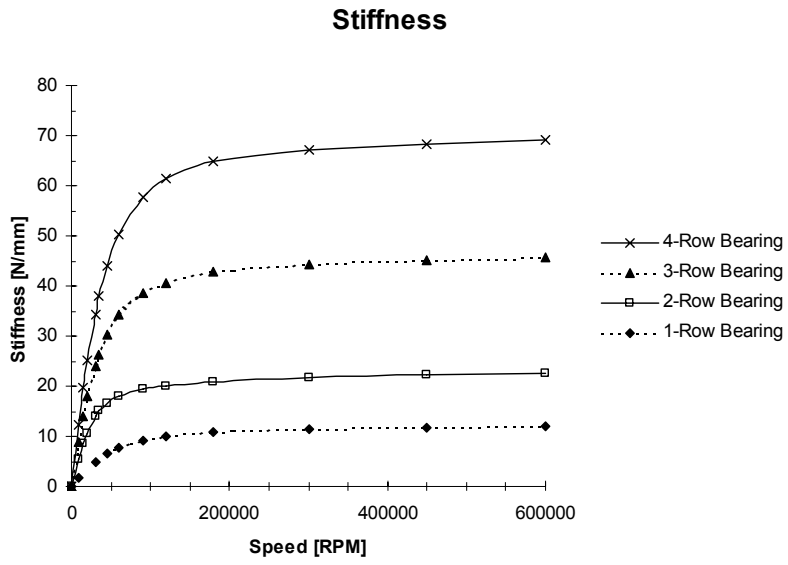


Fig. 6.31. In-plane stiffness versus speed for bearings with different numbers of magnet rows.

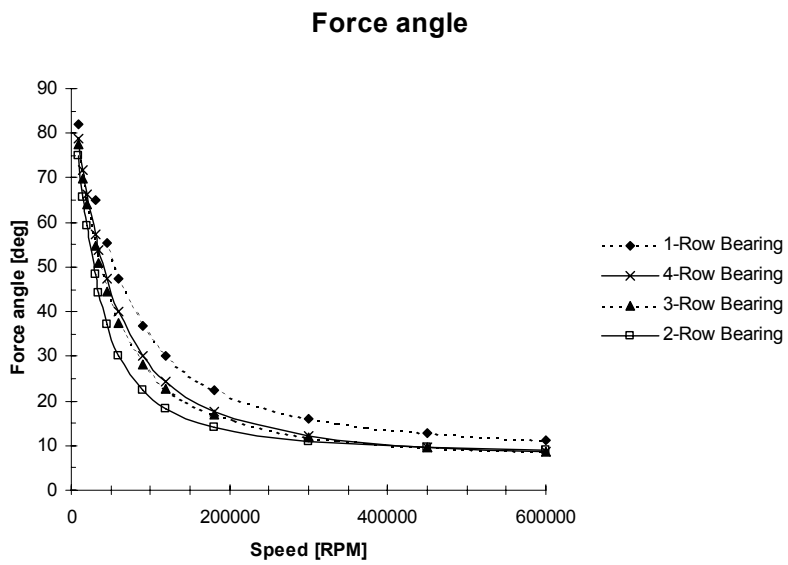


Fig. 6.32. Force angle versus speed for bearings with different numbers of magnet rows.

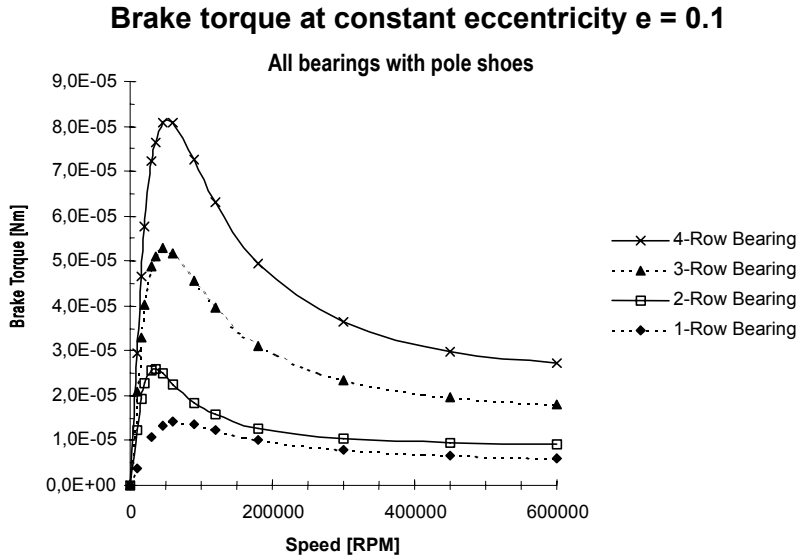


Fig. 6.33. Brake torque versus speed for bearings with different numbers of magnet rows.

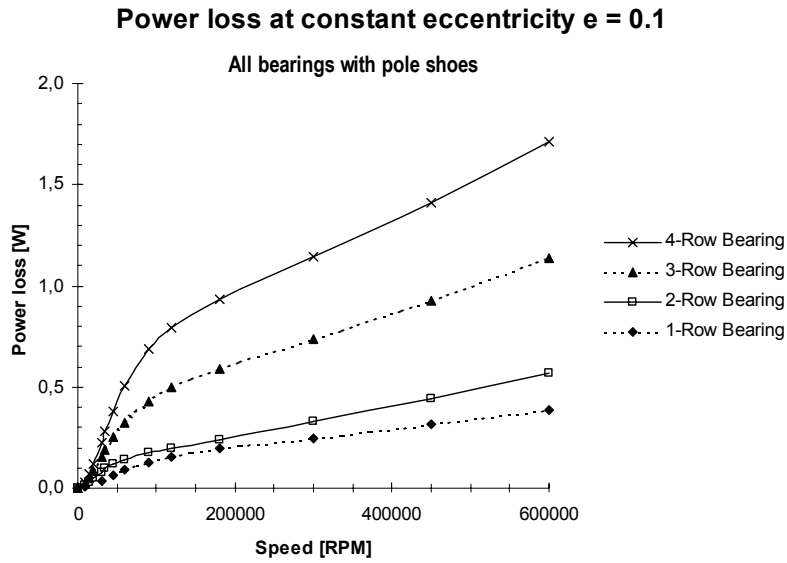


Fig. 6.34. Power loss versus speed for bearings with different numbers of magnet rows.

6.9.4 Optimization of rotor length

We have now optimized the length of the stator, and an interesting question is whether the conducting rotor should be equally long, or if there is a better choice. Fig. 6.37 shows stiffness plotted against relative rotor length for a 2-row bearing spinning at 90,000 rpm. For corresponding force angle, see Fig. 6.38.

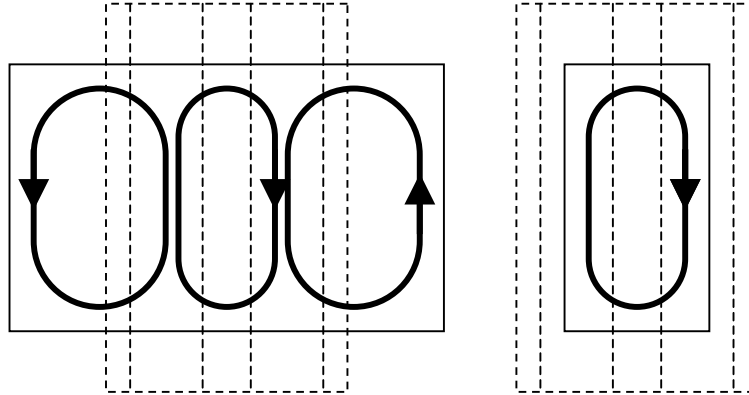


Fig. 6.35. Long rotor to the left, and short rotor to the right. Stator parts dashed.

At first the curves may seem rather confusing, but it is made quite clear when we take a look at the eddy current paths in Fig. 6.35. In the short rotor to the right there is only place enough for the main eddy current. It has no choice, but is forced to circulate close to the magnets where it can produce a large force. But the resistance is comparatively high, since the conductor volume is limited. The long rotor to the left has space enough for stray eddy currents, which help in increasing the active current under the magnets. The worst case, Fig. 6.36, at least when pole shoes are used, is when the rotor is equally long as the stator. There are small and narrow stray currents, and they are situated close to the end plates where they produce negative stiffness, and thus reduce overall bearing performance. Thus, the conducting rotor cylinder should be either somewhat shorter, or much longer than the stator.

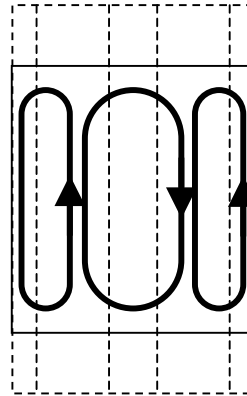


Fig. 6.36. Equally long rotor and stator.

6.9 Parametric optimization of bearing geometry

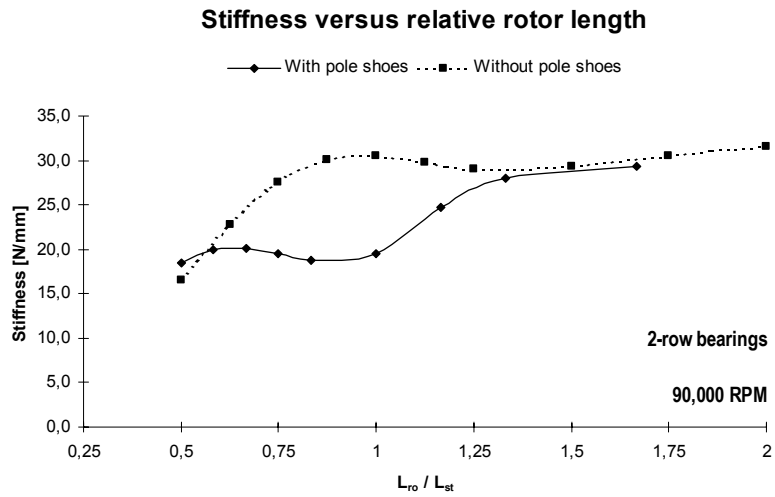


Fig. 6.37. Stiffness versus rotor length in relation to stator length.

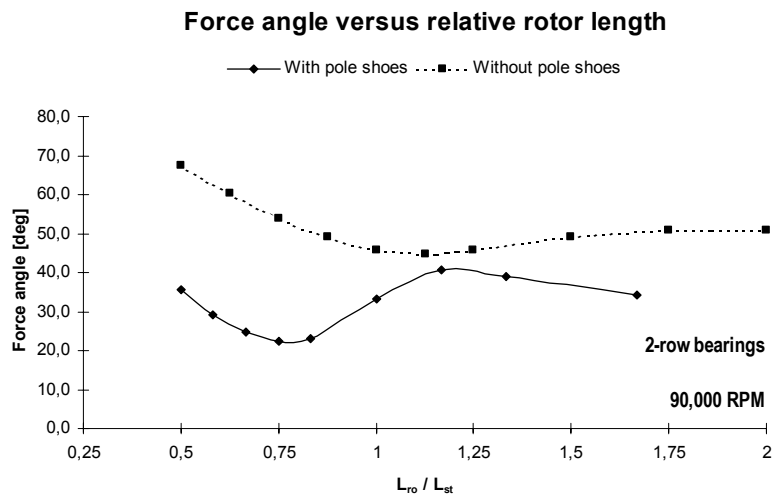


Fig. 6.38. Force angle versus rotor length in relation to stator length.

6.9.5 Optimization of magnet width

We shall now study how the cross-section width of the magnets affects the stiffness and force angle. Consider the following bearing:

Description: Intermediate bearing without pole shoes

Magnets: 2 outer ring magnets. $D_{om} \times 59 \times 8$ mm

2 inner ring magnets $49 \times d_{im} \times 8$ mm

Rotor: Copper cylinder $58 \times 50 \times 18$ mm

In Fig. 6.39-6.41 bearing data are found for two different speeds. The diagrams are plotted against the magnet cross-section width to length ratio, w/l . Thus $w/l = 1$ means that the magnets has a square cross section of 8×8 mm, and that $D_{om} = 75$ mm and $d_{im} = 33$ mm. As expected stiffness increases fast with increased width, but from Fig. 6.40 it can be seen that it is not very economical to increase width too much. For this bearing, the optimum ratio, from an economical point of view, is $w/l = 0,5$.

If higher stiffness is required, the designer has the choice between either more magnets, which is the most economic choice, or wider magnets, which is better if rotor length is critical.

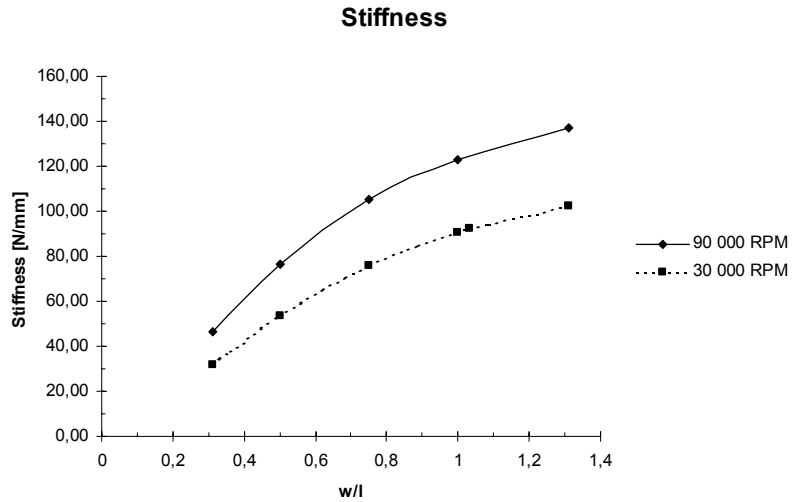


Fig. 6.39. Stiffness versus relative cross section width of magnet.

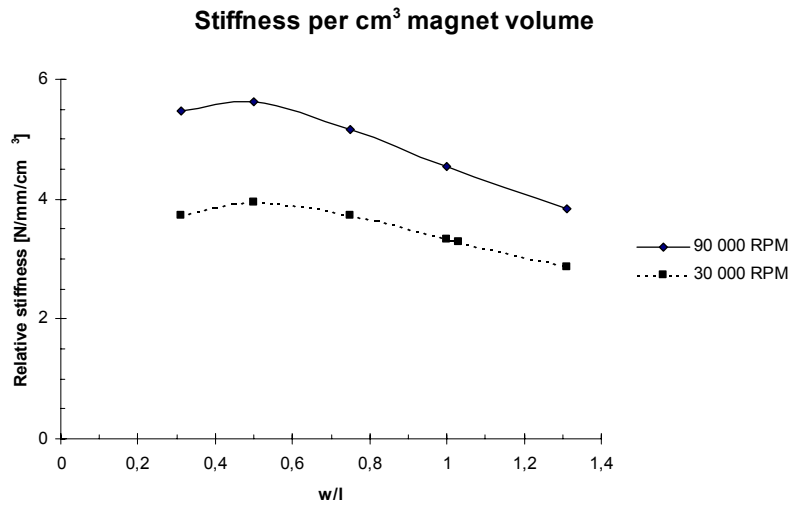


Fig. 6.40. Relative stiffness versus relative cross section width of magnet.

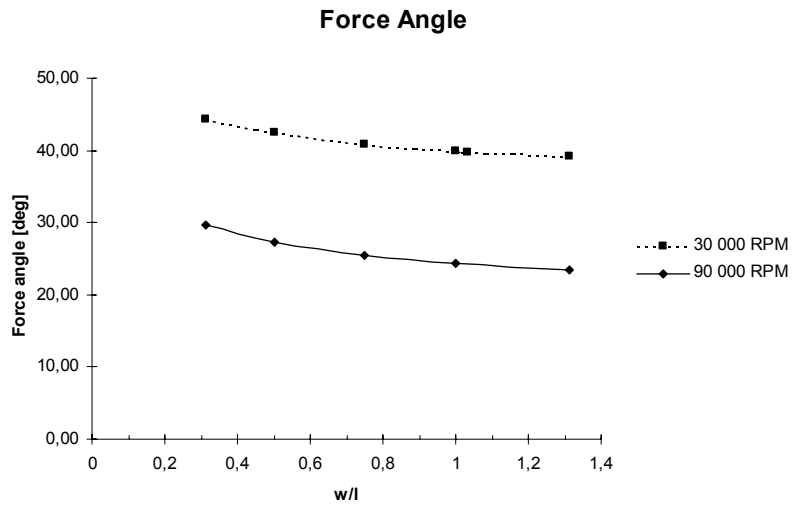


Fig. 6.41. Force angle versus relative cross section width of magnet.

6.9.6 Leakage flux reduction

The radial flux in the iron pole shoes does unfortunately leak to the outside of the bearing as well as through the conducting rotor, Fig. 5.1. A way to reduce this leakage is to reduce the size of the pole shoe washer on the side where no leakage is desired, as has been done to some extent in Fig. 5.1. This will increase the leakage flux in the air gap.

Which diameter of the iron washer is optimal? Let us study a flywheel bearing with the following data:

Description: Flywheel bearing with pole shoes

Magnets: 4 inner axial ring magnets $24 \times 10 \times 7$ mm

Pole shoes: 3 inner intermediate washer $24 \times d_{iw} \times 3.50$ mm
2 inner end plates $24 \times d_{iw} \times 1.75$ mm

Rotor: Copper cylinder $35 \times 25 \times 37.5$ mm

We shall now optimize the inner diameter d_{iw} of the iron washer and replace it with a non-magnetic distance ring as shown in Fig. 4.4. The results are shown as dashed lines in Fig. 6.42-6.43, and we can conclude that 13 mm would be the best choice. If we chose 24 mm, which is the same as not having any iron pole shoe at all, the stiffness is high, but the force angle is dramatically increased due to the reduced inductance.

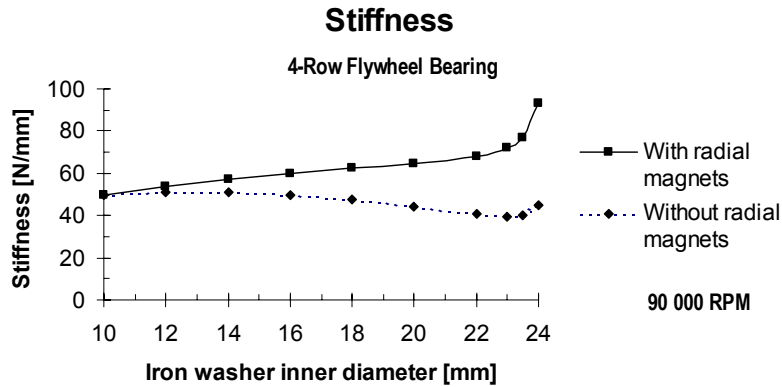


Fig. 6.42. Stiffness versus pole shoe inner diameter. With and without radial magnets for leakage reduction.

6.9 Parametric optimization of bearing geometry

For comparison we shall also replace the distance rings for radially magnetized ring magnets, the direction of magnetization being opposite to the leakage flux. This is very efficient to reduce the leakage flux and to increase stiffness. Unfortunately such magnets are very expensive and are not yet suited for mass production.

If they will ever reach the same price level as axially oriented magnets, Fig. 6.44 is useful for optimization with regard to cost. A good compromise with regard to stiffness, cost and stability would be to choose the diameter in the interval between 16 and 18 mm.

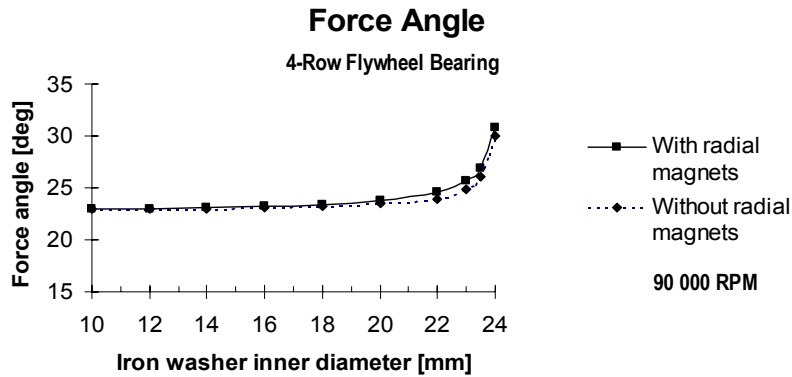


Fig. 6.43. Force angle versus pole shoe inner diameter. With and without radial magnets for leakage reduction.

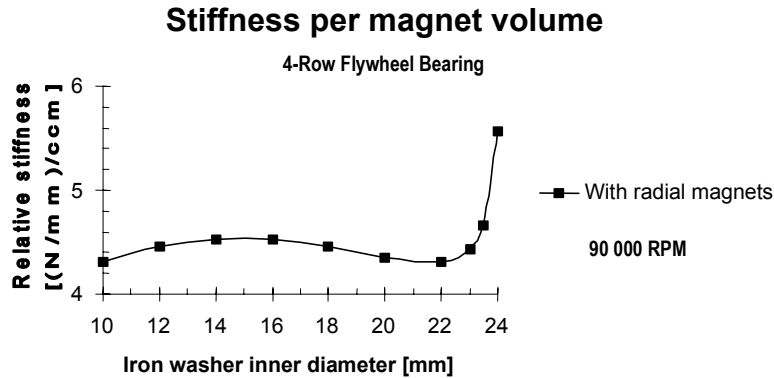


Fig. 6.44. Relative stiffness versus pole shoe inner diameter. With radial magnets for leakage reduction.

7 Motor

A motor has been developed during the project, which comprises three different advanced motor concepts. 1) It is an airgap motor, and 2) the rotor has a Halbach magnet structure and 3) the stator has a helical winding. All together they form an ideal motor for high speed applications.

7.1 Background

Almost every motor on the market are made and optimized for low speed operation. Sometimes these machines are converted for high-speed operation, which usually results in costs much beyond what was expected. And still, the solution may not work. It is either overheated or produces so much noise and vibrations that it is impossible to sell. To summarize, a conventional low speed motor is unsuitable for high speeds due to:

- Too large flux variations from the teeth.
- Too small airgap, specially in induction motors
- Too high negative radial stiffness



Fig. 7.1. Tool spindle.

7 Motor

- Bearing life too short at high speed
- Too high bearing stiffness, which results in unbalance problems
- Shaft bending stiffness too weak, or unsymmetrical
- Creeping due to large centrifugal forces

When the high speed bearing project begun, an investigation was also carried out concerning the choice of a suitable motor. Especially the third point above was considered a major problem. In most motor types the destabilizing radial forces are up to ten times higher than the desired tangential torque producing forces.

No suitable motor was found on the market, though some experimental motors were reported. The best choice seemed to be the coreless bell type PM motor used in a 520 l/s turbomolecular vacuum pump from Pfeiffer Vacuum. The motor operates so smoothly that it can be used with passive magnetic bearings without problems. But the power of that motor type is too low for electrical power systems.

It was decided to develop a new motor/generator based on the Pfeiffer design, but modified for much higher power.

Fig. 7.1 shows a complete grinding spindle with the new motor. It has three hybrid ceramic angular contact ball bearings for highest precision. This spindle was used for driving the induction bearing rotor in prototype nr. 2.

7.2 Concept

The new motor concept has a coreless helical airgap winding, which can be used with three different types of permanent magnet rotors.

1. Outer rotor, bell type
2. Outer rotor conventional
3. Inner rotor

Below a brief description of the motor will be given. For further details on the subject, see the work by Lefevre [8] who has studied the motor and particularly the winding in more detail. A more general description on slotless machines is given by Engström [21].



Fig. 7.2a,b. Helical stator above, and outer rotor below.

7 Motor

Rotors

The **outer rotor of bell type** has only rotating iron parts. The winding back iron rotates with the magnets. Thus the iron losses are zero, except for possible switching losses, if applicable. This rotor has two airgaps around the stator, and one outside the rotor, so three airgaps gives rise to large airdrag when used in atmospheric conditions. That is why this rotor is mostly used in vacuum environments. The advantage is exceptionally low radial forces, and very high efficiency in vacuum. Lefevre [8] estimates the efficiency in a flywheel drive to be 99,1% at 100,000 rpm.

The **outer rotor of “conventional”** type is shown in Fig. 7.2b and 7.3a. It is an all-purpose four-pole quasi Halbach rotor with 16 magnets inserted in an aluminum squirrel cage. The outer rotor is especially aimed for flywheels. The carbon composite rim, such as the one shown in Fig. 9.1, allow such high speeds that the only possible way to arrange the magnets due to the centrifugal forces is on the inside of the hollow flywheel. The magnets have to be segmented, otherwise they will crack when the rotor expands at high speed.

Finally the **inner rotor** is the one used in the machine spindle shown in Fig. 7.1. It has a 4-pole Halbach rotor with 8 magnets. It is illustrated with the winding layout in Fig. 7.5. The inner rotor has no squirrel cage, but is completely filled with magnets for better performance. Since it is a Halbach rotor, no iron back is required. The rotor shaft may be magnetic though, but it makes hardly any difference.



Fig. 7.3a,b. Perspective view of the rotor and the helical winding.

Stator

The stator is a four layer helical winding, shown in Fig. 7.2a and 7.3b. The winding layout is shown in Fig. 7.4 where one phase is set out in a diagrammatic development. Fig. 7.5 shows a cut through the middle of the rotor where the winding is symmetric. Lefevre [8] studied this winding in detail, using both analytical and 2D-FEM simulations. The concept is flexible, so that for one stator, all three rotor concepts can be used.

The winding has 3 hall sensors for maximum flexibility, which may or may not be used. The idea behind the sensors is that though a commercial sensorless drive is cheaper, there are still no reported successful operation of such a drive above 100,000 rpm. For hall sensors this frequency is not a problem at all.

Consider the inner rotor in Fig. 7.5 again. It has the same 4-layer winding, but has an 8-magnet 4-pole Halbach rotor. The advantage with a Halbach array instead of conventional surface mounted magnets, is that the leakage flux between the poles is reduced, which allows a thicker airgap winding.

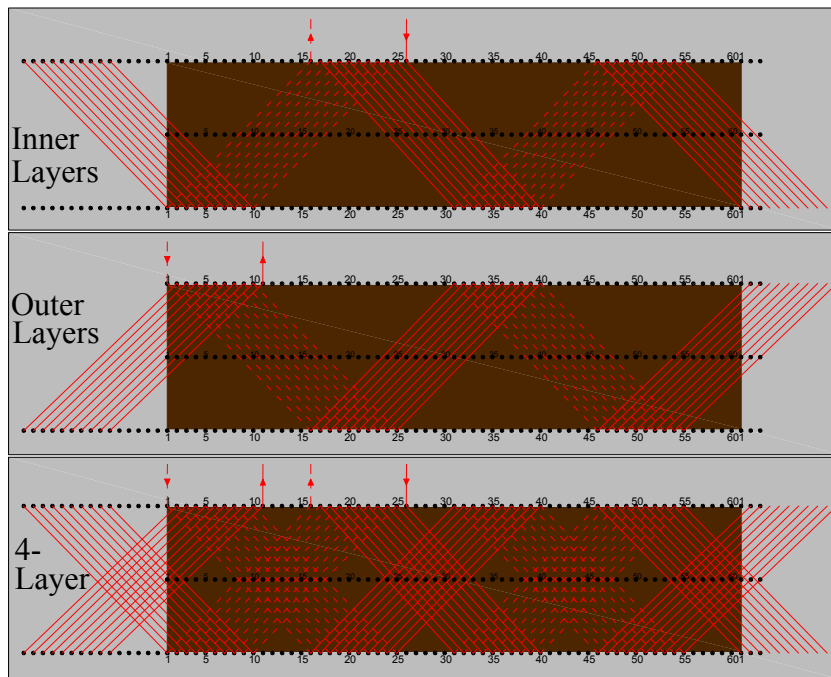


Fig. 7.4. 4-layer helical winding. Above are the inner layers that are wound first on the bobbin.

7 Motor

The flux from the Halbach magnets is almost sinusoidal, and the winding has automatically a very smooth MMF-curve, at least through the centre of the rotor, which could best be described as an enhanced trapezoidal one. Lefevre has studied the MMF-curves and the flux in detail for different sections of the rotor. This arrangement is ideally suited for a sinewave converter, but due to speed requirements, a specially developed six step converter is used instead.

Flywheel Drive

For flywheel operation, no standard drive unit is available that can handle such high frequencies. However, a separate PM motor drive was developed during the project, making use of the three hall sensors. It can be operated in either voltage control mode or current control mode. In the latter case the switching frequency is 56kHz, which can be increased to 100 kHz. The flywheel drive has also been used for the high-speed tool spindle, and in this case the current control is also quite useful as a torque control to protect the tools.

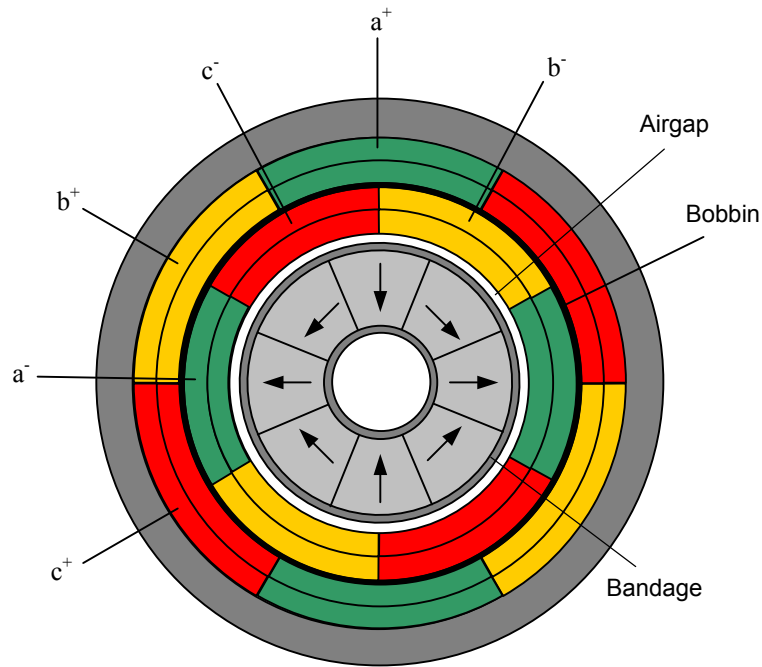


Fig. 7.5. Spindle motor with 4-layer helical winding and 4-pole rotor with a Halbach magnet array. Cut through middle of winding.

7.3 Back-EMF

The no load line voltage has been measured [18] for the spindle with the windings in Y-connection. The outer 3-phase and the inner 3-phase winding are series connected for low speed operation. The converter is specified for a DC input in the range 12 - 48V. Fig. 8.9 shows the spindle (a), the converter (b) and the DC-supply (c). The line voltage is measured directly on the DC-supply. Thus it includes the voltage drop over the converter switches.

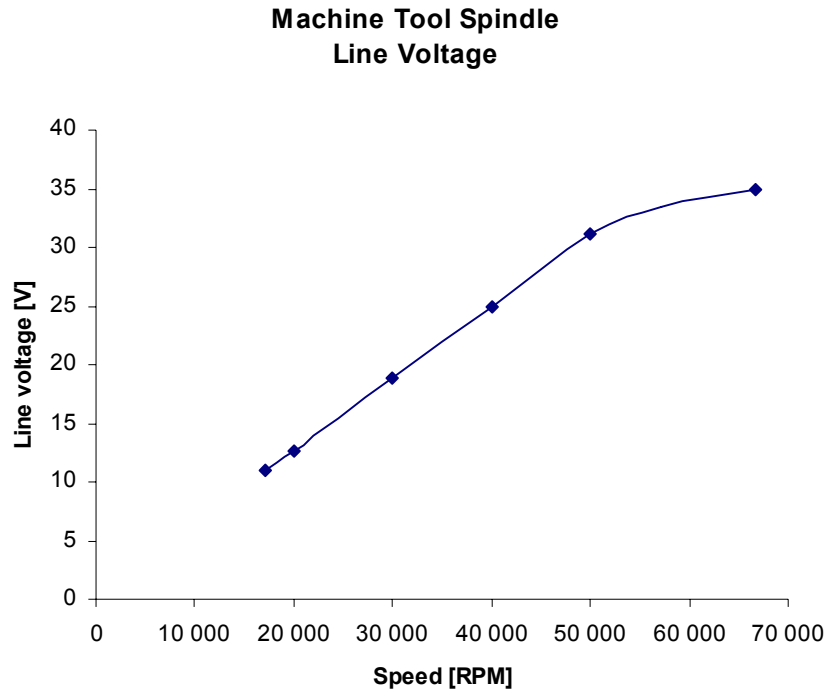


Fig. 7.6. Measured values and interpolated line voltage plotted versus speed for the spindle motor when operated in voltage control mode. The two 3-phase windings are Y-connected in series for low speed operation.

8 Experimental validation of the prototypes

Two prototypes have been built to verify the simulated and analytically obtained bearing data. The first one is a rebuilt turbomolecular vacuum pump. These pumps are normally equipped with one passive magnetic bearing and one ball bearing. Exchanging the passive bearing for an induction bearing is not complicated, and the pump has been tested up to 90,000 rpm.

The second test rig was made to perform accurate measurements on bearing forces and losses. It is a movable spring suspended scales in which the bearing stators are mounted. The rotor is fixed, and is powered by the tool spindle which is also developed during the project, and which is briefly described in Chapter 7.

Test data are found in Section 8.6, and are compared to FEM-results in Section 8.7. An experimental thermal analysis is performed in Section 8.8.

8.1 Prototype 1; Vacuum pump

To study the dynamics of an application equipped with electrodynamic bearings, an existing commercially available turbomolecular vacuum pump from Balzers Pfeiffer GmbH was chosen for an exchange of bearings. The pump is a TMH 071 turbomolecular vacuum pump. These pumps are originally fitted with one ball bearing and one passive radial outer rotor magnetic bearing consisting of three stator rings and three rotor ring magnets. It also has one auxiliary ball bearing inside of the magnetic bearing.

Modifying the passive bearing into an induction bearing was simple, and in order to improve low speed stability one of the magnets in the outer rotor was not removed. The other two were exchanged for a copper cylinder. See Fig. 8.1 and Fig. 8.2. All original stator magnets were kept unchanged.

Vibration damping on the original vacuum pump is done on the ball bearing side. There is no damping on the magnetic bearing side. According to the analysis external damping is necessary when using electrodynamic bearings, and it was not evident that the damping on the ball bearing side would be enough to achieve stability. Unfortunately there was no space left for an external damper on the magnetic bearing side. To reduce the need for additional damping it would be advantageous to use long magnets, as can be

8 Experimental validation of the prototypes

seen in the diagram in Fig. 6.30. However, the original magnets had to be kept due to space limitations.

For safety considerations an additional explosion protection was inserted, and the pump was remotely controlled in case of any failure at 90,000 rpm.

The ball bearing in the lower end of the shaft was unchanged. The original motor, which is a permanent magnet brushless DC motor, was kept unchanged. It is slightly unstable in the radial direction due to reluctance forces, but since one of the rotor magnets is not removed, this stiffness is more than enough to compensate for the motor.

The following changes were made, some of them shown in Fig. 8.2 to 8.4a,b.

- The turbine blades were removed to reduce air drag losses.
- The stator blades were also removed and replaced with a protective cylinder inside the vacuum housing.
- Three eddy current sensors were mounted through the vacuum chamber with vacuum seals.
- Two of the rotor magnets were replaced with a copper cylinder.
- For some experiments thin iron or aluminum washers were inserted between the stator magnets.

In addition a tilt- and vibration table was manufactured, including a remote controller.

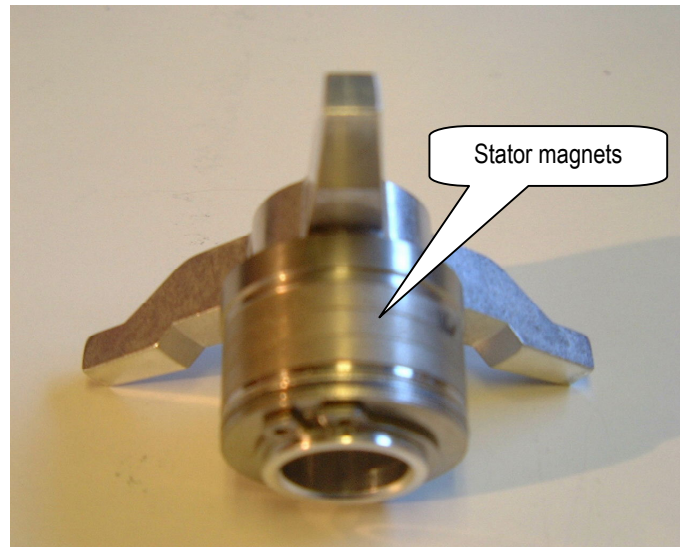


Fig. 8.1. The induction bearing stator.

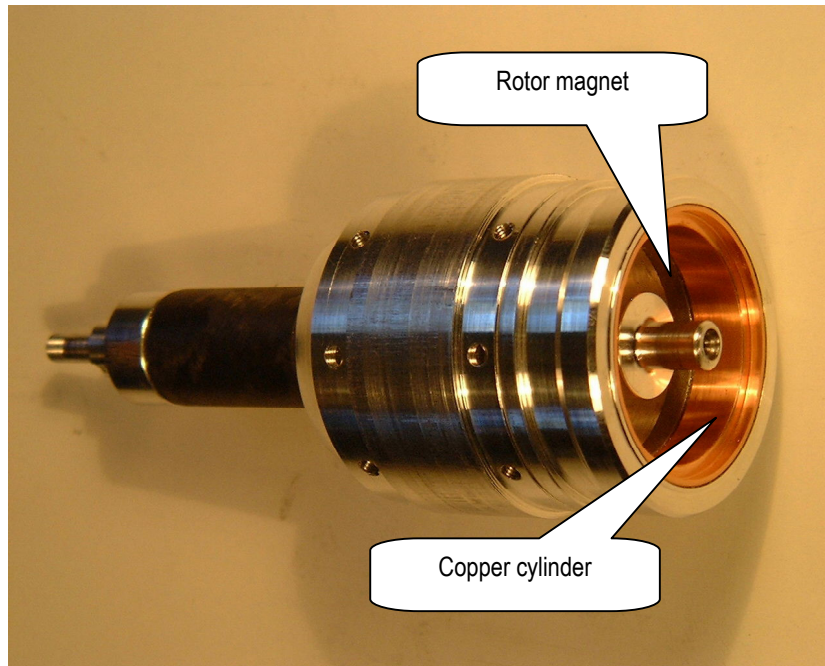


Fig. 8.2. The induction bearing copper rotor mounted inside the hollow shaft.

8.2 Test runs

The pump was mounted on a vibration table, see Fig. 8.3, and accelerated to 90,000 rpm several times. At first in vertical position, later on tilted and finally during different vibration modes.

The motor has an integrated variable speed drive and is able to run between 18,000 and 90,000 rpm, though the speed control was not very accurate since it was not tuned for the low moment of inertia that was the result of removing the blades.

Radial displacement sensors of eddy current type were attached through the chamber with vacuum seals, Fig. 8.5a,b and are calibrated using a micrometer screw, Fig. 8.6. Radial forces were obtained by leaning the vacuum chamber in the y-direction, Fig. 8.7a,b. This results in a speed dependent angle deviation of the rotor in the x- and y- directions with respect to the stator. The deviations were then measured with the displacement sensors. A third sensor, Fig. 8.5a, was used to measure the rotor angle for balancing purpose. The rotor was tilted at different speeds to obtain

8 Experimental validation of the prototypes

force/displacement curves, and finally the rotor was forced into emergency bearing contact by violent vibrations.

Dynamic effects

Measuring restoring forces and side forces was done using the displacements sensors in Fig. 8.5 when the pump was tilted, Fig. 8.7. This however, also affected the ball bearing behaviour, and also the damping coefficient of the support of the pump. Thus the calibrations of the sensors were continuously altered. Since much more accurate measurements were done using the scales in Section 8.3, no results will be presented in this section. Instead one important dynamic effect will be studied, which proves that the traditional theory on rotating damping is not applicable to eddy current devices having a certain inductance.

During the tests the damping was altered, until the stability limit was reached, which occurred at 33,000 rpm. According to the traditional theory, a small increase in damping has a small effect on the stability limit, and there is always an upper stability limit, regardless of damping amount. Not so for this test rig. A small amount of additional damping eliminates the stability limit, and speeds of 90,000 rpm can be reached.

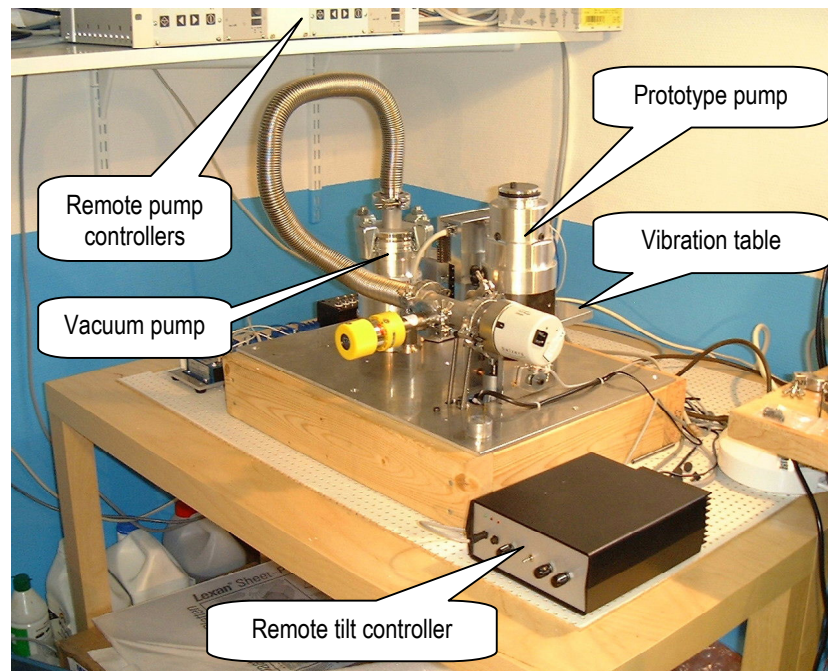


Fig. 8.3. The test rig mounted on the vibration table. See also Fig. 8.7a,b.

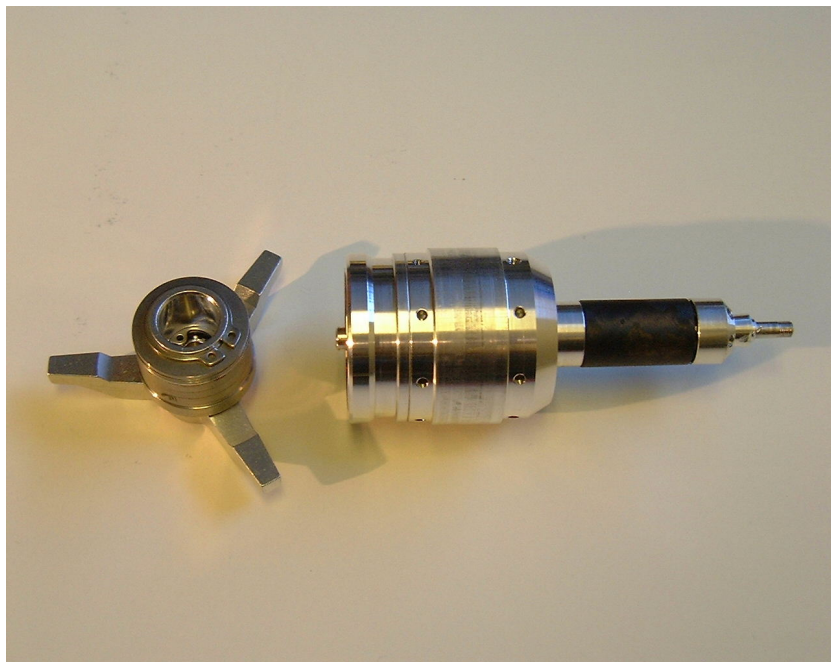
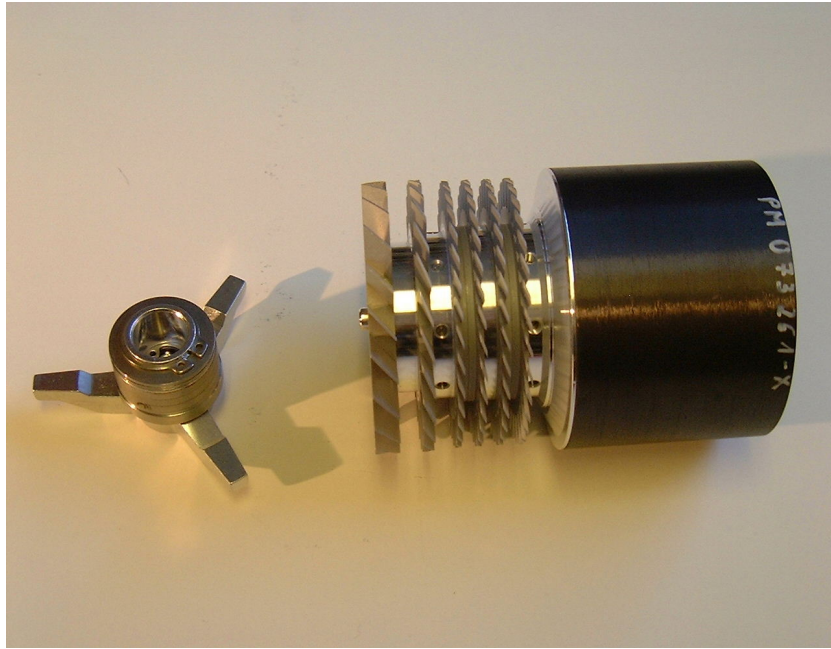


Fig. 8.4a,b. Bearing stator and pump rotor before and after modification.

8 Experimental validation of the prototypes

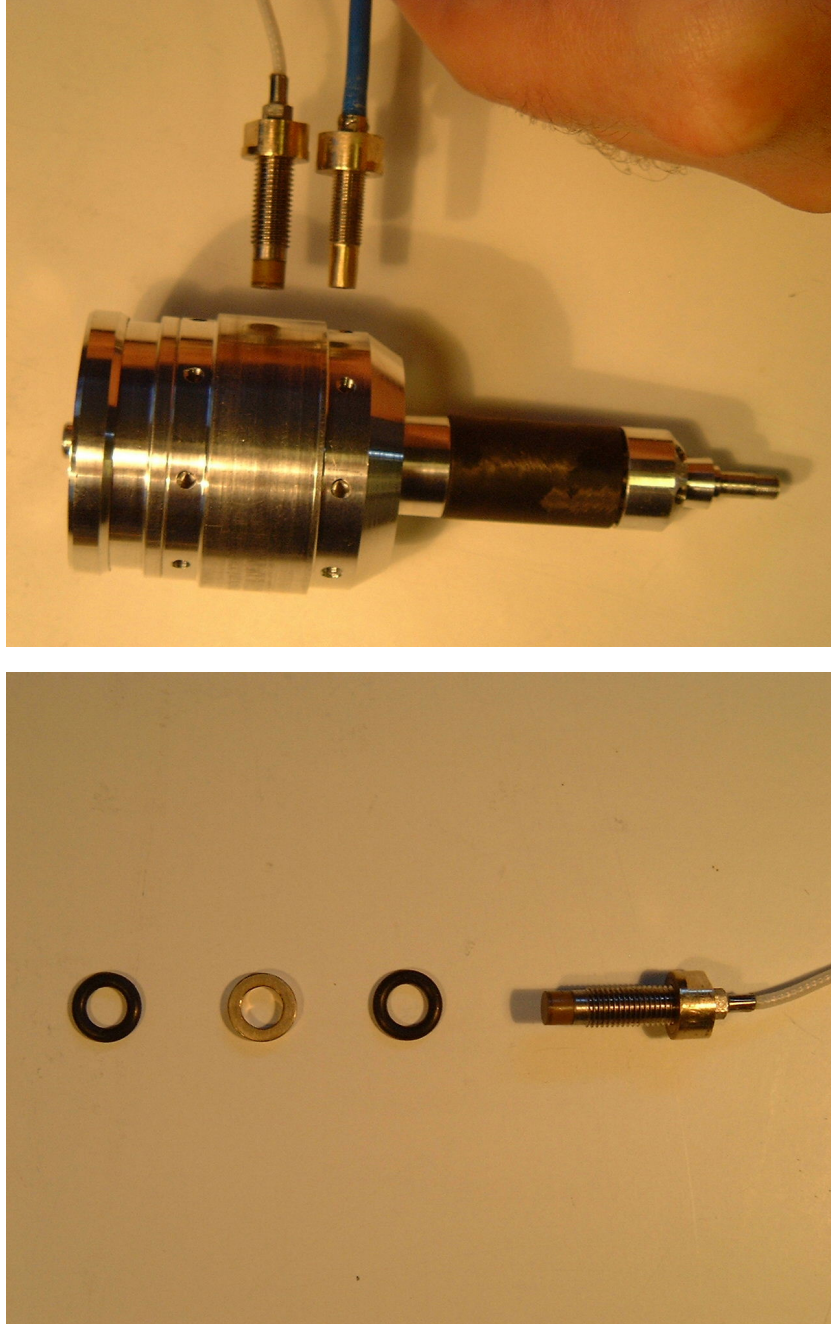


Fig. 8.5a,b. Eddy current sensors and seals.

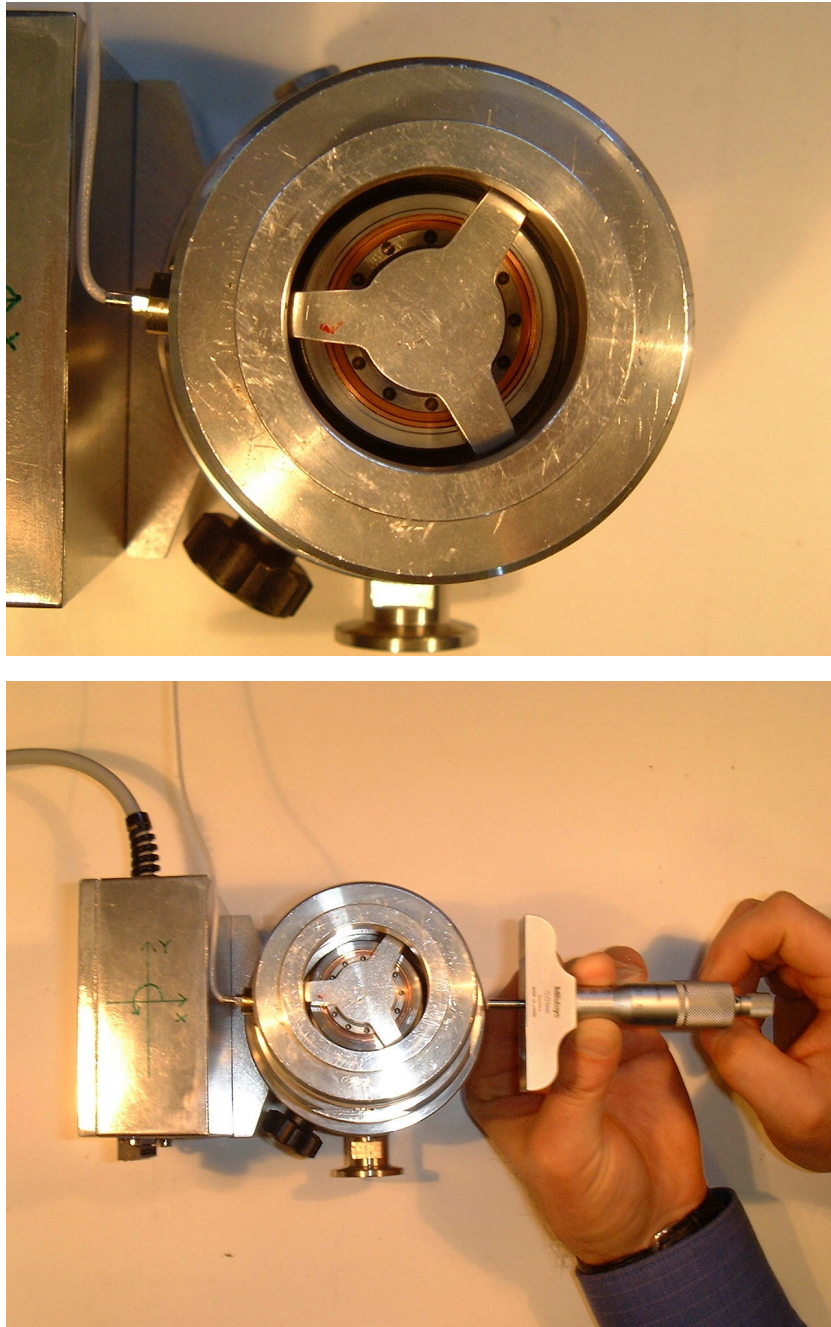


Fig. 8.6a,b. Calibration of sensors with a micrometer screw.

8 Experimental validation of the prototypes

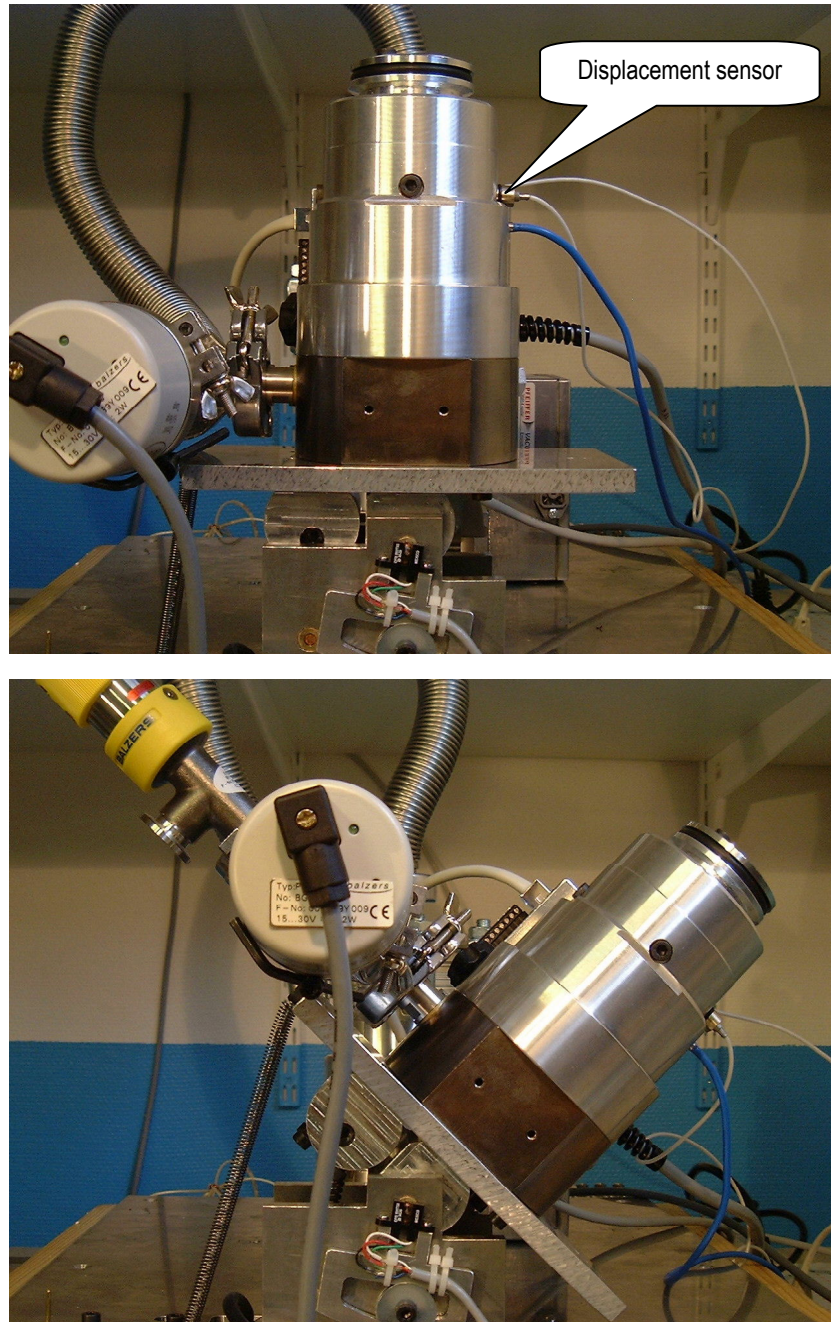


Fig. 8.7a,b. Experiments with different radial load.

8.3 Prototype 2; Spring suspended scales

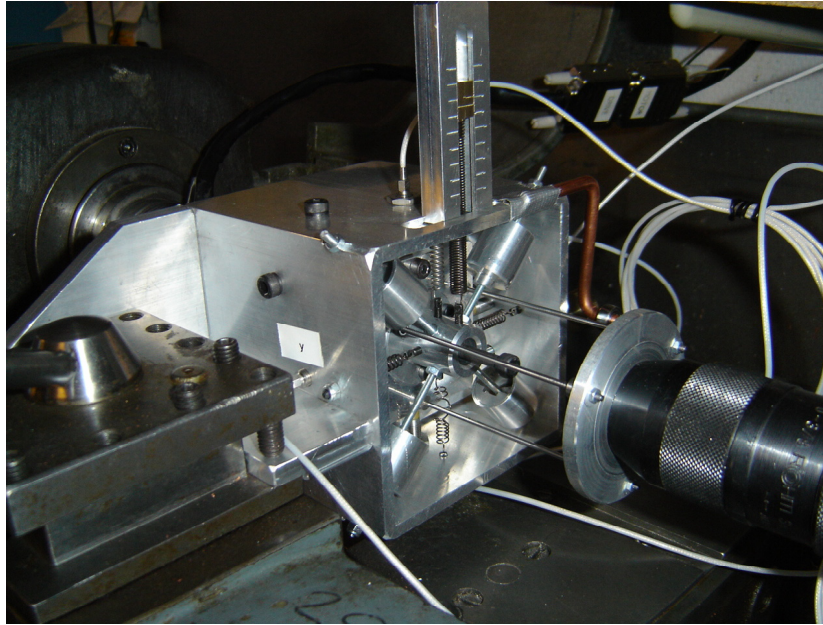


Fig. 8.8. The spring suspended scales.

The test rig consists a fixed machine spindle (1), see Fig. 8.12, on which a short (2) or a long (3) rotor can be attached, see Fig. 8.11. The stator magnets (4) are mounted on holders, an outer (5) and an inner (6) holder. These holders are in turn mounted on the spring mount (7) on which eight springs (8) and four dampers (9) are attached, see Fig. 8.10. Together, the stator including the holders and the mount, form a resilient and movable scales. The movements can be measured with eddy current sensors (10) see Fig. 8.12. One of the springs is adjustable (11), see Fig. 8.10, and can be used to vary the bearing load.

Once the stiffness of the scales is calibrated and known, the force can be calculated using the eddy current signals. These signals represent the bearing eccentricity in x and y directions. The resolution is $1\ \mu\text{m}$ in the x direction, and has been extended to $0.035\ \mu\text{m}$ in the y-direction. The reason is that a linear relationship in the x-direction and a quadratic behaviour in the y-direction is expected, the latter requiring higher precision to verify experimentally.

Experiments have been performed with various numbers of magnets. The maximum number of magnets is six, three inside and three outside the rotor.

8 Experimental validation of the prototypes

All magnets (4) in Fig. 8.11 have a cross section of 4x4 mm. It is also possible to mount larger magnets (12) with a cross section of 7x7 mm, also shown in Fig. 8.11, in the rig. This will be done in subsequent tests.

A typical test is performed according to the following procedure:

1. Before the first test, the springs and sensors are calibrated.
2. The bearing, while not rotating, is put off-center to a certain predetermined eccentricity using the adjustable spring (11).
3. The position and torque sensors are nullified.
4. The speed is increased in small steps, and the new x and y positions are noted, and for some measurements also the torque signals are noted.
5. When decelerating, the same values are read once again, to see if there has been any changes. Averaging takes care of possible temperature changes during the time of the test.
6. Post processing of data is done to calculate the new eccentricity and angle for each speed, and the requested forces and stiffnesses are calculated from the data.

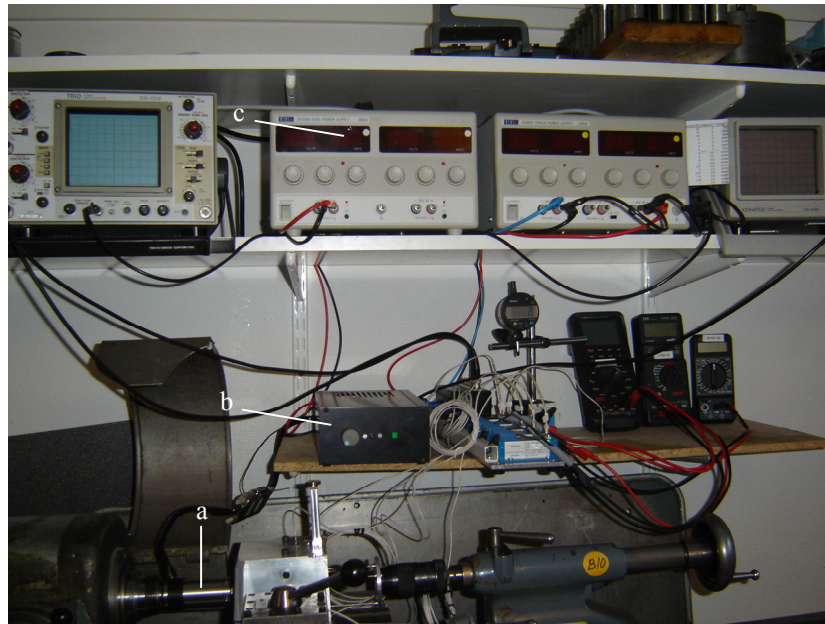


Fig. 8.9. Test rig drive equipment. a) Tool spindle. b) Converter. c) DC-supply.

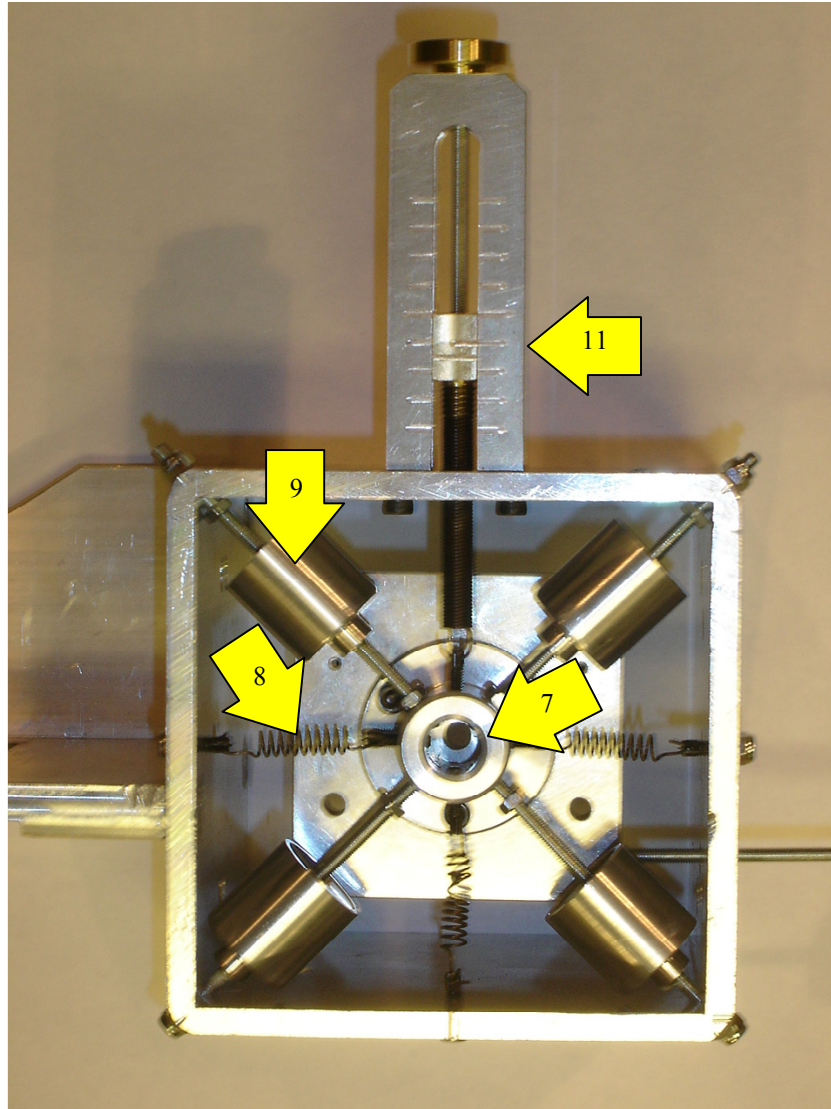


Fig. 8.10. Test rig scales suspended in springs and dampers.

8 Experimental validation of the prototypes

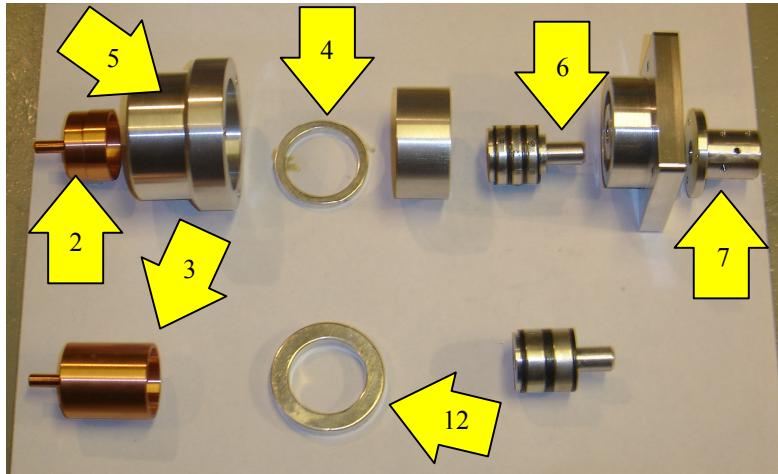


Fig. 8.11. Exploded view of test rig bearing parts and housing.

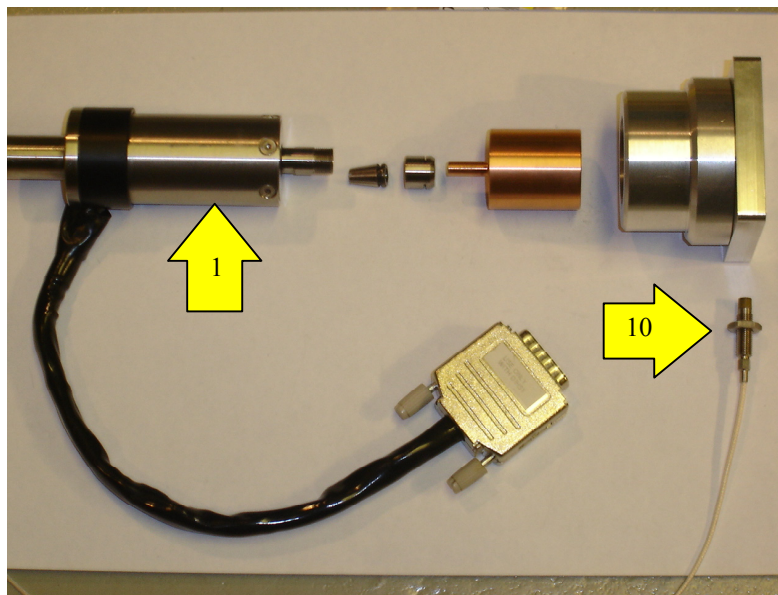


Fig. 8.12. Spindle (1) with clamping rings to attach to rotor. Position sensor (10) measures movements of scales, in which the stator is mounted.

8.3 Prototype 2; Spring suspended scales

The spindle (1) in Fig. 8.12, which is described separately in Chapter 7, is connected to the rotor via clamping rings so that different rotors can be tested. The long rotor (3) in Fig. 8.11, represents the “infinitely” long rotor referred to in Chapter 6. The short rotor (2) is 9 mm long, which is the optimum length for these magnets according to Fig. 6.38. This is the default rotor, which is simulated in the FEM calculations if nothing else is mentioned.

The bearing stator parts (4), (5) and (6) in Fig. 8.11 are mounted on a holder (7), which acts as a very sensitive scales. It is suspended in 8 springs, and its position is measured with 5 eddy current sensors, one of them shown in Fig. 8.12.

The rotor is fixed in space, since the spindle is firmly mounted to the heavy test bench, a Swiss lathe. The spindle has no critical speeds in the measured speed range. However when the cylindrical copper rotors are attached, the first bending critical speed is reduced to 18,000 rpm for the short rotor, and to 12,000 rpm for the long one. This is due to the large overhang of these rotors, and due to the small diameter of the cylinder shaft.

During the measurements, the suspended stator will move according to the equations of motion, Eq. (8.1), which basically is the same as Eq. (5.89), with the difference that the mass m is now the mass of the stator including the scales, and that the external stiffness coefficients $k_{e,x}$ and $k_{e,y}$ are different in the x - and the y -direction because of the adjustable spring in the y -direction.

$$\begin{cases} m\ddot{x} = (-k_{e,x} - K \cos \theta)x + (-d_e - \frac{K}{\omega} \sin \theta)\dot{x} + (-K \sin \theta)y + (\frac{K}{\omega} \cos \theta)\dot{y} \\ m\ddot{y} = (K \sin \theta)x + (-\frac{K}{\omega} \cos \theta)\dot{x} + (-k_{e,y} - K \cos \theta)y + (-d_e - \frac{K}{\omega} \sin \theta)\dot{y} \end{cases} \quad (8.1)$$

The external damping coefficient d_e is relatively high, so it takes about two seconds for the system to reach its final static equilibrium position. When it does, the time derivatives are zero, and the position and corresponding forces can be solved. These results are shown in fig. 8.17 to 8.23.

In order to guarantee repeatability, the dampers are not allowed to have any friction or mechanical contact. This also excludes the use of seals and grease, since they show a hysteretic behaviour. Dampers with these features are not commercially available, so they had to be made separately, and are shown in Fig. 8.13.

8 Experimental validation of the prototypes

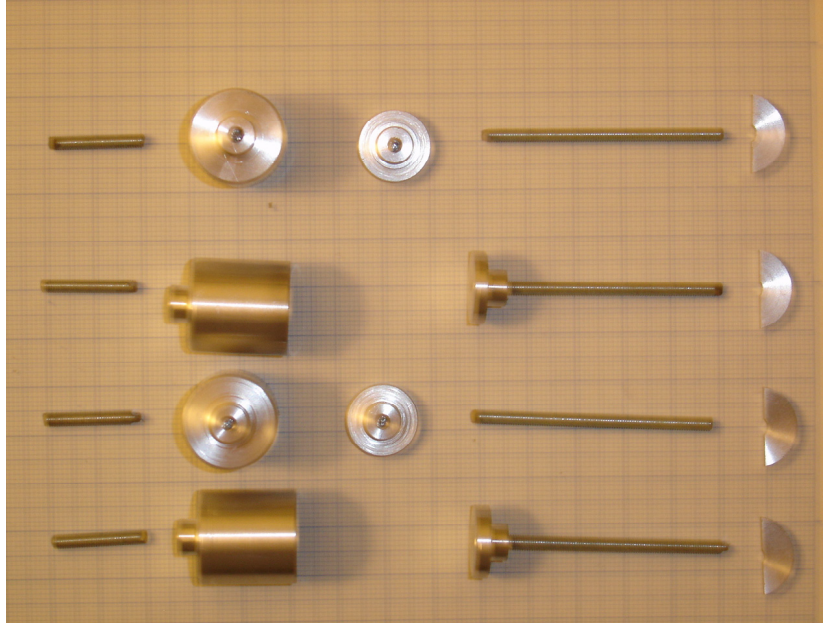


Fig. 8.13. Viscous dampers. Not sealed, and with no mechanical contact anywhere, to avoid any friction or hysteresis.

Several experiments have been performed using different magnet configurations. In the stator there is space enough for bearings with up to 3 rows. All reported experiments were carried out at subcritical speed. However, some experiments were also carried out at supercritical speed up to 22,000 rpm, but generally this caused large vibrations, which deteriorated the measurements. Thus, for future research, in order to perform tests at higher speed, a larger spindle is required with larger diameter clamping rings. The present spindle is intended for Rego-Fix ER-8 clamping rings used for tool diameters of up to 5 mm, which is the size of the current rotor-mounting pin.

8.4 Bearing parts

The bearing parts are shown in Fig. 8.14 and Fig. 8.15. The three magnets in Fig. 8.14 form the inner stator in a 3-row intermediate bearing. Outside the rotor there will be another three magnets mounted, one of them shown in Fig. 8.15. Between the magnets there are pole shoes, made of heat annealed iron washers. These parts are thread on a rod, which is mounted to the scales.



Fig. 8.14. A 3-row bearing assembly. Inner magnets shown only.

The shown magnets in Fig. 8.14 also form a complete outer rotor bearing stator, since no outer magnets are used in this case. Similarly, inner rotor bearings are measured using only the outer magnets, which are mounted inside the housing to the left.

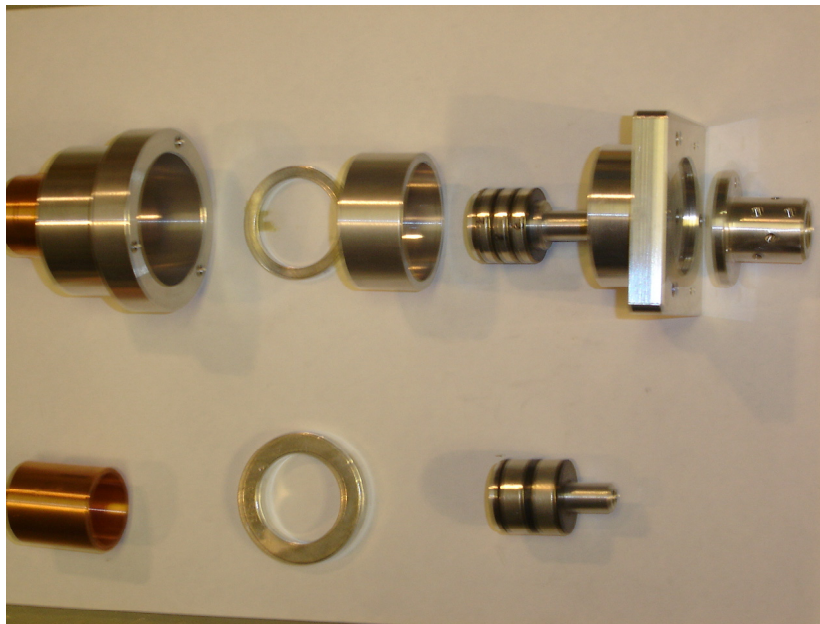


Fig. 8.15. Bearing parts. Above magnets and rings for a 3-row bearing. Below larger magnets for a 2-row bearing.

8.5 Calibration of bearing center

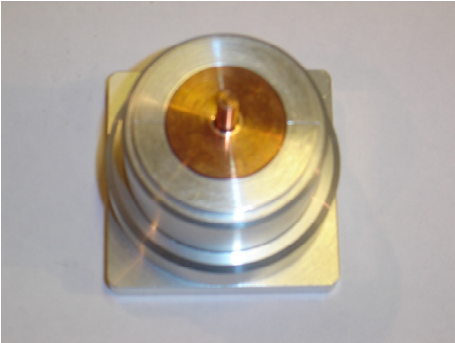
An important task when it comes to bearing calibration, is to find the bearing center, since this is the position from which the rotor displacement and eccentricity is measured. Fig. 8.16 shows how the rotor is centered in the stator using very accurately machined centering ring halves.



An easier way to find the bearing center is to spin the rotor at different speeds. There only exists one stator position, measured as the position of the suspended scales, which does not move when the rotor speed is changed. This point is defined as the magnetic center.



If the flux from the magnets is not perfectly homopolar, then the mechanical center and the magnetic center will be separated. Reasons for this are described in more detail in Chapter 5.6. The separation distance is a way to measure the quality of the magnets.



Throughout the measurements the magnetic center has been used as a reference point, since this is the position that the rotor will use as a reference, when producing forces during eccentric operation.

Fig. 8.16a-c. Calibration of bearing mechanical center.

8.6 Test results

The following test results have been achieved using the bearing described in appendix 2 concerning dimensions and properties of magnets and poles.

The magnet material is NeFeB having a remanent flux of 1.25 T. The following measurements will be presented:

In Chapter 8.6.1

- Forces versus eccentricity
- Force angle versus eccentricity
- Losses versus eccentricity

In Chapter 8.6.2

- Stiffness versus speed
- Force angle versus speed

8.6.1 Eccentricity dependent properties

According to the analysis in Chapter 5, forces are expected to be linearly dependent on eccentricity. The force angle should be constant, and losses should have a quadratic dependence on eccentricity. Measurements of these properties are shown in Fig. 8.17 to Fig. 8.21.

The total bearing force F is shown in Fig. 8.17 for two different speeds. It consists of restoring and tangential force components, F_r and F_b , which are shown in Fig. 8.18 and Fig. 8.19.

The force angle θ is shown in Fig. 8.20 and is constant as expected, though measurement accuracy seems to suffer somewhat at low speed, especially at small eccentricity. This is not surprising, since bearing forces are lowest for this combination of speed and eccentricity.

Finally the losses are shown in Fig. 8.21. These losses include air drag losses at one atmosphere, and are clearly quadratically dependent on eccentricity. The residual losses, including the air drag, are the remaining losses at no eccentricity.

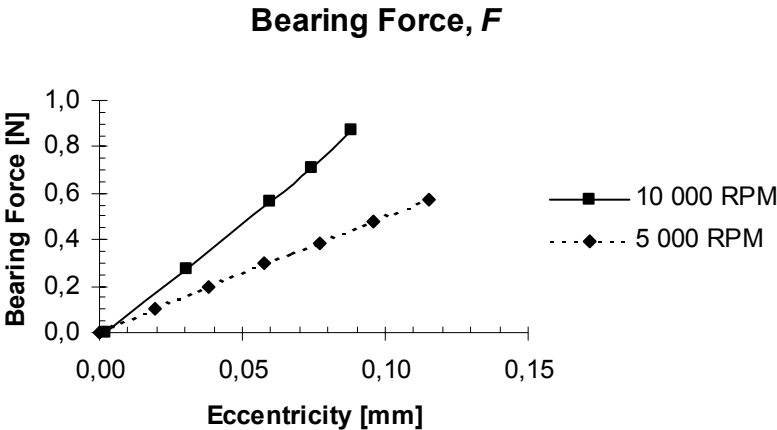


Fig. 8.17. Total bearing force versus eccentricity for a 2-row intermediate rotor bearing.

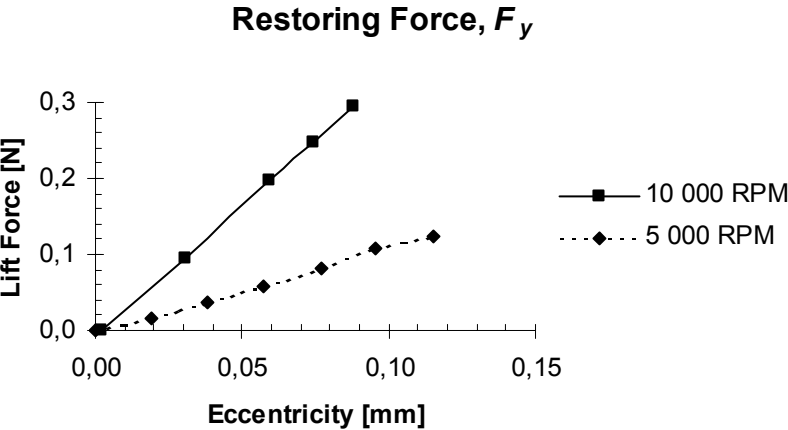


Fig. 8.18. Restoring force versus eccentricity for a 2-row intermediate rotor bearing.

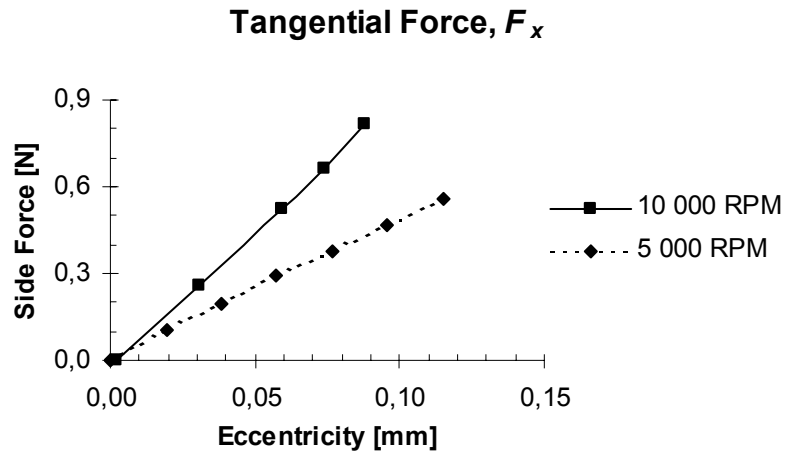


Fig. 8.19. Tangential force versus eccentricity for a 2-row intermediate rotor bearing.

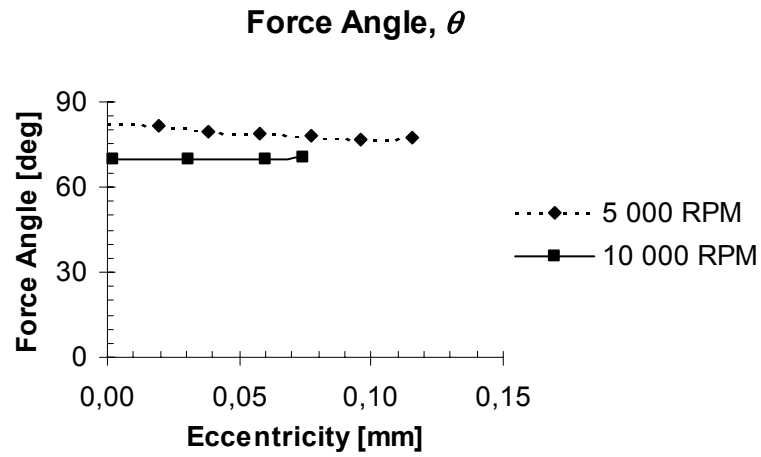


Fig. 8.20. Force angle versus eccentricity for a 2-row intermediate rotor bearing.

8 Experimental validation of the prototypes

The bearing losses consist of different parts. The dominant part is due to the eddy currents induced during eccentric operation. These losses can be calculated directly from the force angle in Fig. 8.20. These losses should be zero at no load. However, losses due to magnet inhomogeneities have a residual loss even at zero eccentricity. The same is true for air drag losses. In Fig. 8.21 below all these losses are included.

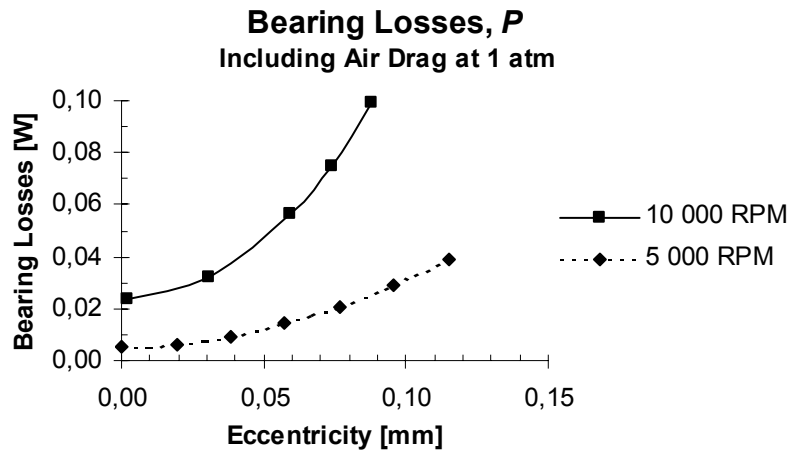


Fig. 8.21. Bearing losses versus eccentricity for a 2-row intermediate rotor bearing.

8.6.2 Stiffness versus speed

The total force F is, according to the analysis in Chapter 5, expected to increase linearly with speed in the low speed region. Thus the "in-plane" stiffness K is also expected to increase linearly. Measured values of F are recalculated into K and are shown in Fig. 8.22 and 8.24.

The restoring force F_y increases quadratically with speed in the low speed region. Thus the rotordynamic stiffness k_y is also expected to be quadratic in this region. Measured values of F_y are recalculated into k_y , which are shown in Fig. 8.23 and Fig. 8.25.

The force angle θ is shown in Fig. 8.26, and shows a decreasing relationship with speed, as expected.

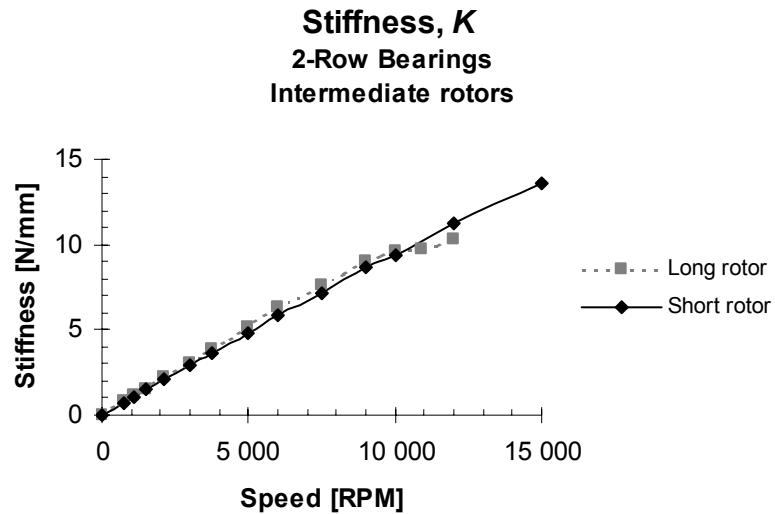


Fig. 8.22. In-plane stiffness for a 2-row bearing with different rotors.

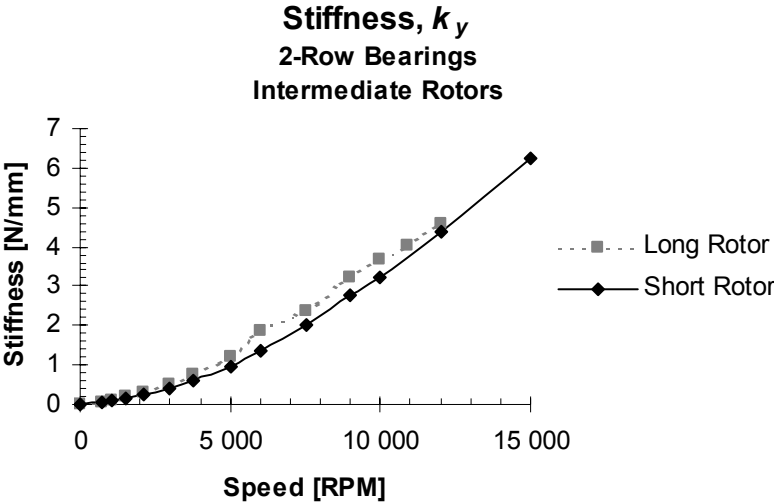


Fig. 8.23. Rotordynamic stiffness for a 2-row bearing with different rotors.

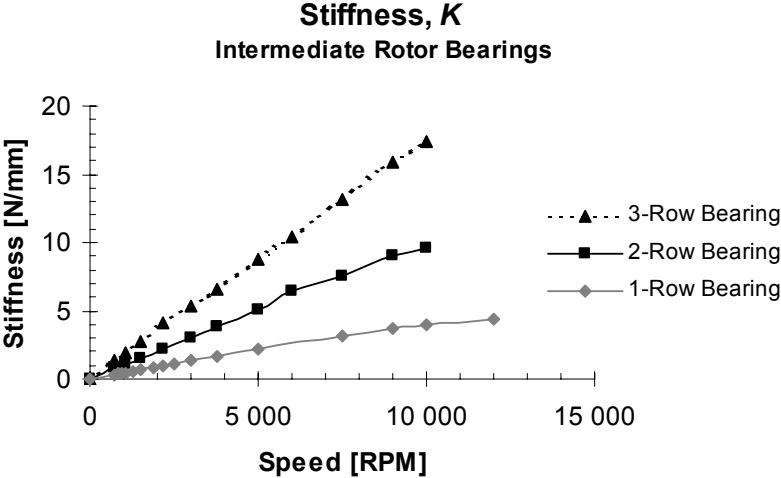


Fig. 8.24. In-plane stiffness for intermediate bearings with up to 3 rows.

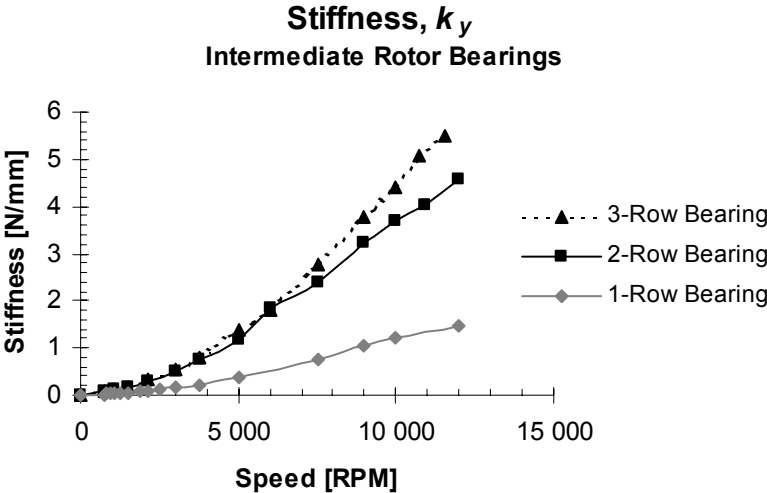


Fig. 8.25. Rotordynamic stiffness for intermediate bearings with up to 3 rows.

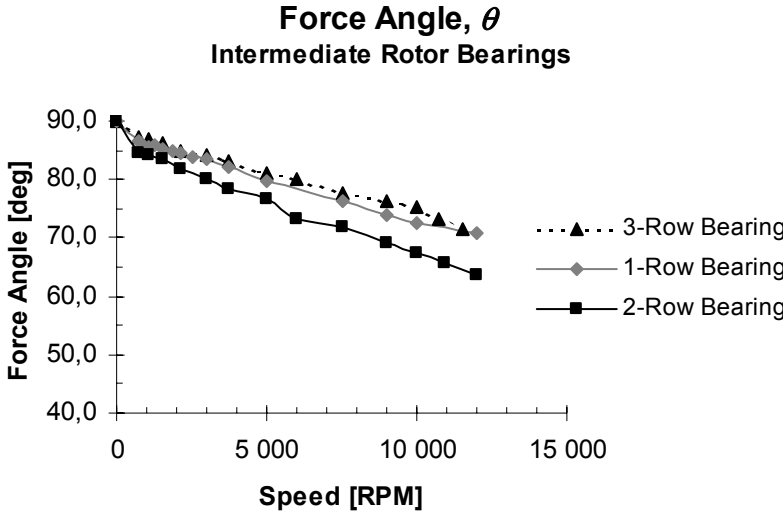


Fig. 8.26. Force angle for intermediate bearings with up to 3 rows.

8.7 Comparison with FEM calculations

The experimental values will now be compared to the data from the FEM analysis. The comparison is only possible to do in the low speed region, since measurements have only been performed up to between 12,000 and 22,000 rpm depending on rotor choice. The FEM-analyses on which this comparison is based, is found in Fig. 6.23, where the analyses has been performed for speeds up to 600,000 rpm. The analytical values shown in Fig. 8.27 constitute the low speed range of Fig. 6.23.

Before the comparison can be made, it is necessary to compensate for the fact that the FEM analyses has been performed for cobalt magnets having a remanent flux of 1 T, while the measurements were made on NeFeB magnets having a remanence of 1.25 T. Thus the analytical values of the stiffness referring to cobalt magnets, K_{CoSm} , have to be recalculated according to Eq. (8.2), which is valid as long as the pole shoes are not saturated. The flux B_0 at the pole shoe surface is normally less than 1 T when cobalt magnets are used.

$$K_{NeFeB} = K_{CoSm} (B_{r,NeFeB} / B_{r,CoSm})^2 = K_{CoSm} (1.25 / 1)^2 \quad (8.2)$$

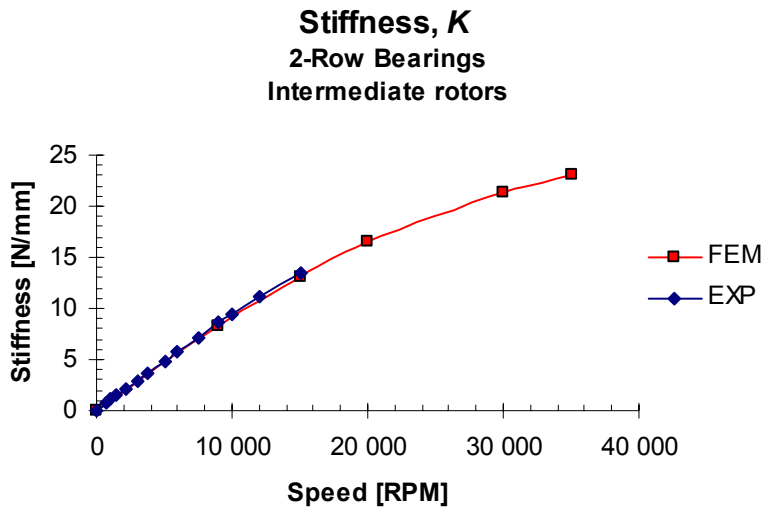


Fig. 8.27. Comparison between experimental data and FEM simulations for a 2-row bearing.

8.8 Thermal analysis

With the extremely low losses reported, both analytically and experimentally, it is expected that there will be no thermal problem using this bearing type. To verify this, the bearing was mounted to the tool-spindle, and a certain radial load was applied to ensure eddy currents in the copper rotor. The spindle was run for between one and one and a half hour, until the temperature was stabilized.

The results are shown in Fig. 8.28 and shows that the temperature rise in the bearing is only 2°C, for both speed and load combinations tested, while the temperature rise in the motor was higher. Thus a conclusion can be drawn that the bearing, when operated in air, can be regarded as a heat sink to the motor.

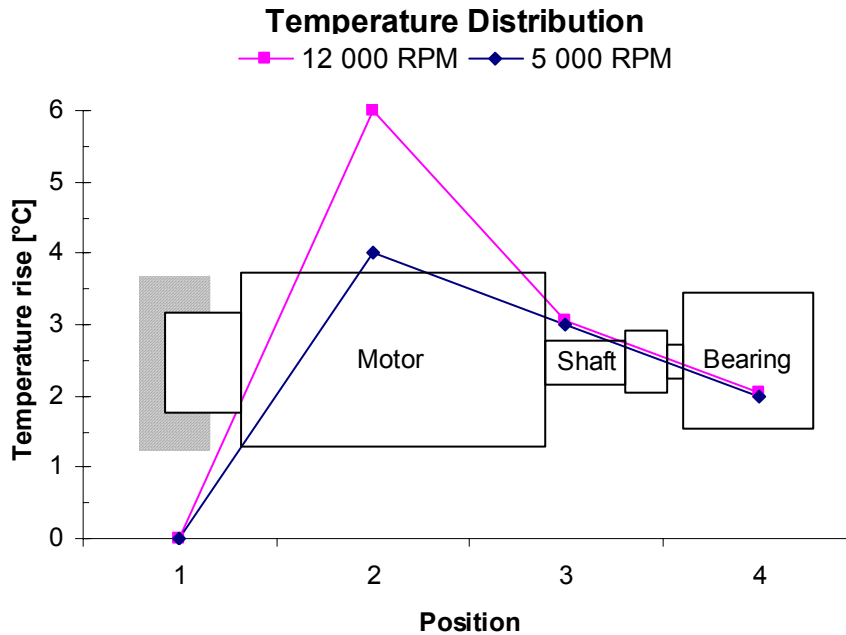


Fig. 8.28. Temperature rise due to long time operation.

9 Conclusions and suggestions for future research

This dissertation presents the design and analysis of a novel magnetic bearing specially aimed for high-speed rotating machines. It operates according to the electrodynamic levitation principle, which is here applied to an equally novel radial flux homopolar magnet topology.

It also proposes a high efficiency motor design compatible with the bearing, and a concept for how to apply the bearing and the motor together with dampers, permanent magnet unloaders and auxiliary bearings in such a way as to levitate a heavy rotor like a flywheel, virtually without any losses.

The bearing has been analyzed in several steps.

- An extensive 3D FEM analysis was performed, including parametric optimization of the bearing geometry. This is the major part of this work.
- A completely new analytical model has been developed. It makes use of the fact that the rotor behavior during eccentric operation has much in common with an induction generator squirrel cage, spinning in a 2-pole flux with large slip.
- Studies on bearing dynamics was done on a rebuilt vacuum pump from Balzers Pfeiffer, which was equipped with a homopolar induction bearing.
- Experimental evaluation of bearing forces was made on several bearing geometries. A special type of a spring suspended scales was made for this purpose, which can measure eccentricities with a resolution down to ± 35 nm (nanometer).

9.1 Conclusions

Based on the measurements, the finite element simulations and the analytical model developed, the following conclusions can be made.

1. Due to the homopolar flux from the ring magnets, the rotor does not experience any change of flux when it is spinning in its center position. Thus no eddy currents are induced, and no losses are generated. This is the normal operating condition, since the static loads are normally supposed to be carried by separate unloaders.
2. As soon as the rotor position deviates from its centered position, the conductor will see a periodic flux change which is proportional to the eccentricity, and eddy currents will be induced. These currents produce a force, which has a restoring as well as a tangential force component.
3. A similar flux change is caused by lateral motion and vibration of the rotor, which gives rise to speed dependent currents. These currents produce a delayed damping force, which might have a tangential and a restoring force component as well, depending on rotor speed and vibrational frequency.
4. Some residual losses occur in a no load condition due to magnet inhomogeneities. Also air drag losses are present when not applied in a vacuum environment.
5. External non-rotating damping is necessary for system stability.
6. Small changes in damping may have a large effect on the stability limit, an effect that cannot be explained by the theory on rotating damping as it is traditionally applied to eddy currents, treating conductors as purely resistive devices.
7. FEM simulations agree very well with measured data, and can be used for optimization of the bearing geometry.
8. The motor that is developed is particularly well suited for vacuum applications, since it is compatible with magnetic bearing requirements on low radial forces, and since it is not likely to cause thermal problems due to its high efficiency.

9.2 *Suggestions for future research*

The bearing, in the current state as it is presented in this report, has enough stiffness and is well suited for many stationary vacuum applications. To facilitate its use in industrial applications it is suggested that future research is initially focused on:

- the development of a low-frequency damper compatible with vacuum requirements and material standards
- reducing the need for damping by optimizing the bearing geometry for lower force angle
- develop models taking ferromagnetic members in the rotor into consideration
- continue and improve the ongoing flywheel concept, which is shown in Fig. 9.1.

With some improvements the bearing is likely to attract future interest in mobile environments, biochemistry and in the fuel cell industry. Then research has to focus on

- improvement of the model by adding a reluctance grid for the repulsive airgap flux
- getting better understanding of system dynamics without making either high frequency or low frequency assumptions
- performing iterative studies on bearing geometry to optimize properties with regard to production economy
- develop analytical expressions for angular stiffness and cross-coupling stiffness coefficients, and their related damping coefficients.



Fig. 9.1. Ongoing flywheel project.

References

- [1] Earnshaw, S., "On the Nature of the Molecular Forces which Regulate the Constitution of the Luminiferous Ether", *Trans. Camb. Phil. Soc.*, 7, pp 97-112 (1842)
- [2] J. Powell and G. Danby, "Electromagnetic Inductive Suspension and Stabilization System for a Ground Vehicle," U.S. Patent 3 470 828, Oct.7, 1969.
- [3] Richards, P.L., Tinkham, M., "Magnetic Suspension and Propulsion Systems for High-Speed Transportation", *J. Appl. Phys.* Vol. 43, No. 6, Jun. 1972, pp. 2680-2690.
- [4] Sacerdoti, G., Catitti, A., Soglia, L. " Self Centering Rotary Magnetic Suspension Device", US Patent No: 3811740, Publication date 1974-05-21.
- [5] Lembke, T., " Design of Magnetic Induction Bearings", M.Sc. thesis, Chalmers University of Technology, Göteborg 1990.
- [6] Lembke, T., "Eddy Induced Magnetic Bearing", European patent No. 0594033, Publication date 1994-04-27.
- [7] Post, R., "Dynamically stable Magnetic Suspension/Bearing System". US patent No. 5495221, Publication date 1996-02-27.
- [8] Lefevre, L., "Helical Air-gap Winding Permanent Magnet Machine", *Electrical Machines and Drives*, Royal Institute of Technology, Stockholm 1998.
- [9] Lang, M. and Fremerey, J.K., "Optimization of Permanent-Magnet Bearings", 6th International Symposium on Magnetic Suspension Technology, Turin, October 2001.
- [10] Filatov, A., "'Null-E' Magnetic Bearings", Ph.D. dissertation, University of Virginia, August 2002.
- [11] Post, R.F.; Fowler, T.K.; Post, S.F., "A high-efficiency electromechanical battery", *Proceedings of the IEEE* , Vol. 81 (1993), pp.462 – 474

References

- [12] Schweitzer G., Bleuler H., Traxler A., "Active Magnetic Bearings", vdf Hochschulverlag AG an der ETH Zürich, 1994.
- [13] Filatov A. V., Maslen EH, Gillies G. T., "A method of noncontact suspension of rotating bodies using electromagnetic forces", Journal of Applied Physics, Vol. 91 (2002) pp. 2355-2371
- [14] Filatov A. V., Maslen, E. H., and Gillies, G. T., "Stability of an Electrodynamic Suspension" Journal of Applied Physics, Vol. 92 (2002), pp. 3345-3353.
- [15] Lembke T., "Induction Bearings –A Homopolar Concept for High Speed Machines", Dep. of Electrical Machines and Power Electronics, Royal Institute of Technology, Stockholm, 2003
- [16] Lembke T., "3D-FEM Analysis of a Low Loss Homopolar Induction Bearing", International Symposium on Magnetic Bearings, ISMB9, Lexington, KY, USA 2004.
- [17] Krämer E., "Dynamics of Rotors and Foundations", Springer Verlag, Berlin, 1993
- [18] Lembke T., "Assessment and Experimental Verification of the Homopolar Induction Bearing", Internal report for Magnet AB, Uppsala, 2005.
- [19] J. K. Fremerey, M. Kolk: A 500-Wh power flywheel on permanent magnet bearings, Proceedings of the 5th International Symposium on Magnetic Suspension Technology, 1-3. 12. 1999, Santa Barbara, CA
- [20] Boden K., Fremerey J.K., "Industrial Realization of the "System KFA-Jülich" Permanent Magnet Bearing Lines" Proceedings of MAG '92, Alexandria, Virginia, July 29-31, 1992
- [21] Engström J., "On Design of Slotless Permanent Magnet Machines", Licentiate thesis, Department of Electrical Machines and Drives, Royal Institute of Technology, 1999
- [22] Slemon G. R., "Electric Machines and Drives", ISBN 0-201-57885-9, Addison-Wesley Publishing Company, 1992.
- [23] "M3A 100kW Flywheel Power System" Data Sheet, AFS Trinity Power Corporation 2005, www.afstrinity.com
- [24] "Annual Report 2001", Magnet AB, Uppsala, 2001

- [25] Lang, M. "Berechnung und Optimierung von passiven permanentmagnetischen Lagern für rotierende Maschinen, VDI-Verlag, Düsseldorf, 2004, ISBN 3-18-335721-6
- [26] Mega Manual, Department of Electronic and Electrical Engineering, University of Bath, Claverton Down, Bath BA2 7AY, United Kingdom
- [27] Lembke. T. "Compliant foil fluid film bearing with eddy current damper", US Patent 6,469,411
- [28] R. G. Gilbert: "Magnetic suspension", US Patent 2,946,930, 1955

Appendix 1

Simple hands-on rules for designing induction bearings

Based on the analysis above we can summary the design phase of a homopolar induction bearing into a few simple hands on rules.

1. Choose configuration:

1. Inner rotor, with ring magnets on the outside.
2. Outer rotor, with ring or disc magnets on the inner stator.
3. Intermediate rotor type, comprising a tubular rotor with magnets both on the inside and on the outside of the rotor.

2. Choose rotor material with as high conductivity as possible.

3. Decide the lowest rotational speed during continuous operation.

Let the wall thickness of the cylinder equal one skin depth or more for this frequency. For intermediate rotors do not use too thick walls. A thickness of between one and one and a half skin depth is recommended for best use of the magnets.

Choose the pole width of the magnets, including pole shoes, to two times the sum of the airgap and the skin depth at this frequency.

4. Decide the maximum rotational speed.

Choose the maximum rotor diameter with respect to constraints like centrifugal acceleration or other design criteria. Use bandage only on outer rotor type bearing in order to keep the airgap small.

5. Choose magnet arrangement.

Halbach array will give the highest stiffness, but is expensive and need high speed to utilize the stiffness.

Flux concentration with pole shoes gives high stiffness at low speed. Other advantages are simple magnet arrangement, flat stiffness versus speed curve and small side forces.

Appendix 1

6. Choose magnet cross section depending on optimization criteria.

Maximum stiffness: Let the width of the magnet equal at least two times the pole width plus two times the axial length of a pole shoe, if the latter are used.

Economic stiffness: Let the width be about 60% of the value above. This will result in maximum stiffness per kilo magnet.

7. Choose number of magnets for desired stiffness.

Adjust by changing diameter or bearing width.

8. Choose type of bearing end.

Reduce the axial length of the end pole shoe to 50%.

If there is place enough, let this pole shoe cover the airgap and some of the conducting cylinder.

Do not make the cylinder slightly longer than the stator package. Make it either somewhat shorter or much longer.

Appendix 2

Model geometries

Model 1

Description:	Intermediate bearing without pole shoes	
Magnets:	2 outer ring magnets.	38 × 30 × 4 mm
	2 inner ring magnets	24 × 16 × 4 mm
Pole shoes:	None	
Rotor:	Copper cylinder	29 × 25 × 9 mm

Model 2

Description:	Intermediate bearing with pole shoes	
Magnets:	2 outer ring magnets.	38 × 30 × 4 mm
	2 inner ring magnets	24 × 16 × 4 mm
Pole shoes:	1 outer intermediate washer	38 × 30 × 2 mm
	2 outer end plates	38 × 30 × 1 mm
	1 inner intermediate washer	24 × 16 × 2 mm
	2 inner end plates	24 × 16 × 1 mm
Rotor:	Copper cylinder	29 × 25 × 9 mm

Model 3

Description:	Flywheel outer rotor bearing with pole shoes	
Magnets:	4 inner ring magnets	24 × 10 × 7 mm
Pole shoes:	3 inner intermediate washers	24 × 16 × 3,50 mm
	2 inner end plates	24 × 16 × 1,75 mm
Rotor:	Copper cylinder	35 × 25 × 9 mm

Appendix 3

Patents

The magnetic bearings presented in this dissertation are protected by the following patents and patent applications:

US6469411	Compliant foil fluid film bearing with eddy current damper
TW471568Y	Magnetic bearing
AU2285002	Compliant foil fluid film bearing with eddy current damper
WO0248561	Compliant foil fluid film bearing with eddy current damper
US6118199	Magnetic bearings
US6050782	Magnetically suspended high velocity vacuum pump
EP0960277	Magnetically suspended high velocity vacuum pump
EP0956457	Electrodynamic magnetic bearing
JP10281158	Magnetic suspension device
AU5788298	Magnetically suspended high velocity vacuum pump
AU5788198	Electrodynamic magnetic bearing
SE508445	Magnetically suspended high velocity vacuum pump
SE508442	Magnetic bearings
SE9700257	Integrating rate gyroscope
SE9700256	High velocity vacuum pump
SE9700255	Device for magnetic suspension
WO9832981	Electrodynamic magnetic bearing
WO9832973	Magnetically suspended high velocity vacuum pump

Readers interested in the patents above are kindly requested to contact Magnetel on the address below.

Magnetel AB
Axel Johanssons gata 4D
754 50 Uppsala
Sweden